SHEAR BEHAVIOUR AND DESIGN OF COLD-FORMED CHANNEL SECTIONS WITH ELONGATED OPENINGS BASED ON DIRECT STRENGTH METHOD

DUY KHANH PHAM

THE UNIVERSITY OF SYDNEY

Supervisors:
Dr. Cao Hung Pham
Prof. Gregory J. Hancock

A thesis submitted in fulfilment of
the requirements for the degree of
Master of Philosophy

School of Civil Engineering
Faculty of Engineering
The University of Sydney
Australia

Nov 2019

ABSTRACT

This thesis presents a detailed study on shear buckling and shear strength of high strength cold-formed channel sections with elongated openings. The main purposes are to investigate experimentally and numerically the shear behaviour of perforated cold-formed steel plain C-lipped sections and to further develop a Direct Strength Method (DSM) of design to predict the shear capacity of such sections.

Firstly, in order to achieve the primary aims as stated, an experimental program of thirty tests was performed to observe the shear behaviour of channel members with both non-elongated and elongated web holes. Based on the capability of minimising the bending moments at two ends of the shear span, a testing apparatus namely 'Dual Actuator Test Rig' previously developed at the University of Sydney was used throughout the test program to capture a state close to pure shear and to obtain the predominantly shear capacity of perforated members with an aspect ratio (shear span / web depth) up to 2.0. The experimental results were used to study the shear strength reduction due to enlarged web openings. Further, these test results were also used as the input to the current Direct Strength Method (DSM) equations for further comparisons, calibrations and validations.

Secondly, in order to achieve more insights into the shear behaviour of cold-formed members with elongated web openings, numerical nonlinear simulations based on the Finite Element Method (FEM) using ABAQUS/Standard were developed to compare with and calibrate against the experimental results. Moreover, to study shear buckling behaviour and to generate shear buckling loads which is also a required input to the DSM in shear, a simplified method for shear buckling analysis using simplified finite element (FE) models including web holes were introduced in this study. The buckling results obtained from these models were calibrated against those of the full FE models which have the same configuration as the actual tests. On the basis of the accuracy of the finite element modelling, the FE models for both shear buckling and shear strength analyses were employed for parametric studies to extend the result database used for further verification of new proposals in this study.

Finally, on the basis of the results from experimental and numerical investigations, a new DSM design for cold-formed channel sections subjected to shear with both non-elongated

and elongated web openings was introduced. The new proposal is based on the use of the existing DSM design rules for shear together with introduced modifications of the shear yield loads as a result of the Vierendeel mechanism approach. As a consequence of the parametric study for shear buckling analyses, a dimensional transformation was also proposed to determine the equivalent hole dimensions in design.

Keywords: Cold-formed channel section, Shear behaviour, Elongated openings, Direct Strength Method.

STATEMENT OF ORIGINALITY

This is to certify that to the best of my knowledge, the content of this thesis is my own work. This thesis has not been submitted for any degree or other purposes.

I certify that the intellectual content of this thesis is the product of my own work and that all the assistance received in preparing this thesis and sources have been acknowledged.

Duy Khanh Pham

PUBLICATIONS

This thesis contains material accepted or submitted for publication, based on the work presented in the thesis, for which I am the main author. The material is distributed throughout Chapters 3, 4, and 5.

Journal Papers:

Pham, D.K., Pham, C.H., Pham, S.H. and Hancock, G.J. (2019). "Experimental Investigation of High Strength Cold-formed Channels with Elongated Openings in Shear", *Journal of Constructional Steel Research*, 2019 (accepted for publication)

Pham, D.K., Pham, C.H., and Hancock, G.J. (2019). "Numerical Investigation of High Strength Cold-formed Channels with Elongated Openings in Shear", *Journal of Constructional Steel Research*, 2019 (being prepared)

Conference Papers:

Pham, D.K., Pham, C.H., Pham, S.H. and Hancock, G.J. (2019). "The Behaviour of Cold-formed Channel Sections with Elongated Web Holes in Shear", *Fifth Congrès International de Géotechnique - Ouvrages – Structures*, University of Transport Technology (UUT), Hanoi, Vietnam, 2019

Pham, D.K., Pham, C.H., and Hancock, G.J. (2019). "Elastic Buckling Solution to Perforated Thin-walled Channel Sections in Shear with an Aspect Ratio of 2.0", *Fifth Congrès International de Géotechnique - Ouvrages – Structures*, University of Transport Technology (UUT), Hanoi, Vietnam, 2019

Duy Khanh Pham

ACKNOWLEDGEMENTS

Firstly, I would like to express my sincere gratitude to my supervisors, Dr Cao Hung Pham and Prof Gregory J. Hancock, for the continuous support of my M.Phil study, for their motivation and immense knowledge. Their guidance helped me in all the time of research and writing of this thesis.

Besides my supervisors, I would like to sincerely thank Dr Song Hong Pham for his enthusiastic support of my research and for the stimulating discussions, especially for enlightening me the first glance of research.

I would like to thank Bluescope Steel for supply of the test specimens for the research program performed at the University of Sydney.

I am grateful to the technical staffs at the J.W. Roderick Laboratory for Materials and Structures including Mr Garry Towell, Mr Paul Bustra, Mr Paul Burrell, Mr James Ryder for their assistance during the experimental program and for their friendship in the labs.

I wish to thank many friends and colleagues in the “Blue Room” (Room 360) for their friendship and great moments we have had.

I am greatly indebted to my parents (Van Thieng Pham and Anh Hong Pham) and my parents-in-law (Van Huy Pham and Thi Dinh Nguyen) for supporting me spiritually, and for providing me with a loving environment throughout my study in Sydney.

Lastly, and most importantly, I wish to give special thanks to my wife,Thi Quynh Hoa Pham, who always stays with me to inspire me and never ceases to bring happiness into my life.

Duy Khanh Pham

ABBREVIATIONS

AISI	:	American Iron and Steel Institute
ANN	:	Artificial Neutral Network
AR	:	Aspect ratio
DoF	:	Degrees of Freedom
DSM	:	Direct Strength Method
EA	:	Equal Angle
EWM	:	Effective Width Method
FE	:	Finite Element
FEM	:	Finite Element Method
ISFSM	:	Isoparametric Spline Finite Strip Method
LMS	:	Low Moment Side
LVDT	:	Linear Variable Displacement Transducer
MPC	:	Multi-Point Constraint
SAFSM	:	Semi-Analytical Finite Element Method
SFSM	:	Spline Finite Strip Method
TFA	:	Tension Field Action

NOTATIONS

τ_{cr}	=	Shear elastic buckling stress (MPa)
μ	=	Poisson's ratio
A	=	Cross-sectional area of gauge portion (mm^2)
A_h	=	Original area of a slotted hole (mm^2)
$A_{h\text{-}eq}$	=	Area of transformed hole (equivalent hole area) (mm^2)
AR_h	=	Aspect ratio of opening
A_w	=	Cross-sectional of web element (mm^2)
b	=	Gauge width (mm)
B	=	Overall flange width (mm)
D	=	Overall web depth (mm)
d_h	=	Overall hole depth (mm)
$d_{h,m}$	=	Depth of the holes with $d_h/h = m$ (mm)
$d_{h\text{-}eq}$	=	Depth of transformed hole (equivalent hole depth) (mm)
E	=	Young's modulus
f_y	=	Average yield stress (MPa)
$f_{y,0.2\%}$	=	Nominal proof stress (MPa)
h	=	Depth of flat web portion (mm)
Imp	=	Imperfection scaling factor
k_v	=	Elastic shear buckling coefficient of perforated member
l	=	Overall lip size (mm)
L	=	Length of shear span (mm)
L_h	=	Overall hole length (mm)
$L_{h,m}$	=	Length of the holes with $d_h/h = m$ (mm)
L_h'	=	Critical opening length (distance between plastic hinges along the span length) (mm)
$L_{h\text{-}eq}$	=	Length of transformed hole (equivalent hole length) (mm)
M	=	Bending moment (kNm)

M_{pv}	=	Plastic bending capacity of top (or bottom) segment above (or below) the opening (kNm)
r	=	Filleted corner radius of opening (mm)
t	=	Member thickness (mm)
V	=	Shear force (kN)
V_{cr}	=	Elastic shear buckling load (kN)
$V_{cr,full}$	=	Elastic shear buckling load generated from full finite element models based on actual tests (kN)
$V_{cr,simplied}$	=	Elastic shear buckling load generated from simplified finite element models (kN)
v_i	=	Vierendeel parameter
V_n	=	Shear strength of channel members with original openings (kN)
$V_{n,FEM}$	=	Shear strength of channel members by FEM (kN)
$V_{n,test}$	=	Shear strength of members by actual tests (kN)
$V_{n\text{-}eq}$	=	Shear strength of channel members with equivalent openings (kN)
V_{vrd}	=	Shear yield load based on the Vierendeel mechanism (kN)
$V_{vrd,0.6}$	=	Shear yield load of the holes with $d_h/h = 0.6$ based on the Vierendeel mechanism (kN)
$V_{vrd,m}$	=	Shear yield load of the holes with $d_h/h = m$ based on the Vierendeel mechanism (kN)
V_y	=	Shear yield load of unperforated section (kN)
$V_{y,FEM}$	=	Peak load extracted from finite element models restrained laterally in the web and the lips (kN)
$V_{y,net}$	=	Shear yield load based on web net area (kN)
$V_{y,proposed}$	=	Modified shear yield load based on the new proposal for the DSM design for channel sections in shear with non-elongated and elongated web openings (kN)
V_{yh}	=	Shear yield load based on the Vierendeel model with non-elongated openings (kN)
ε	=	Average engineering strain
ε_{true}	=	True strain
λ_v	=	Non-dimensional slenderness

σ	=	Average engineering stress (MPa)
σ_{true}	=	True stress (MPa)
φ_p	=	Angle taken from low moment side and vertical centre line of web opening

TABLE OF CONTENTS

LIST OF FIGURES

LIST OF TABLES

Chapter 1
INTRODUCTION

1.1 RESEARCH BACKGROUND

Cold-formed steel structures have been commonly used in the construction industry (Winter [1], Yu [2] and Hancock [3]) for both structural and non-structural components such as columns, beams, joists, studs, frames, structural decks, wall panels, girts and purlins. The wide application of high strength cold-formed steel in building construction is attributed to the high strength-to-weight ratio, ease of prefabrication, easy and fast erection and installation compared to conventional hot-rolled steel.

Cold-formed steel members are fabricated by press-braking or cold-rolling from flat steel plates, sheet metal or strip materials at ambient temperature. This process causes a change in the mechanical properties of the material including yield stress and stiffness as a result of the cold working of the metal. Further, with the improvement of rolling and forming technology, various members with complex section shapes can be fabricated and used in the building industry as individual structural framing members and decks or panels.

In floor and roof systems, high strength steel profiled sheeting is commonly fastened to cold-formed purlins of lipped C or Z-sections. The design of such purlin members is currently incorporated into the North American Specification AISI S100-16 [4] and the Australian/New Zealand Standard AS/NZS 4600:2018 [5]. In these codes, the newly developed Direct Strength Method (DSM) of design for cold-formed members have been recently standardised with the aim of simplifying the design process and revoking the conventional Effective Width Method (EWM) which involves complicated computations.

The Direct Strength Method (DSM) design rules for unperforated cold-formed steel members in shear have been recently incorporated into AISI S100-16 [4] and AS/NZS 4600:2018 [5]. Elastic shear buckling loads (V_{cr}) and yield shear loads (V_y) are two required inputs in the DSM. In order to determine the elastic buckling loads (V_{cr}) of channel sections in

pure shear, Pham & Hancock [6, 7] have used the Spline Finite Strip Method (SFSM) developed by Lau & Hancock [8] or the new theory of the Semi-Analytical Finite Strip Method (SAFSM) using multiple series terms (Hancock & Pham [9]) developed to investigate the shear elastic buckling characteristics of channel sections with two simply supported ends. For shear elastic buckling analysis of channel sections with holes, C.H. Pham [10, 11] used the SFSM encoded in the isoparametric spline finite strip method (ISFSM) developed by Eccher [12] to provide solutions of shear buckling loads for lipped channel sections with central square and circular holes in the web. The SFSM was also benchmarked against the Finite Element Method (FEM) using software package ABAQUS/Standard in all cases of stress distributions by C.H. Pham [11]. In S.H. Pham [13], the shear buckling loads and the shear buckling modes generated from the FEM models for shear buckling solutions for channel sections with central square and circular web holes were proven to be similar to those by the SASFM.

For the determination of yield shear load of an unperforated web, the equation, $V_y = 0.6 f_y A_w$, is used in AISI S100-16 [4] where A_w is the area of the flat web portion and f_y is the average yield stress. This expression implies that the shear resistance depends only on the flat portion of the web and the flat web is fully effective. With perforated channel sections, Unabia B. [14] proposed the use of web net section area at the opening location referred to $V_{y,net}$ for the calculation of the shear yield load of a web section with holes. However, the use of $V_{y,net}$ has been proven to be conservative for sections with relative small perforations but unconservative for sections with large holes as reported in C.H. Pham et al. [15] and S.H. Pham [13]. S.H. Pham et al. [16] presented a new proposed model to obtain the shear yield loads for members with central circular and square openings subjected to pure shear with an aspect ratio (*AR*) of 1.0. The sizes of holes employed in this practical model vary from very small dimensions where traditional shear yielding predominates to substantial large reduced web areas where the proposed Vierendeel action dominates. Later, it was also proven in S.H. Pham [13] that the proposal by S.H. Pham et al. [16] is capable of being used for pure shear members with square and circular holes with an aspect ratio up to 2.0.

1.2 PRESENT PROBLEM

High-strength cold-formed steel members are commonly manufactured with perforations for the purpose of minimising the effects of service systems on the ceiling clearance height and the internal architecture by providing access for the building service systems through web holes as shown in **Figs 1.1** and **1.2**. The presence of the web openings leads to changes in buckling characteristics and ultimate strengths because of changes in stress distributions. This has resulted in a considerable number of studies into the effect of web cut-outs on cold-formed steel members including compression in columns, flexural and shear in beams.

Fig 1.1: Cold-formed framing system (image courtesy of ClarkDietrich Building Systems)

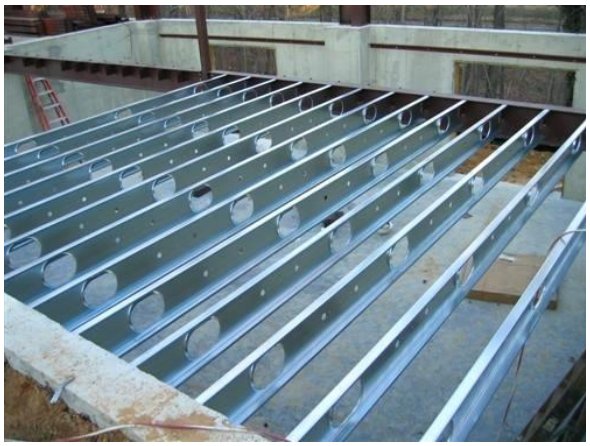

Fig 1.2: Cold-formed floor system (image courtesy of IMGLABS.co)

The effects of evenly spaced web holes on both the buckling-controlled failures and the ultimate strengths of compression and flexural perforated members were investigated by Moen [17] and Moen & Schafer [18, 19] based on a database of earlier tests on cold-formed members with holes, and parametric nonlinear finite-element models with a wide range of hole sizes, hole spacings, hole shapes, and dimensions of members. The Direct Strength Method (DSM) approach developed from these studies were incorporated into the North American Specification AISI S100-12 [20] and recently in the Australian/New Zealand Standard AS/NZS 4600:2018 [5]. For perforated members in shear, experimental investigations of channel sections with square holes were performed by C.H. Pham et al. [21] and C.H. Pham et al. [15] at the University of Sydney (USYD) to observe the predominantly shear failure modes and the shear strength reduction when the sizes of web holes vary from 40 to 120 mm in a 200 mm

deep section. With the aim of minimising bending moments to obtain close to pure shear capacity, C.H. Pham et al. [21] and C.H. Pham et al. [15] used central point load tests with an aspect ratio (shear span / web depth) of 1.0. Commercially available plain channel members of 200 mm web depth were chosen with various thicknesses including 1.5, 1.9, and 2.4 mm in the USYD's studies. Tests in shear with different sizes of circular web openings were carried out by Keerthan & Mahendran [22] at the Queensland University of Technology (QUT) with a wide range of web depths of 120, 160 and 200 mm. The shear test results from USYD and QUT were subsequently collected and calibrated by S.H. Pham et al. [16] as a database to verify the proposal for the DSM of design for C-sections in shear with central circular and square web openings.

Although the Direct Strength Method (DSM) has been recently developed for design for cold-formed members in shear, only DSM design rules for unperforated members subjected predominantly to shear based on the research by Pham & Hancock [7] were included in AISI S100-16 [4]. The DSM design formulae for channel sections in shear with central web openings were also proposed by S.H. Pham et al. [16]. However, this proposal only focused on square and circular web holes. In order to increase the applicability for all service systems in practice, the web openings are likely to be enlarged along the span length of members due to a limited web depth. As a result, the behaviour of channel sections with web holes with elongated shapes such as rectangular and slotted holes should be studied. The DSM of design for perforated channel sections with the elongated web holes in compression and bending was extended by Moen & Schafer [18, 19] and was standardised currently in AISI S100-16 [4] and AS/NZS 4600:2018 [5]. The past research by Shan et al. [23], Schuster et al. [24] and Eiler et al. [25] on channel sections investigated the influence of rectangular and slotted web openings on the shear strength reduction. The design method based on the results from these studies has been retained in AISI S100-16 [4] and AS/NZS 4600:2018 [5]. These standards still adopt the empirical approach from the research findings in the 1990s. According to this design methodology, the shear strength of a perforated member is calculated by multiplying the shear strength of an unperforated section by the reduction factor (q_s) mainly based on experiments. Detailed formulae for this approach were expressed in Section C3.2.1 of NAS S100-2016. Despite the computational convenience, it was proven by Keerthan & Mahendran [26] that the empirical method for determination of shear strength of members with holes is conservative

for perforated channel sections with small cut-outs, but unconservative with substantially large openings. Further, there is a restricted applicability of the empirical method due to limited number of available tests and data range.

Hence, rectangular and slotted hole shapes (elongated holes) are chosen for a shear test program presented in this thesis to observe the influence of elongated openings on the shear behaviour of cold-formed channel sections.

1.3 RESEARCH SCOPE AND OBJECTIVES

The main objective of this thesis is to provide an understanding of the shear behaviour of cold-formed channel purlins and beams with the presence of both non-elongated and elongated central web openings. Both experimental and numerical investigations were performed followed by proposals for DSM design guidelines. In order to achieve these objectives, main tasks in this thesis are addressed as follows:

(i) To investigate experimentally the behaviour of perforated cold-formed C-lipped sections with both non-elongated and elongated central web openings (circular, square, rectangular and slotted holes) subjected to predominantly shear.

(ii) To develop numerical nonlinear simulations of the shear tests on members with web holes to calibrate against the test results and to extend the test database by conducting parametric studies.

(iii) To study the shear elastic buckling of whole channel sections with a variety of web hole dimensions in different cases of stress distributions resulting from shear and bending moments acting at two end sections of the members.

(iv) To compare the experimental results with current proposals for design for channel sections in shear with holes to evaluate the applicability of these proposals to the presence of elongated web openings.

(v) To propose a modified DSM design for shear to predict the shear strength of cold-formed channel members with different hole shapes in the web.

1.4 RESEARCH METHODOLOGY

In order to achieve the objectives as mentioned above, an integrated approach including experimental, theoretical and numerical investigations is implemented.

For the experimental investigation, a total of thirty shear tests included in two test series are carried out at the University of Sydney. Plain C-lipped channel sections with the thickness of 1.5 mm and the depth of 200 mm (C20015) are used in all the shear tests. Aspect ratios of openings (AR_h = hole length / hole depth) for the investigation are chosen as 1.0, 2.0 and 3.0 together with various hole depths including 40, 80 and 120 mm. The dual actuator test rig developed by S.H. Pham et al. [27] is utilised throughout the shear tests to obtain predominantly shear capacity with an aspect ratio of 2.0 and to observe the shear behaviour of channel members with elongated holes. The experimental results from the test program are compared with the strength predictions using the current DSM of design for shear with and without Tension Field Action (TFA). The test outcomes and results provide a clearer understanding of the shear behaviour of perforated cold-formed sections with elongated holes.

For numerical study, nonlinear finite element simulation using the finite element package ABAQUS 6.14 (ABAQUS 6.14-2 [28]) is employed to develop finite element (FE) models. The FE models are firstly built to optimise the experimental design before setting up the actual tests. The simulations are then calibrated against the test results followed by a performance of parametric studies. The finite element method modelling utilising Abaqus/CAE is also employed for shear elastic buckling analyses of channel sections with elongated web openings. The shear buckling loads from these analyses serve as the input V_{cr} of the DSM design method.

The results from shear elastic buckling analyses and shear ultimate strength analyses are collected for the comparison of the Direct Strength Method design loads for shear including the influence of the elongated web holes. Further, the modified DSM design rules for shear are proposed on the basis of resulting database from both experimental and numerical studies to predict the shear strength of cold-formed channels with various sizes of web openings.

Chapter 2

LITERATURE REVIEW AND SHEAR STRUCTURAL BEHAVIOUR

2.1 SHEAR ELASTIC BUCKLING OF SLENDER UNPERFORATED PLATES

For thin plates in shear, the shear buckling strength of unperforated rectangular plates has been thoroughly investigated by many studies including Timosenko & Gere [29], Allen & Bulson [30], Bleich [31], and Bulson [32]. For a slender plate simply supported along its edges and subjected to shear stresses distributed uniformly along all the edges, shear stresses are assumed to be equal to the shear elastic buckling stress (τ_{cr}) when the plate buckles. The shear elastic buckling stress of an infinitely long plate was formulated by Timosenko & Gere [29] as:

$$\tau_{cr} = \frac{k_0 \pi^2 E}{12(1-\mu^2)\left(\frac{h}{t}\right)^2} \tag{2.1}$$

where k_0 is the shear buckling coefficient of the plate without holes depending on the boundary conditions and the ratio of the length of the plate (a) to the depth of the plate (h); E is the Young's modulus; μ is Poisson's ratio; t is the thickness of the plate. For simply supported rectangular plates, the value of k_0 as a function of the aspect ratio of the plates (a/h) can be determined by using the following approximate formulae:

$$\text{When } \frac{a}{h} \le 1, \qquad k_0 = 4.00 + \frac{5.34}{(a/h)^2} \tag{2.2a}$$

$$\text{When } \frac{a}{h} > 1, \qquad k_0 = 5.34 + \frac{4.00}{(a/h)^2} \tag{2.2b}$$

According to ***Eq (2.2)***, in the cases that plates are simply supported on all edges, the value of k_0 is increased from 5.34 for a very long plate to 9.34 for a square plate respectively.

2.2 SHEAR ELASTIC BUCKLING OF SLENDER PERFORATED PLATES

An analysis of elastic shear buckling of perforated square plates with circular holes was investigated by Rockey et al. [33] using the Finite Element Method (FEM). The reduction of the buckling coefficient (k_v) for both simply supported and clamped edges in the study by

Rockey et al. [33] is shown in **Fig 2.1**. A comparison between the values of k_v by Rockey et al. [33] and those by C.H. Pham [11] employing the Spline Finite Strip Method (SFSM) is shown in **Fig 2.2.**

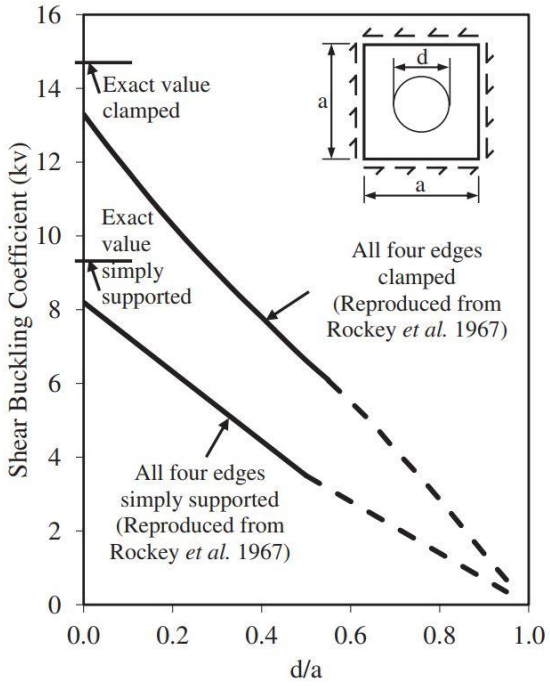

Fig 2.1: Effect of circular hole on shear buckling coefficient (Rockey et al. [33])

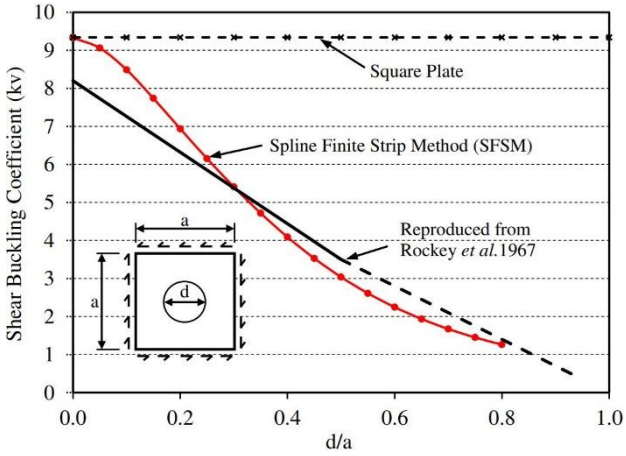

Fig 2.2: Shear buckling coefficient of square plate with circular hole using FEM (Rockey et al. [33]) and SFSM (C.H. Pham [11])

Further, Narayanan & Der Avanessian [34] conducted finite element studies to compute the elastic buckling coefficients and proposed approximate formulae for many cases of slender plates under shear with hole dimensions not greater than half the width of the plate. The relationship for plates with a central circular hole was suggested as:

$$k = k_0 \left[1 - \alpha_c \frac{d}{\sqrt{(h^2 + b^2)}} \right] \tag{2.3}$$

where k and k_0 are the shear buckling coefficients of perforated and unperforated plates having the same plate dimension, α_c equals 1.8 for simply supported edges and 1.5 for clamped edges respectively; d is the diameter of the circular opening; h and b are the depth and the length of the plates respectively. When the cut-outs are larger, the values of k might be calculated by:

$$k = k_0\left[1-\frac{d}{h}\right] \tag{2.4}$$

In the case of a plate containing a central rectangular opening, the values of k can be estimated as:

$$k = k_0\left[1-\alpha_r\frac{A_c}{A}\right] \tag{2.5}$$

where α_r equals 1.25 and 1.50 for clamped and simply supported edges respectively; A_c is the area of the hole; A is the area of the unreduced plate. When the openings become larger, the shear elastic buckling coefficient (k) shall be taken as the smaller of the two values given as:

$$k = k_0\left[1-\frac{b_0}{b}\right] \text{ or } k = k_0\left[1-\frac{d_0}{h}\right] \tag{2.6}$$

where d_0 and b_0 are the depth and the length of the opening respectively.

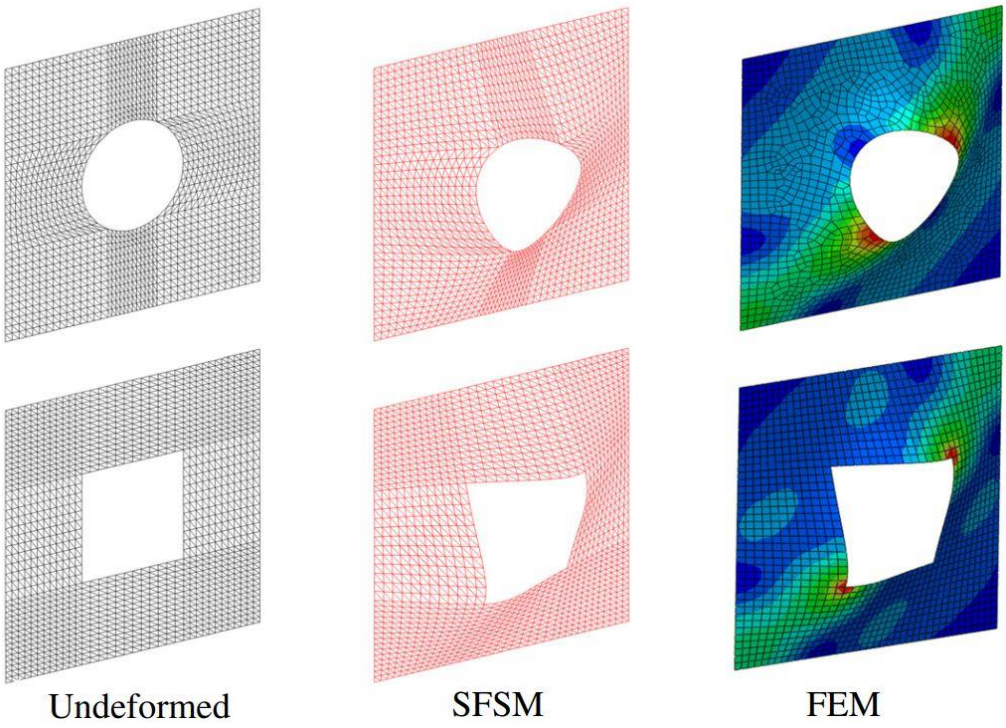

Fig 2.3: Shear buckling modes from SFSM and FEM of square plate with circular and square openings (C.H. Pham [11])

The shear buckling of simply supported plates with holes in shear have been also studied by C.H. Pham [11] based on the FEM using ABAQUS/Standard. The results from FEM analyses have been validated successfully against the shear buckling analyses using the SFSM

on the same dimensions. Good agreement in shear elastic buckling coefficients between the two methods were obtained with a maximum variance of less than 2%. In addition, the same shear buckling modes from SFSM and FEM of plates with different hole shapes were also generated as shown in **Fig 2.3**. New approximate relations for the shear buckling coefficient (k_v) for square slender plates with central circular and square holes have been also proposed by C.H. Pham [11] as follows:

- For square plates with circular openings:

When $\frac{d}{a} \le 0.2$: $$k_v = k_0\left[1-0.5\left(\frac{d}{a}\right)-4.2\left(\frac{d}{a}\right)^2\right] \quad (2.7a)$$

When $0.2 < \frac{d}{a} < 0.6$: $$k_v = k_0\left[1.15-2.3\left(\frac{d}{a}\right)+1.3\left(\frac{d}{a}\right)^2\right] \quad (2.7b)$$

When $0.6 \le \frac{d}{a}$: $$k_v = k_0\left[0.6-0.6\left(\frac{d}{a}\right)\right] \quad (2.7c)$$

- For square plates with square openings:

When $\frac{d}{a} \le 0.2$: $$k_v = k_0\left[1-0.8\left(\frac{d}{a}\right)-4.5\left(\frac{d}{a}\right)^2\right] \quad (2.8a)$$

When $0.2 < \frac{d}{a} < 0.6$: $$k_v = k_0\left[1.15-2.9\left(\frac{d}{a}\right)+2.1\left(\frac{d}{a}\right)^2\right] \quad (2.8b)$$

When $0.6 \le \frac{d}{a}$: $$k_v = k_0\left[0.4-0.4\left(\frac{d}{a}\right)\right] \quad (2.8c)$$

2.3 SHEAR ELASTIC BUCKLING OF UNPERFORATED COLD-FORMED CHANNEL MEMBERS

A cold-formed channel section is commonly composed of three components including web, flanges and lips. A study of the shear buckling of thin-walled channel sections with and without lips was carried out by Pham & Hancock [6] using the Spline Finite Strip Method (SFSM) to investigate the effect of flanges and lips on the shear elastic buckling capacity and buckling modes. This study was performed with different variables in flange width, boundary conditions and shear stress distribution as shown in **Fig 2.4**.The critical buckling stresses of both lipped and unlipped channel sections in shear are calculated by ***Eq (2.1)*** where k_0 is replaced by the shear buckling coefficient for the whole section and h is presumed as the depth of flat portion of the web.

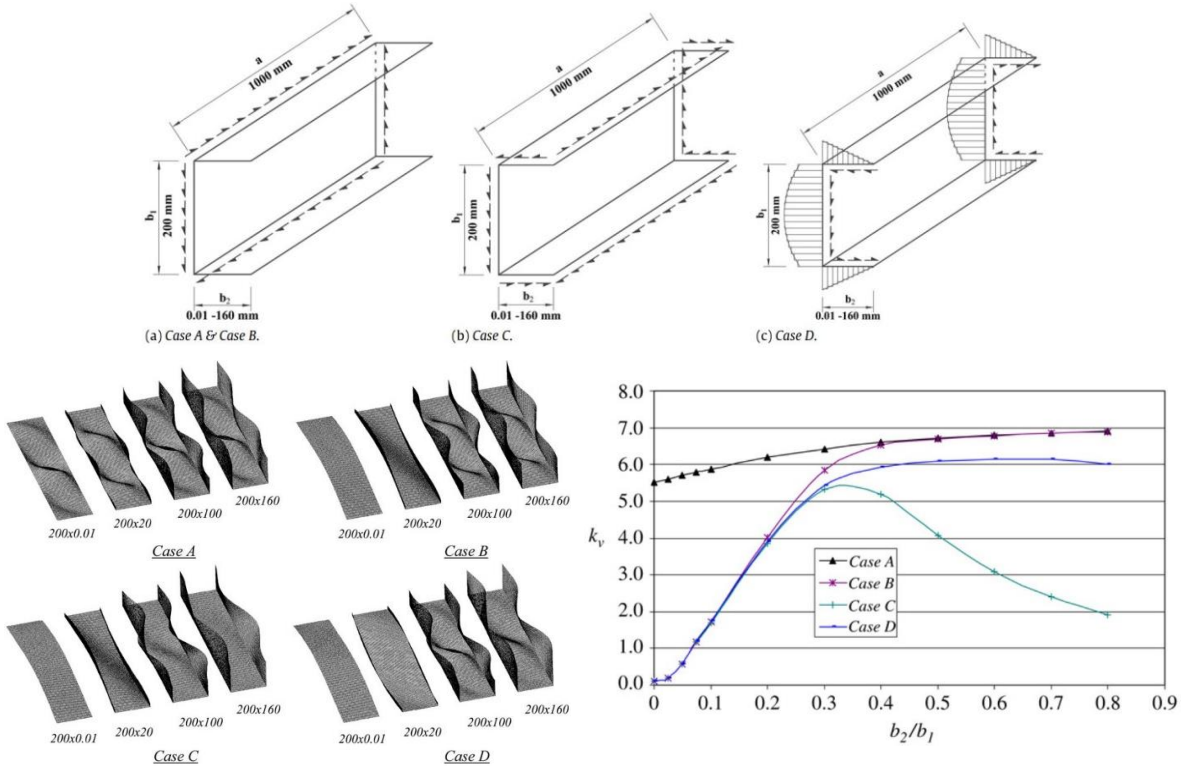

(a) With unlipped channels of b_1/a = 0.2

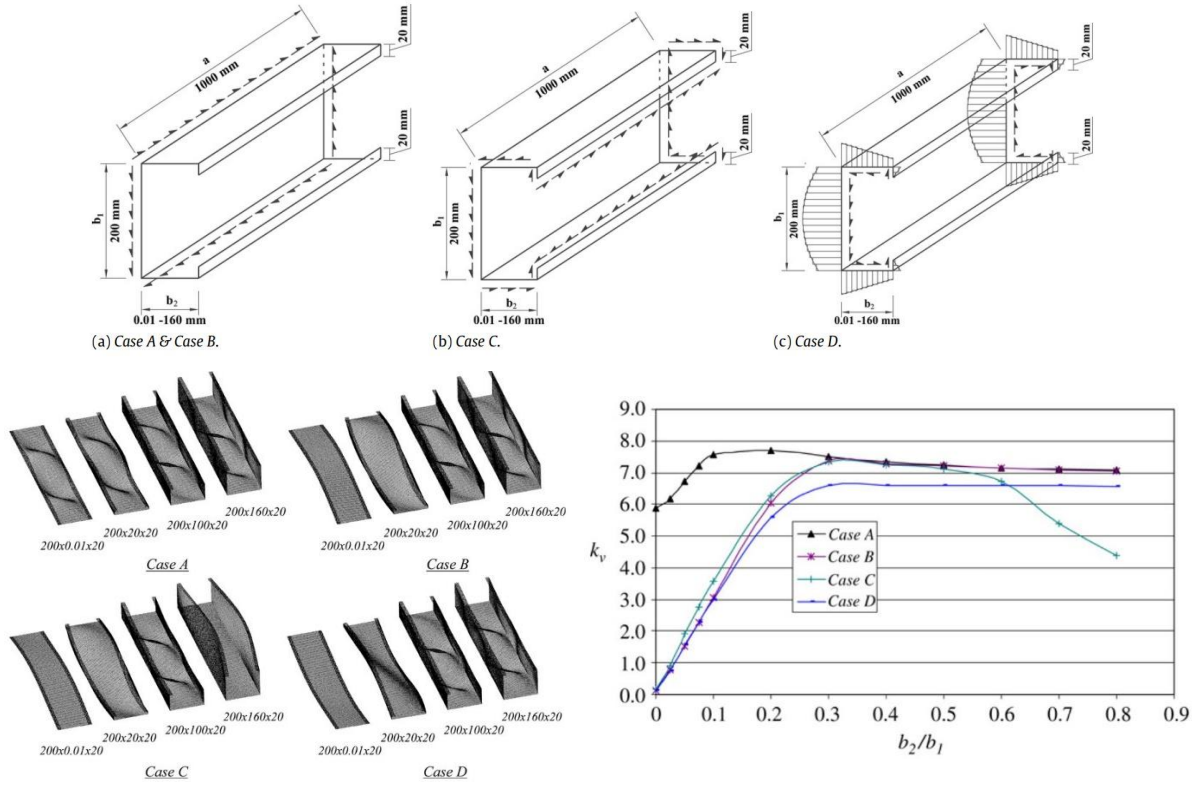

(b) With lipped channels

Fig 2.4: Shear flow distributions, shear buckling modes and shear buckling coefficients (Pham & Hancock [6])

Detailed explanations of shear buckling behaviours of channel sections with and without lips including the buckling mode shapes, the changes in the value of the shear buckling coefficient, the significant improvement in shear buckling capacity due to the presence of flanges and lips were also provided in Pham & Hancock [6]. The cases for the ratio of web depth to shear span (b_1/a) of 1.0 were also considered in this study.

Solutions to the elastic buckling of simply supported channel sections including flanges and lips in pure shear with the stress distribution as in Case D were provided by Pham & Hancock [35]. The elastic buckling loads (V_{cr}) were computed from the use of the SFSM. The shear buckling coefficients (k_v) were then back calculated from the shear buckling capacities and were plotted in the format of interaction charts. Designers can look up the charts derived from the shear buckling analyses using the SFSM to determine directly the shear buckling coefficients (k_v) without using the SFSM software. The charts of (k_v) for design are shown in **Fig 2.5** with a wide range of channel dimensions. Unlipped channel sections are supposed to be lipped members with a very small lip size of 0.01 mm.

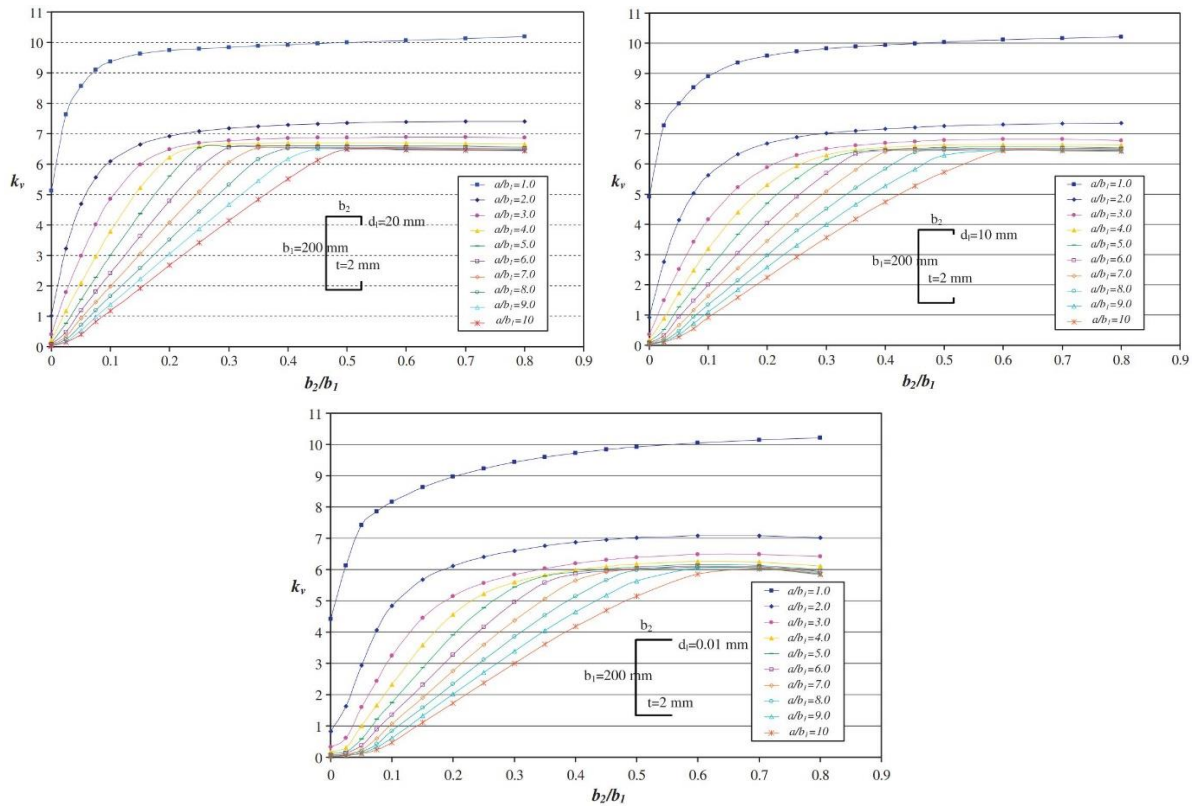

Fig 2.5: Interaction charts for elastic shear buckling coefficients (Pham & Hancock [35])

In addition, Keerthan & Mahendran [36] realised that the restraint level at the web-flange juncture is about 23 % fixity level (i.e. fixed condition between flange and web). A proposal for the determination of the elastic shear buckling coefficients of lipped channel beams (LCBs) were formulated as follows:

When $\frac{b_f}{d_1} \geq 0.3$: $$k_{LCB} = k_{ss} + 0.23(k_{sf} - k_{ss}) \quad (2.9a)$$

When $\frac{b_f}{d_1} \leq 0.3$: $$k_{LCB} = k_{ss} \quad (2.9b)$$

With $\frac{a}{d_1} \geq 1$: $$\begin{cases} k_{ss} = 5.34 + \dfrac{4}{(a/d_1)^2} \\ k_{sf} = 8.98 + \dfrac{5.61}{(a/d_1)^2} - \dfrac{1.99}{(a/d_1)^3} \end{cases} \quad (2.9c)$$

With $\frac{a}{d_1} < 1$: $$\begin{cases} k_{ss} = 4 + \dfrac{5.34}{(a/d_1)^2} \\ k_{sf} = \dfrac{5.34}{(a/d_1)^2} + \dfrac{2.31}{(a/d_1)} - 3.44 + 8.39\left(\dfrac{a}{d_1}\right) \end{cases} \quad (2.9d)$$

where k_{LCB} is the shear buckling coefficient of lipped channel beams; k_{ss} and k_{sf} are the buckling coefficients associated with simple-simple and simple-fixed boundary conditions respectively; b_f is the flange width; d_1 is the clear web height; a is the shear span of the web.

2.4 SHEAR ELASTIC BUCKLING OF PERFORATED COLD-FORMED CHANNEL MEMBERS

On the basis of a good agreement between the Spline Finite Strip Method (SFSM) and the Finite Element Method (FEM) using ABAQUS/Standard in shear elastic buckling analyses of cold-formed channels with holes, C.H. Pham [11] developed FE models including square and circular holes in the web element to determine the critical buckling loads of channels in shear with an aspect ratio of 1.0 (span length / web depth). The shear buckling coefficient (k_v) of perforated channels in this study were also back calculated with the same method as used by Pham & Hancock [35]. It is worth noting that the effect of bending moments balancing with two coupling shear forces at two ends of channels with web openings in practice have been investigated in Case B and C as shown in **Fig 2.6**. The uniform shear stress acting throughout the web panel edges was also studied in Case A.

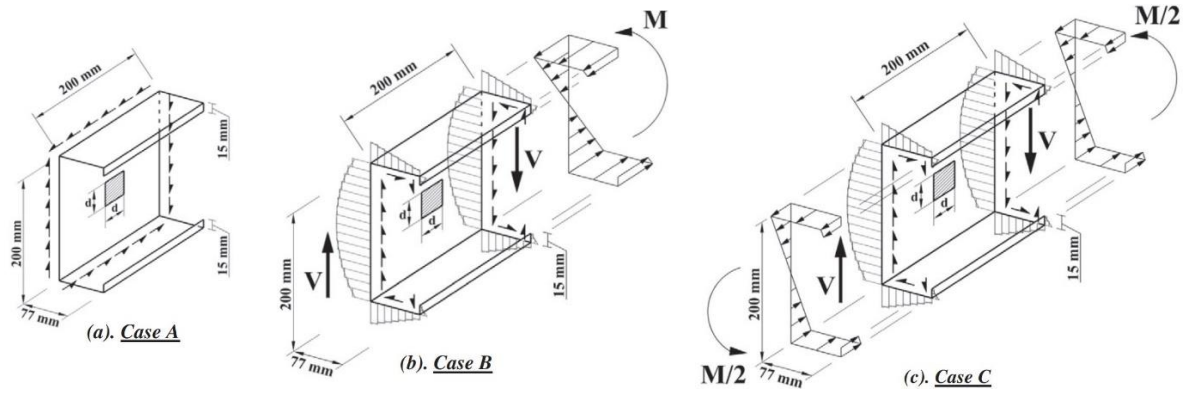

Fig 2.6: Stress distribution of lipped channel with central square hole (C.H. Pham [11])

Fig 2.7 shows the shear buckling modes of channel sections with a central square web hole by C.H. Pham [11]. The buckling mode shape for Case C where a pair of bending moments with half value ($M/2 = V.a/2$, a is the member length) acting at both end sections in the same direction is symmetrical about the diagonal axis across the web. When a bending moment applied at one end to balance with two couple shear force in Case B, the buckling pattern concentrated at one corner of the web hole. A design proposal by C.H. Pham [11] for the determination of shear buckling coefficients of channels with central circular and square web openings was also formulated based on a generated database of (k_v) as follows:

- For channel sections with circular holes:

When $\frac{d}{a} \le 0.2$: $$k_v = k_0\left[1-0.5\left(\frac{d}{a}\right)-4.2\left(\frac{d}{a}\right)^2\right] \quad (2.10a)$$

When $0.2 < \frac{d}{a} < 0.6$: $$k_v = k_0\left[1.15-2.35\left(\frac{d}{a}\right)+1.5\left(\frac{d}{a}\right)^2\right] \quad (2.10b)$$

When $0.6 \le \frac{d}{a}$: $$k_v = k_0\left[0.6-0.53\left(\frac{d}{a}\right)\right] \quad (2.10c)$$

- For channel sections with square holes:

When $\frac{d}{a} \le 0.2$: $$k_v = k_0\left[1-0.8\left(\frac{d}{a}\right)-4.5\left(\frac{d}{a}\right)^2\right] \quad (2.11a)$$

When $0.2 < \frac{d}{a} < 0.6$: $$k_v = k_0\left[1.15-2.95\left(\frac{d}{a}\right)+2.2\left(\frac{d}{a}\right)^2\right] \quad (2.11b)$$

When $0.6 \le \frac{d}{a}$: $$k_v = k_0\left[0.4-0.33\left(\frac{d}{a}\right)\right] \quad (2.11c)$$

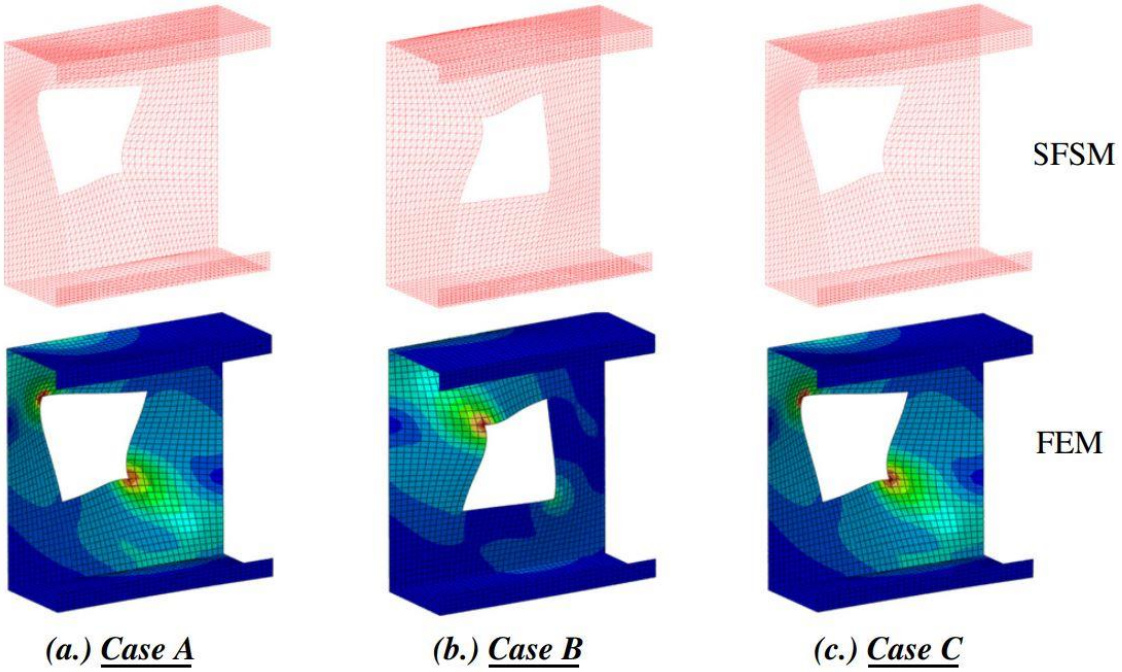

Fig 2.7: Buckling mode shapes of lipped channel with a central square web hole using SFSM and FEM (C.H. Pham [11])

For perforated channel members in shear with higher aspect ratios, S.H. Pham et al. [37] suggested an approximate equation for shear buckling coefficient (k_v) for the cases of central web openings using the artificial neutral network model (ANN) as:

$$k_v = 5.39\frac{h}{a} - 3.33\frac{d_h}{h} - 17.7\frac{L_h}{a} + 11.9\frac{A_0}{A} + 5.27 \qquad (2.12)$$

where a is the length of the shear span; h is the flat web depth; L_h is the width of web opening; d_h is the depth of web opening; A_0 is the area of web hole; A is the area of the flat web surface excluding web hole. However, in order to take account of the effect of the flange width, a larger database of results from seven hundred and sixty-eight FE models were analysed by S.H. Pham [38] using the same methodology (ANN) to generate a new approximate formula including a term of b_f (flange width) as follows:

$$k_v = 6.15\frac{h}{a} - 3.63\frac{d_h}{h} - 19.58\frac{L_h}{a} + 13.88\frac{A_0}{A} + 0.57\frac{b_f}{h} + 4.86 \qquad (2.13)$$

Further, S.H. Pham et al. [16] proposed a linear relationship $d = 0.825\ D$ to transform a circular hole size into an equivalent square hole where d is the square hole size, and D is the circle diameter. This dimensional transformation has been also used for cases of an aspect ratio up to 2.0 by S.H. Pham [38].

2.5 SHEAR STRENGTH OF UNPERFORATED COLD-FORMED CHANNEL MEMBERS

In a highly slender member, the stress redistribution in the web occurs after the member buckles in shear allowing the development of a diagonal tension band across the web termed as Tension Field Action (TFA). The Tension Field Action within a stiffened shear panel is shown in **Fig 2.8** where diagonal principal stresses are distributed along a diagonal band. Further, the formation of the TFA is controlled by the flanges and transverse stiffeners surrounding the shear panel. Throughout historic investigations of Tension Field Action, there were several different models developed to predict the shear strength of plate girders including Basler [39], Hoglund [40], Marsh [41], Höglund [42] and Davies et al. [43]. Remarkably, the simplified model established by Höglund [42] and the shear model developed by Basler [39] were acceptable to determine shear strengths of I-shaped members and channels including and excluding Tension Field Action (TFA) as specified in sections G2.1 and G2.2 in the American Specification for Structural Steel Buildings AISC 360-16 (ANSI [44]).

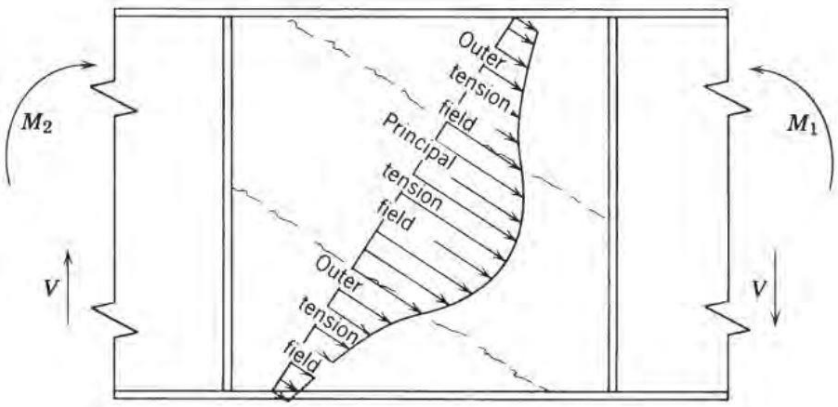

Fig 2.8: Tension field action (Ziemian [45])

For cold-formed steel structures, both the North American specification AISI S100-16 [4] and the Australian Standard AS/NZS 4600:2018 [5] provide two different methods to predict the shear strength of the web for both unstiffened and stiffened web panels. For members without transverse stiffener, either elastic shear buckling, inelastic shear buckling or shear yielding governs the shear capacity of unperforated webs. The failure modes of unperforated members depend on the web slenderness, geometrical properties of sections and boundary conditions. For members with thick webs (low slenderness), shear strength can be determined based on shear yielding in the web as per the following equation:

$$V_y = 0.6 f_y A_w \tag{2.14}$$

where A_w is the flat web area; f_y is the design yield stress. For webs with high slenderness where elastic shear buckling governs the member strength, shear strength is determined as the shear buckling load as:

$$V_n = V_{cr} = \tau_{cr} A_w \tag{2.15}$$

where τ_{cr} is calculated as per ***Eq.(2.1)***. For webs with moderate slenderness. The members are likely to fail by inelastic shear buckling. Basler [39] provided a formula to predict the shear strength in inelastic and strain hardening ranges ($\tau_{cr\ (inelastic)}$) as follows:

$$\tau_{cr(inelastic)} = \sqrt{\tau_{pr}\tau_{cr(elastic)}} \tag{2.16a}$$

$$\tau_{pr} = 0.8(f_y / \sqrt{3}) \tag{2.16b}$$

where $\tau_{cr(inelastic)}$ is the inelastic shear buckling stress; τ_{pr} is the proportional limit in shear; $\tau_{cr(elastic)}$ is the initial elastic shear buckling stress. The shear strength of webs in the inelastic range can be determined by substituting the values of $\tau_{cr(elastic)} = \tau_{cr}$ as:

$$V_n = \tau_{cr(inelastic)} A_w = \sqrt{\tau_{pr}\tau_{cr(elastic)}} A_w = 0.64 t^2 \sqrt{k_v f_y E} \tag{2.17}$$

A provision based on the Direct Strength Method for design for unperforated channels without holes in web and without web stiffeners excluding Tension Field Action (TFA) have been incorporated in AISI S100-16 [4] and AS/NZS 4600:2018 [5] as follows:

For $\lambda_v \le 0.815$: $V_n = V_y$ (2.18a)

For $0.815 < \lambda_v \le 1.227$: $V_n = 0.815 \sqrt{V_{cr} . V_y}$ (2.18b)

For $\lambda_v > 1.227$: $V_n = V_{cr}$ (2.18c)

The nondimensional slenderness (λ_v), the yield shear load (V_y) of the web based on an average shear yield stress of 0.6 f_y, and the elastic shear buckling load of the whole section (V_{cr}) are computed respectively as follows:

$$\lambda_v = \sqrt{V_y / V_{cr}} \tag{2.19}$$

$$V_y = 0.6 A_w f_y \tag{2.20}$$

$$V_{cr} = \frac{k_v \pi^2 E A_w}{12(1-\mu^2)\left(\frac{h}{t}\right)^2} \tag{2.21}$$

For unperforated members with transverse stiffeners (stiffened panels), the shear strength might be increased as a result of the Tension Field Action (TFA). The nominal shear strength (V_n) of unperforated channels on web including Tension Field Action (TFA) is specified in Section G2.2 in AISI S100-16 [4] as follows:

For $\lambda_v \leq 0.776$: $$V_n = V_y \quad (2.22a)$$

For $\lambda_v > 0.776$: $$V_n = \left[1 - 0.15\left(\frac{V_{cr}}{V_y}\right)^{0.4}\right]\left(\frac{V_{cr}}{V_y}\right)^{0.4} V_y \quad (2.22b)$$

This DSM equations for shear were developed by Pham & Hancock [7] based on shear test results using a central point load test rig with an aspect ratio of 1.0. Further, the DSM for design for channels in shear including the TFA have been also validated with the shear tests using the Basler test rig and the dual actuator test rig by S.H. Pham et al. [46] and S.H. Pham et al. [27] respectively with aspect ratios up to 2.0.

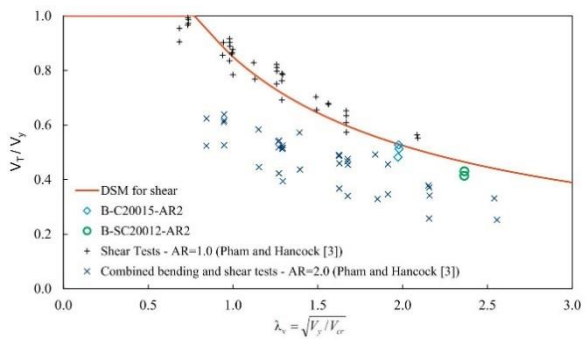

Fig 2.9: Test results with the Basler test rig plotted against the DSM shear curve (S.H. Pham et al. [46])

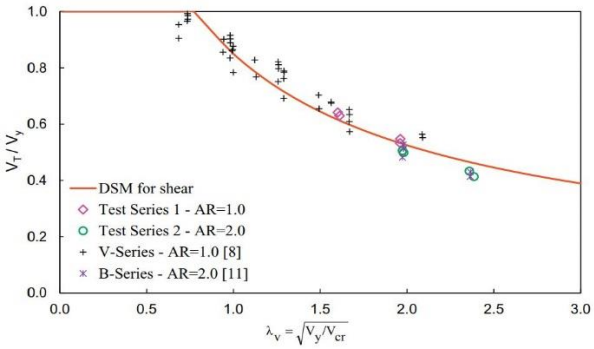

Fig 2.10: Test results with the dual actuator test rig plotted against the DSM shear curve (S.H. Pham et al. [27])

Fig 2.9 shows a comparison of DSM design loads for shear with shear test results of channel sections and SupaCee sections using the Basler test rig developed by S.H. Pham et al. [46]. It was found that the results from combined bending and shear tests with an aspect ratio of 2.0 by Pham & Hancock [47] lie below the DSM curve for shear due to the effect of bending when using the central point load test with a high shear span (AR = 2.0). The predominantly shear test results of plain lipped channel sections and SupaCee sections using the dual actuator test rig developed by S.H. Pham et al. [48] are plotted in **Fig 2.10** against the current DSM design curve with the TFA. All the resulting points from the shear tests by Pham & Hancock

[47] using the central point load test with *AR* = 1.0, from the shear tests using the Basler test rig by S.H. Pham et al. [46] with *AR* = 2.0, and from the pure shear tests using the dual actuator test rig by S.H. Pham et al. [48] with *AR* = 1.0 and 2.0 lie close to the DSM shear curve. This demonstrates that the DSM shear curve with TFA is also applicable to unperforated channel sections with aspect ratios up to 2.0.

2.6 SHEAR STRENGTH OF PERFORATED COLD-FORMED CHANNEL MEMBERS

In order to allow access for all service systems in practice, high strength cold-formed steel members are likely to be manufactured with perforations in the web. This has resulted in a considerable number of studies into the effect of web cut-outs on channel sections in shear. Current AISI S100-16 [4] and AS/NZS 4600:2018 [5] Specification/Standard still adopt an empirical method based on studies by Shan et al. [23], Schuster et al. [24], Eiler et al. [25]. According to the approach methodology, the shear strength of a perforated member is calculated by multiplying the shear strength of an unperforated section by the reduction factor (q_s) based purely on experiments. The formulae for this approach are expressed in Section C3.2.1 of NAS S100-2016 as follows:

When $c/t \geq 54$: $$q_s = 1 \quad (2.23a)$$

When $5 \leq c/t < 54$: $$q_s = \frac{c}{54t} \quad (2.23b)$$

For circular holes: $$c = \frac{h}{2} - \frac{d}{2.28} \quad (2.24a)$$

For non-circular holes: $$c = \frac{h}{2} - \frac{d}{2} \quad (2.24b)$$

where h is the depth of flat portion of the web; t is the web thickness; d is the hole depth. Despite the computational convenience compared to the DSM approach which requires two inputs (V_{cr} and V_y), it was proven by Keerthan & Mahendran [22, 26] that the empirical method for determination of shear strength of members with holes is conservative with small cut-outs, but unconservative with substantially large openings. Further, there is a restricted applicability for the empirical method due to limited number of tests and range. By using the central point load tests, Keerthan & Mahendran [22] carried out a shear test program at the Queensland University of Technology (QUT) on lipped channel sections with aspect ratios of 1.0 and 1.5 with various sizes of circular web holes and a wide range of web depths including 120, 160,

200 mm. By fitting the results generated from the shear tests, Keerthan & Mahendran [22] established two design options for the shear capacity (V_{nl}) of lipped channel beams (LCBs) with web openings. The more accurate equations were formulated as follows:

When $\frac{d_{wh}}{d_1} \le 0.85$: $$V_{nl} = q_s V_v \quad (2.25)$$

For $0 < \frac{d_{wh}}{d_1} \le 0.3$: $$q_s = 1 - 0.6\left(\frac{d_{wh}}{d_1}\right) \quad (2.26a)$$

For $0.3 < \frac{d_{wh}}{d_1} \le 0.7$: $$q_s = 1.215 - 1.316\left(\frac{d_{wh}}{d_1}\right) \quad (2.26b)$$

For $0.7 < \frac{d_{wh}}{d_1} \le 0.85$: $$q_s = 0.732 - 0.625\left(\frac{d_{wh}}{d_1}\right) \quad (2.26c)$$

where V_{nl} is the shear capacity of perforated LCBs; V_v is the shear capacity of LCBs without web openings; d_{wh} is the depth of web openings; d_1 is the clear height of web. The effect of flange straps on the shear capacity of the members was also considered by Keerthan & Mahendran [22]. Two graphs in **Fig 2.11** show the relationship between the shear capacity reduction factor (q_s) and the ratio d_{wh}/d_1 based on the proposal for design for LCBs with circular web openings.

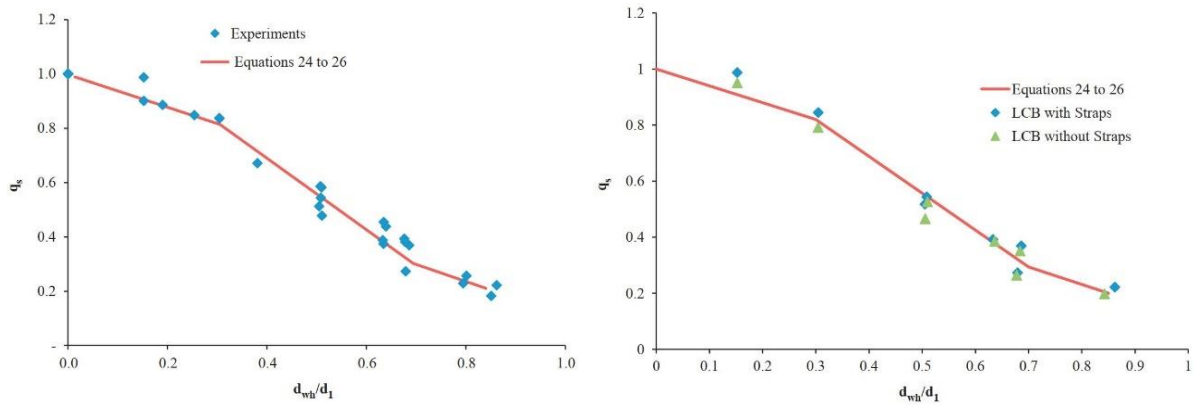

Fig 2.11: Shear capacity reduction factor (q_s) versus d_{wh}/d_1 for LCBs with web openings (Keerthan & Mahendran [22])

C.H. Pham et al. [21] and C.H. Pham et al. [15] performed experimental investigations of channel sections with web square holes at the University of Sydney (USYD) using the same central point test rig to observe the predominantly shear failure modes and the shear strength reduction when the sizes of web holes vary from 40 to 120 mm. Commercially available plain

channel members of 200 mm web depth with *AR* = 1.0 were employed with various thicknesses of 1.5, 1.9, and 2.4 mm in the USYD's studies. The shear test results from USYD and QUT together with the test results of the studies by Shan et al. [23], Schuster et al. [24] and Eiler et al. [25] were subsequently collected by S.H. Pham [38] to affirm a poor prediction of shear strengths of perforated channels using the empirical design method currently retained in AISI S100-16 [4] and AS/NZS 4600:2018 [5] as shown in **Fig 2.12**.

C.H. Pham et al. [15] proposed a DSM design equation for channel sections with square and circular holes where the conventional shear yield loads (V_y) is replaced by a shear yield load based on net web area referred to $V_{y,net}$ formulated as:

$$V_{y,net} = 0.6(h - d_h) f_y t \tag{2.27}$$

where h is the depth of the web plate, d_h is the depth of the hole, t is the thickness of the web, and f_y is the design yield stress. However, S.H. Pham et al. [16] demonstrated that the use of $V_{y.net}$ can be acceptable for relatively small perforations, but unconservative with large web holes as shown in **Fig 2.13**.

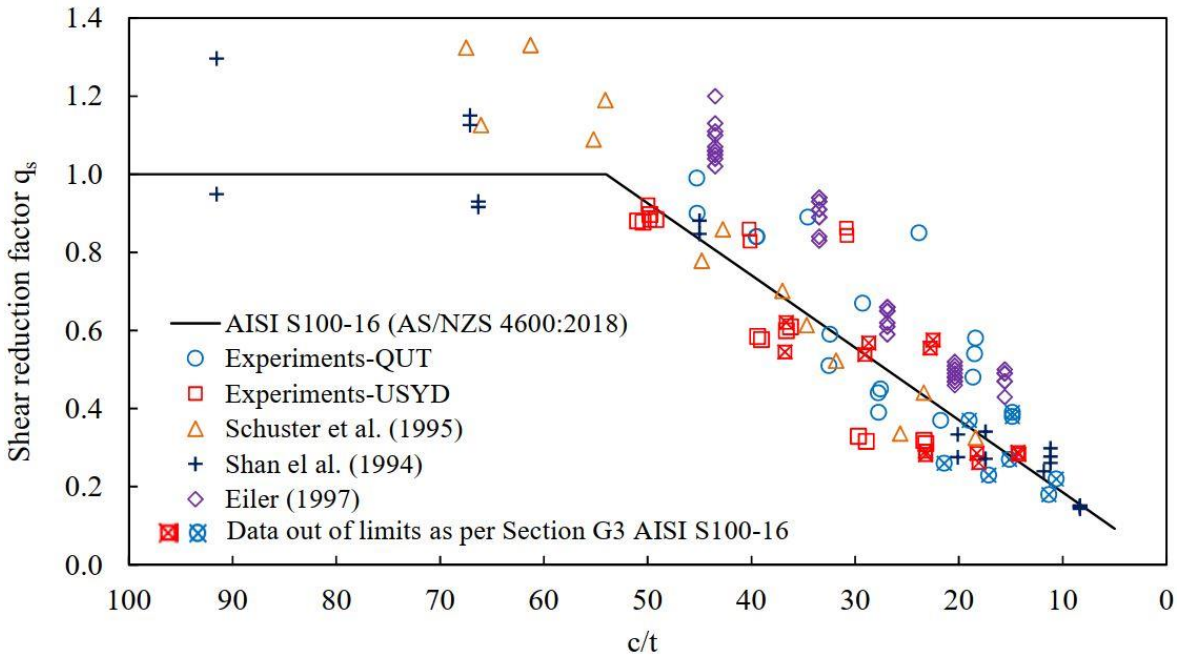

Fig 2.12: Shear reduction factor comparison between tests and current standards for perforated channels in shear (S.H. Pham [38])

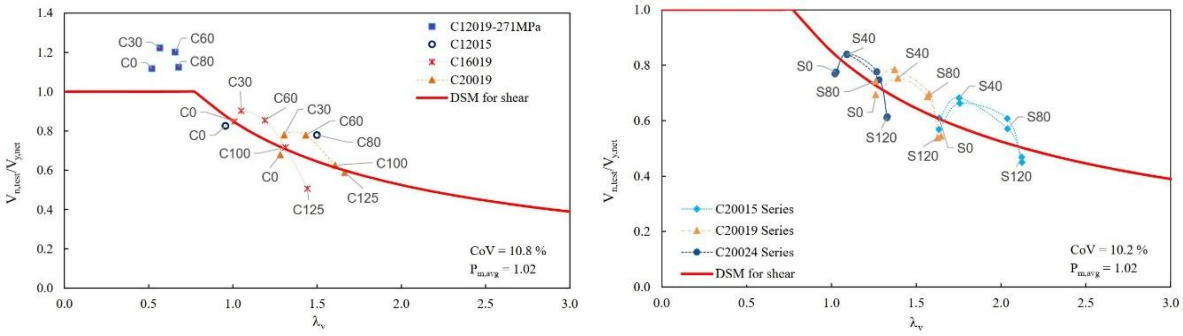

(a) Test database at QUT (Keerthan & Mahendran [22])

(b) Test database at USYD (C.H. Pham et al. [21] and C.H. Pham et al. [15])

Fig 2.13: Predominantly shear tests at QUT and USYD on channels with circular and square web openings with the use of $V_{y,net}$ (S.H. Pham et al. [16])

On the basis of the limited applicability of the suggestion by C.H. Pham et al. [15], S.H. Pham et al. [16] proposed a model based on the Vierendeel mechanism recognised by Chung et al. [49, 50] accounting for both local and global actions around the web openings when the members are subjected to high shear. Based on the proposal by S.H. Pham et al. [16], the values of shear yield loads of perforated channels are calculated as:

$$\text{when } 0 < \frac{d_h}{h} \le 0.10, \qquad V_{yh} = V_y \tag{2.28a}$$

$$\text{when } 0.10 < \frac{d_h}{h} < 0.60, \qquad V_{yh} = V_y - 2\left(\frac{d_h}{h} - 0.1\right)\left(V_y - V_{vrd,0.6}\right) \tag{2.28b}$$

$$\text{when } 0.60 \le \frac{d_h}{h}, \qquad V_{yh} = V_{vrd} \tag{2.28c}$$

where d_h is the depth of the hole, h is the depth of the web plate. The shear load (V_{vrd}) of perforated sections with substantially large openings based on the Vierendeel mechanism is computed by:

$$V_{vrd} = \frac{4M_{pv}}{L_h} \tag{2.29}$$

where M_{pv} is the plastic bending capacity of the top (or bottom) segment above (or below) the opening, including the flanges and lips. The hole is centrally located, and L_h is the length of the hole. $V_{vrd,0.6}$ is the value of V_{vrd} computed for the perforated section with the ratio d_h/h = 0.6. The proposal using the Vierendeel model has been also recently recommended by S.H. Pham [38] for channels with circular and square web holes with shear aspect ratios up to 2.0 based on a good validation as shown in **Fig 2.14**.

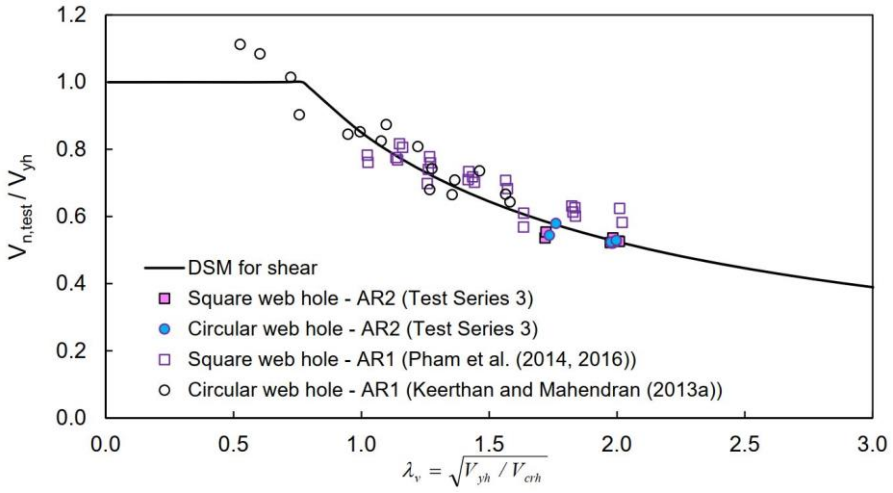

Fig 2.14: Shear test results on perforated beams with aspect ratios of 1.0 and 2.0 plotted against the DSM curve (S.H. Pham [38])

2.7 TEST RIG DESIGNS FOR SHEAR TESTS OF UNPERFORATED MEMBERS

With the aim of minimising the effect of bending moments, Basler et al. [51] performed a test program on welded plate girders using a test configuration as shown in **Fig 2.15**. The girder was simply supported at a quarter and three-quarter points on its length. The loads were transferred in opposite directions at cantilever ends of the girders. The top and bottom flanges were strengthened at two supported positions with cover plates to develop resistance to high bending. Transverse web stiffeners were welded to the girder at two ends of the test specimen where the shear failure was expected to occur. According to the schematic force diagrams in **Fig 2.15**. The shear panels formed by the transverse stiffeners was subjected to a constant shear force resulting from a small bending moment gradient and a pair of equal and opposite sign bending moments at two ends of the shear span was produced. Aspect ratios (*AR*) of 0.5, 0.75, 1.0 and 1.75 were chosen for this experimental program.

For the same purpose of capturing the shear behaviour of the members, LaBoube & Yu [52] developed a simply supported central load test rig with the aspect ratio of 1.0 as shown in **Fig 2.16a**. By using a short shear span, the member was governed by high shear action rather than bending. In order to observe the shear failure on members with a larger aspect ratio (*AR* = 3.23), LaBoube & Yu [52] used another test design similar to the test configuration

previously developed by Basler et al. [51] as shown in **Fig 2.16b**. The loads were transferred via a simply supported long beam at the top of the structure.

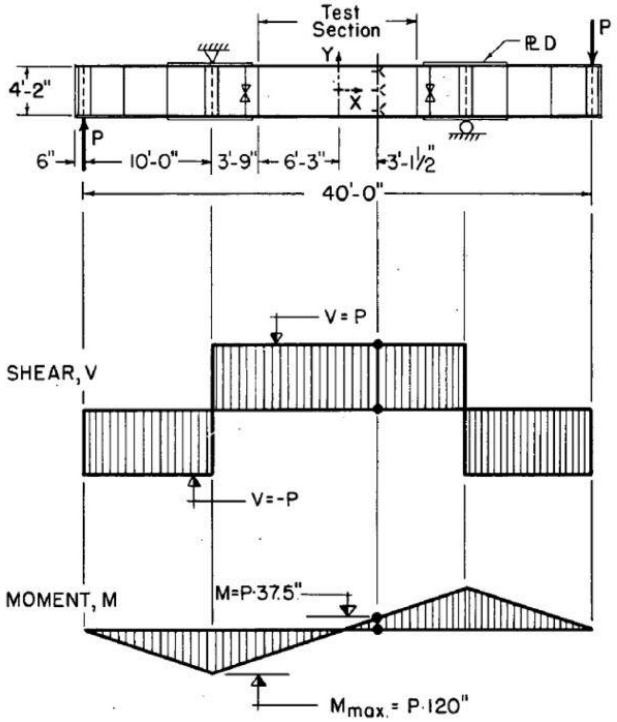

Fig 2.15: Test configuration on welded plate girders under a pure shear (Basler et al. [51])

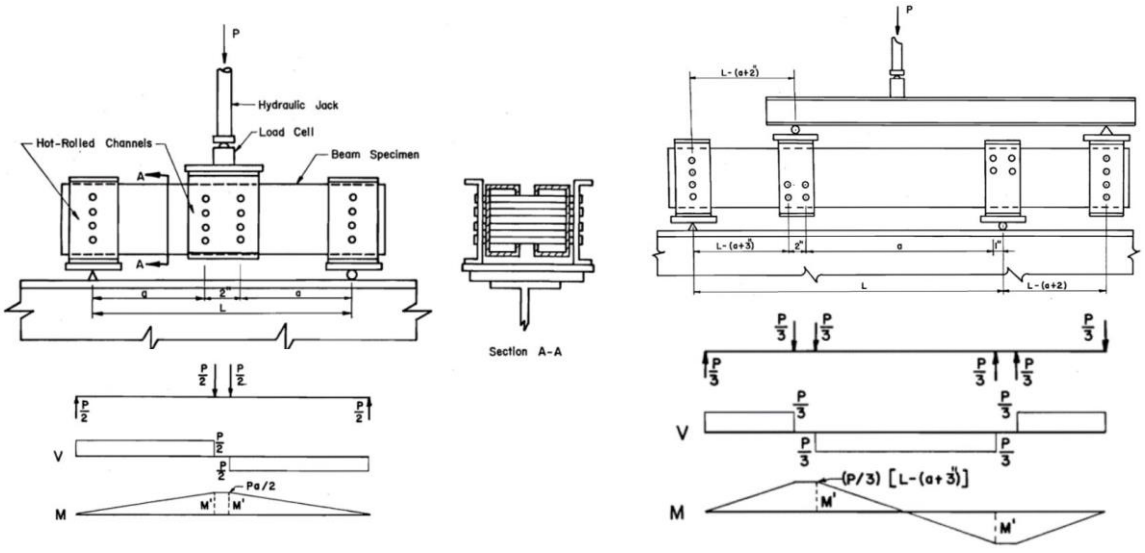

(a) Test configuration of simply supported central load test rig

(b) Test configuration for larger shear aspect ratio

Fig 2.16: Test configurations by LaBoube & Yu [52]

Based on the basic design of the test configuration early developed by LaBoube & Yu [52], an experimental program was performed by Pham & Hancock [47] using a central point load test configuration as shown in **Fig 2.17** to determine the ultimate shear strengths of cold-formed channel sections subjected to predominantly shear with an aspect ratio of 1.0. This test configuration was also further employed to investigate the combined shear and bending interaction of members with an aspect ratio up to 2.0. The tests were performed on two different commercially available lipped channel sections with the depths of 150 and 200 mm and various thicknesses of 1.5, 1.9 and 2.4 mm. The effect of straps on the failure modes and the ultimate strengths were also included. Because of the use of five bolt rows over the full depth of the sections for the development of the full tension field action, higher shear strengths were obtained by Pham & Hancock [47] as compared to those by LaBoube & Yu [52] on the same test setups.

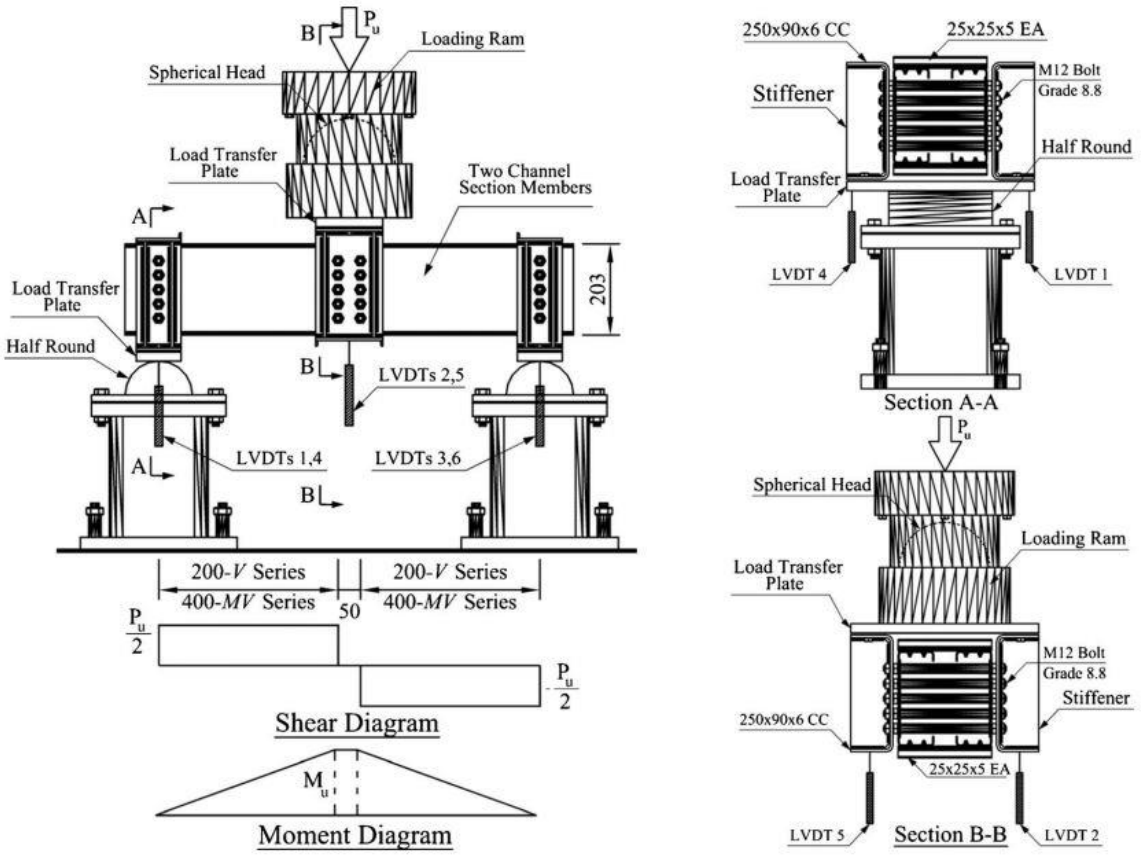

Fig 2.17: Test configuration of simply supported central load test by Pham & Hancock [47]

(a) Failure mode of predominantly shear test (*AR* = 1.0)

(b) Failure mode of combined shear and bending test (*AR* = 2.0)

Fig 2.18: Failure modes shapes of tests by Pham & Hancock [47]

As can be seen in **Fig 2.18** showing the failure mode shapes of channels under pure shear and combined bending and shear by Pham & Hancock [47], it is very clear that the ratio of moment and shear (*M/V*) governs the failure mode of the structure. Specifically, due to small bending, the shear failure was observed very clearly when *AR* = 1.0 (*M/V* = *L* = *b* where *L* and *b* are the shear span and the whole depth of the beam respectively) as shown in **Fig 2.18a**. When the aspect ratio (*AR*) is up to 2.0, bending governed the failure mode of the beam resulting from an increase in the ratio *M/V* which is up to *2b*.

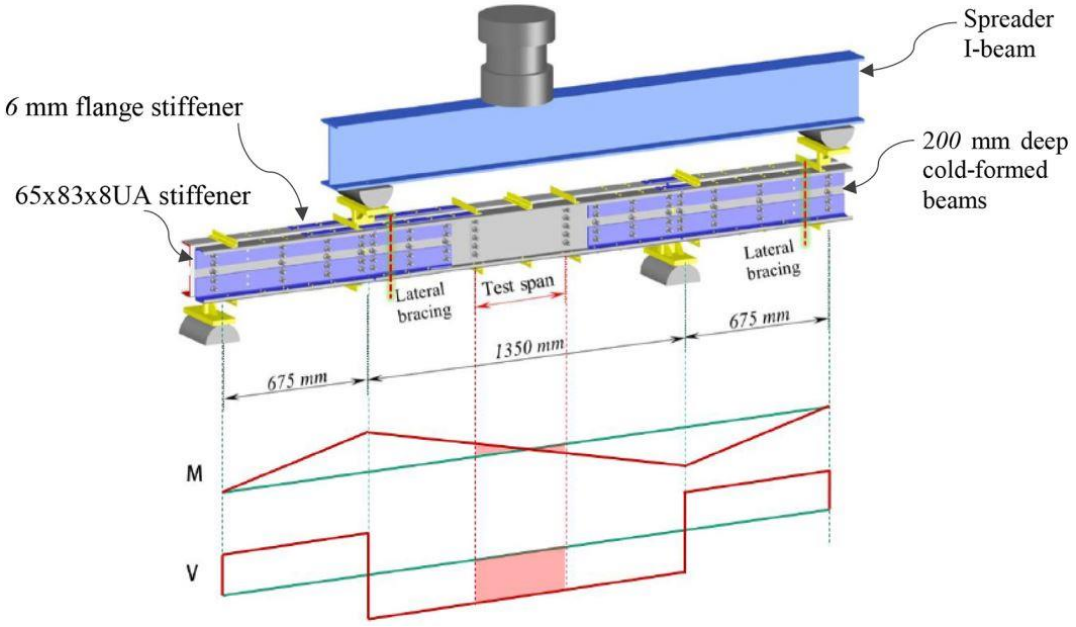

Fig 2.19: Basler test rig set-up by S.H. Pham et al. [46]

In order to study the shear behaviour of cold-formed steel members with greater aspect ratios than 1.0, two new experimental configurations with minimal bending moments namely 'Basler Test Rig' and 'Dual Actuator Test Rig' with aspect ratios up to 2.0 were developed and validated by S.H. Pham et al. [46] and S.H. Pham et al. [27] respectively. As can be seen in **Fig 2.19**, the first new test set-up (Basler Test Rig), which was inspired by the early tests on plate girders in shear by Basler et al. [51], was able to capture a state close to pure shear by producing a pair of equal and opposite sign moments at two ends of the test span. Therefore, the ratio *M/V* generated by Basler Test Rig was only a half of that obtained from the conventional central point load tests of the same aspect ratio (*AR*). With the same approach, a pair of equal and opposite sign moments at two ends of shear span was also generated using the second new test rig (Dual Actuator Test Rig). During the tests using the dual actuator test rig, the desired ratio (M_B/M_C) of -1.0 where M_B and M_C are the applied moments at two ends of the shear span were controlled by adjusting the movement rates of two independent actuators as shown in **Fig 2.20**.

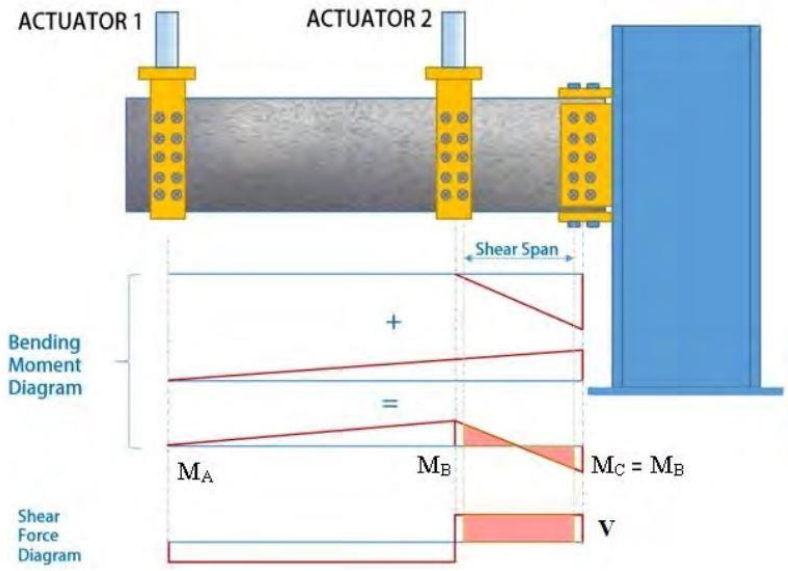

Fig 2.20: Dual actuator test rig set-up by S.H. Pham et al. [27]

As can be seen in **Fig 2.21**, both new test configurations using the Basler test rig and the dual actuator test rig with a shear aspect ratio of 2.0 produced similar shear failure modes on both plain channel and SupaCee sections. These failure modes are also identical to an idealised pure shear failure obtained from earlier test programs on channel members in shear.

(a) Shear failure mode of a plain channel section using Basler Test Rig

(b) Shear failure mode of a SupaCee section using Basler Test Rig

(c) Shear failure mode of a plain channel section using Dual Actuator Test Rig

(d) Shear failure mode of a SupaCee section using Dual Actuator Test Rig

Fig 2.21: Shear failure mode of channel members using Basler Test Rig and Dual Actuator Test Rig with a shear aspect ratio of 2.0 by S.H. Pham et al. [46] and S.H. Pham et al. [27]

2.8 TEST RIG DESIGNS FOR SHEAR TESTS OF PERFORATED MEMBERS

In order to investigate the shear behaviour of channel members with web openings. Shan et al. [23] carried out a total of 26 shear tests on perforated beams with slotted holes using a central point load test configuration as shown in **Fig 2.22a**. Further, Eiler et al. [25] also conducted a test program of 85 tests on beams with non-elongated and elongated openings subjected to linearly varying shear as shown in **Fig 2.22b.** Based on the results from these test programs, a set of formulae were proposed to determine the shear strength reduction factor (q_s) as specified in C3.2.1 of the NAS S100-2016.

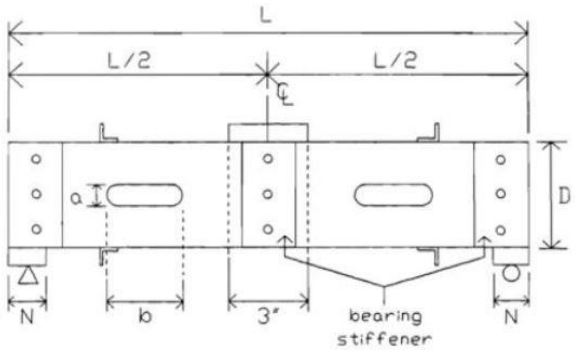

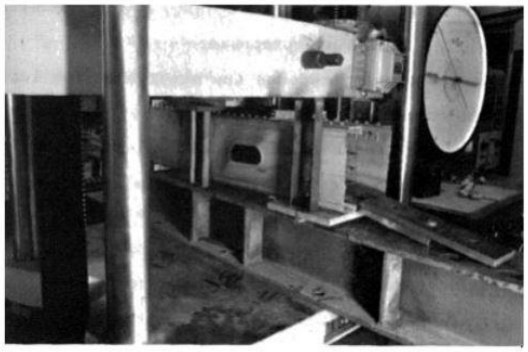

(a) Test program using central point load tests by Shan et al. [23]

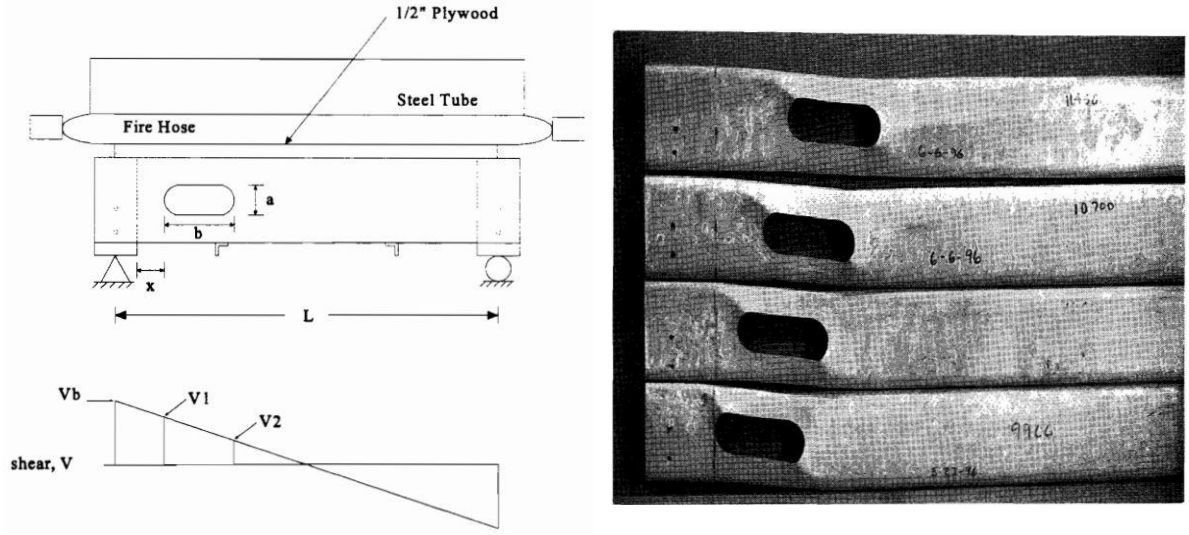

(b) Test program with openings subjected to linearly varying shear by Eiler et al. [25]

Fig 2.22: Shear test setups and shear failure modes by Shan et al. [23] and Eiler et al. [25]

The central point load test setup was also further used by Keerthan & Mahendran [53], Keerthan & Mahendran [22], C.H. Pham et al. [21] and C.H. Pham et al. [15] as shown in **Figs 2.23** and **2.24** to investigate the shear behaviour of perforated LiteSteel beams with and without stiffeners, and of plain lipped channel sections with circular and square web holes. While a new suggestion which is in line with the empirical method (i.e. the shear strength is determined based on reduction factor q_s) was proposed by Keerthan & Mahendran [53] and Keerthan & Mahendran [22], the test results by C.H. Pham et al. [21] and C.H. Pham et al. [15] were plotted against the current Direct Strength Method (DSM) design curves to evaluate the applicability of this design philosophy to the presence of web openings.

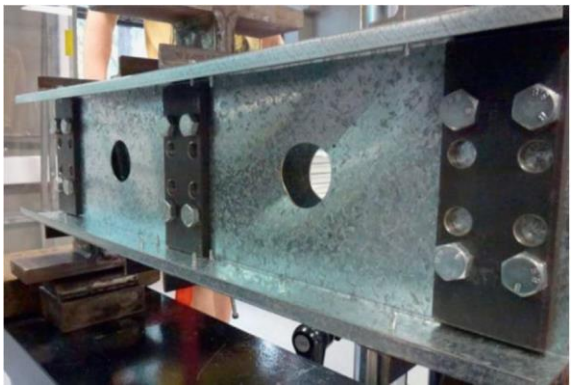

Fig 2.23: Shear failure mode with circular web holes by Keerthan & Mahendran [22]

Fig 2.24: Shear failure mode with square web holes by C.H. Pham et al. [21]

On the basis of the fast and simple test preparation and assembly compared to Basler Test Rig, a dual actuator test rig was further employed by S.H. Pham [38] to investigate the shear behaviour of perforated channel sections with an aspect ratio up to 2.0. A test series of 12 shear tests with circular and square central web holes was conducted. Even though the shear aspect ratio was up to 2.0 in the shear tests using the dual actuator test rig, the failure modes as can be seen in **Fig 2.25** were similar to the shear failure modes observed from early studies with AR = 1.0 by Keerthan & Mahendran [22] and C.H. Pham et al. [21] where diagonal shear bands across the web portion of the shear span were formed from two corners of the holes to two corners of the shear span. Further, on the basis of experimental results, the applicability of the current DSM curve in shear and the shear yield loads (V_{yh}) based on the Vierendeel mechanism for perforated channel sections with non-elongated web holes with shear aspect ratios up to 2.0 has been proven by S.H. Pham [38].

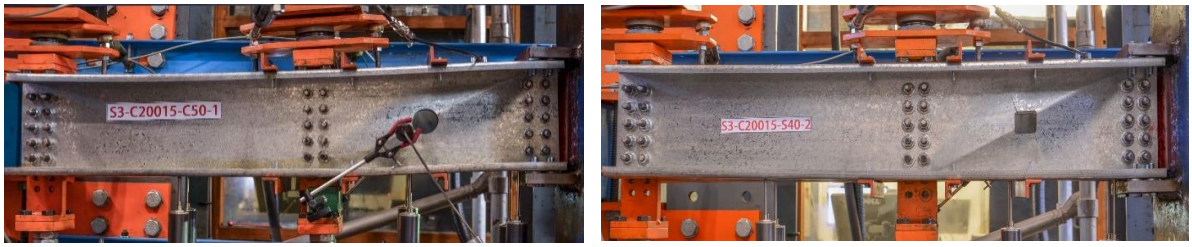

(a) Shear test with a circular web hole (b) Shear test with a square web hole

Fig 2.25: Shear failure modes from the tests using a dual actuator test rig with circular web holes by S.H. Pham [38]

2.9 NUMERICAL METHODS IN THIN-WALLED STRUCTURE ANALYSIS

There are several numerical methods, which have been used in thin-walled structure analysis, including Semi-Analytical Finite Strip Method (SAFSM), Spline Finite Strip Method (SFSM) and Finite Element Method (FEM).

The SAFSM and SFSM are two common numerical methods further developed based on Finite Strip Method (FSM) which subdivides the whole section into longitudinal finite strips. Both of the SAFSM and SFSM use polynomial functions for the transverse displacements. The difference between these numerical methods is that the SAFSM utilises harmonic functions to estimate the longitudinal displacements instead of employing spline functions as used in the SFSM. In order to study the elastic shear buckling of channel sections

in shear with simple support boundary condition, Pham & Hancock [6, 7] have used the Spline Finite Strip Method (SFSM) developed by Lau & Hancock [8] and the new theory of the Semi-Analytical Finite Strip Method (SAFSM) using multiple series terms (Hancock & Pham [9]). Further, the SAFSM plays a role as the basis method of commercial numerical programs such as THIN-WALL 2 and CUFSM developed by Nguyen et al. [54] and Li & Schafer [55] respectively.

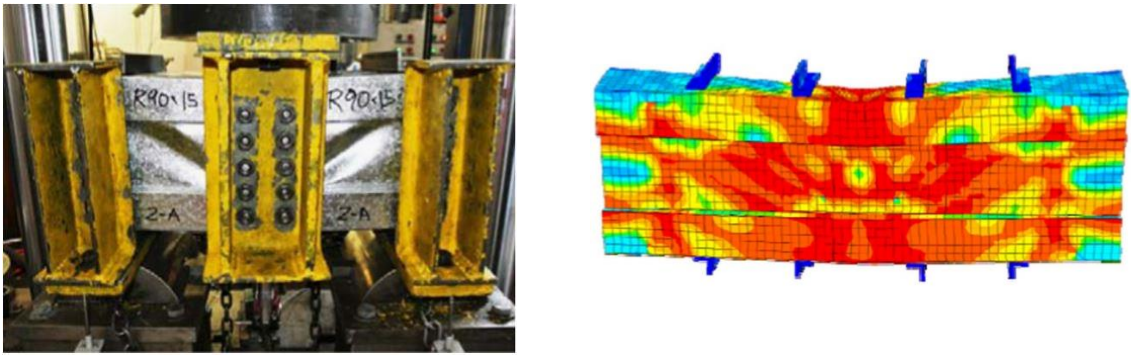

(a) Shear failure modes from experiments and FE models by Pham & Hancock [56]

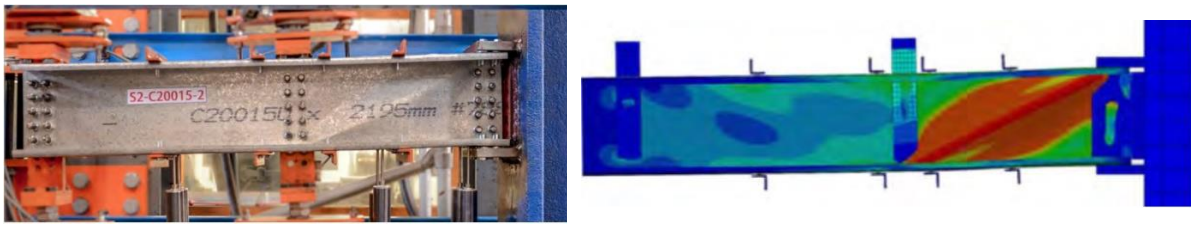

(b) Shear failure modes from experiments and FE models by S.H. Pham [38]

Fig 2.26: Shear failure modes obtained from experiments and FE models using Abaqus

The FEM is a very reliable and powerful method to produce and analyse numerical models. Hence, numerical modelling software based on the FEM including ABAQUS and ANSYS are commonly used to optimise the designs for tests, to validate the results of experiments and to extend the test database. Throughout history, the FE models developed by Pham & Hancock [56, 57], S.H. Pham [38] were successfully calibrated against the test results including the modes of failure and the ultimate loads of cold-formed steel sections in shear (see **Fig 2.26**). Furthermore, the applicability of the FEM used for shear buckling analysis of cold-formed sections was asserted by C.H. Pham [11] and S.H. Pham [38] based on good agreements in both shear buckling loads and shear buckling modes among the FEM, the SFSM and the SAFSM (see **Fig 2.27**).

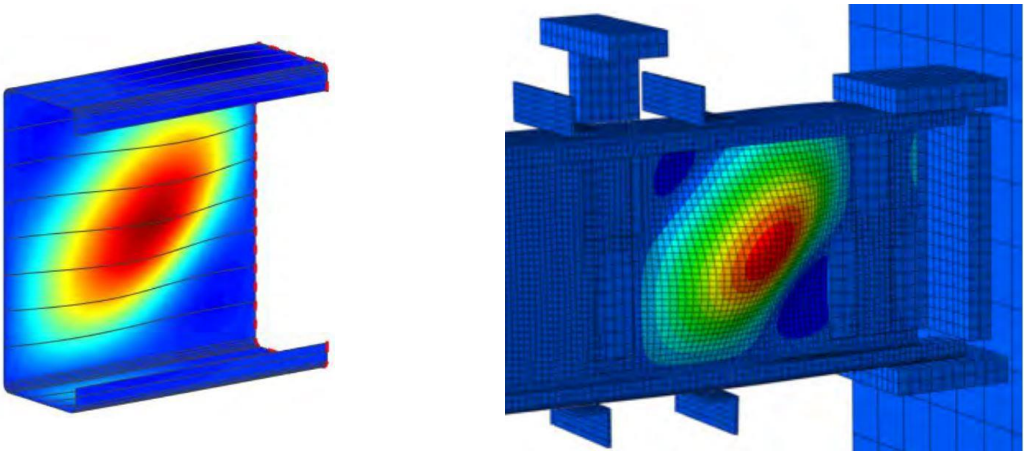

(a) SAFSM (b) FEM

Fig 2.27: Shear buckling modes obtained by SAFSM and full FE models by S.H. Pham [38]

Chapter 3
EXPERIMENTAL INVESTIGATION OF COLD-FORMED MEMBERS WITH ELONGATED WEB OPENINGS IN SHEAR

3.1 CHAPTER INTRODUCTION

This chapter presents an experimental program carried out at the University of Sydney to determine the ultimate strength of high strength cold-formed channel sections with elongated web openings (rectangular and slotted holes) in shear. Shear tests on perforated channels with non-elongated web openings (square and circular holes) have been also conducted to calibrate against test results from the previous experimental investigation by S.H. Pham [38].

Two shear test series comprising a total of thirty tests were performed. The first series was conducted on channels with central square and rectangular web holes. The second series focused on circular and slotted holes at the centre of the channel webs. All tests were undertaken in the J. W. Roderick Laboratory for Materials and Structures of the School of Civil Engineering at the University of Sydney. A standard commercially available plain C-channel with a web depth of 200 mm, a flange width of 75 mm, and a lip size of 15 mm was selected as a preferred section throughout all test series. The chosen aspect ratios of hole length (L_h) to hole depth (d_h) were 1.0, 2.0 and 3.0. A dual test rig was used in all tests with an aspect ratio of 2.0. Details of test rig design was also described in this chapter. Four tensile coupon tests were conducted to determine the material properties of members used in the shear tests including yield stress and Young's modulus.

This chapter summarises the test results serving as the input to the Direct Strength Method (DSM) of design proposal for channel members with elongated web openings as discussed in Chapter 5.

3.2 TENSILE COUPON TESTS AND RESULTS

In order to determine the mechanical properties of the G450 high strength steel material, four tensile coupon tests were conducted in the J. W. Roderick Laboratory for Materials and Structures at the University of Sydney. The specimens for the coupon tests were taken longitudinally from the web of the cold-formed steel members used for the shear tests. The tensile coupon dimensions conformed to AS1391-2005 [58] for the tensile testing of metals using 12.5 mm wide coupons with a gauge length of 25 mm.

The coupon tests were performed using the 50 kN capacity MTS Criterion testing machine operating in a displacement control mode. During the coupon tests, a constant displacement rate of 0.5 mm/min was maintained. The coupons were secured in a pair of vice grips and an extensometer was used to record the elongation. The complete stress-strain curve was determined by resetting the extensometer having displacement range of 3.0 mm several times during test process. The yield stress was obtained by determining the 0.2 % nominal proof stress referred to as $f_{y,0.2\%}$.

Table 3.1: Results of tensile coupon tests

Specimen	Thickness (mm)	b (mm)	A (mm^2)	$f_{y,0.2\%}$ (MPa)	E (MPa)
C20015-W-1	1.52	11.94	18.11	541.35	201147
C20015-W-2	1.51	12.32	18.64	547.75	216228
C20015-W-3	1.53	12.21	18.64	539.80	206370
C20015-W-4	1.52	12.25	18.62	542.60	201167
Mean				**542.87**	**206228**

The specimens for the tensile coupon tests were labelled to indicate the test section and the coupon test number. For instance, "C20015-W-1" means the coupon was cut longitudinally from the web of the channel of 200 mm depth and 1.5 mm thickness. '1' indicates the test order in the coupon series. An average yield stress f_y of 542.87 MPa was obtained. The average Young's modulus of elasticity calculated according to the tensile coupon stress-strain curves

is 206228 MPa. **Table 3.1** shows the detail of all coupon tests where *b* is the gauge width, *A* is the cross-sectional area of gauge portion, *E* is the Young's modulus of elasticity.

It can be seen in **Table 3.1** that Young's moduli in each tensile coupon test approximate to the nominal value of 200000 MPa. However, the yield stresses are significantly higher than the nominal yield stress of 450 MPa. The stress-strain curves of the 1.5 mm thick cold-formed steel material generated from the four tensile coupon tests are shown in **Fig 3.1**. The tests were paused several times to capture the static values of the yield stresses. The resulting curves were also consistent with the typical stress-strain curves of cold-formed steel material where yielding plateaus are unclear and followed by a little strain hardening. The results obtained from the tensile coupon tests in this chapter are used as the input to calculate true stress (σ_{true}) and true plastic strain (ε_{true}) in Chapter 4.

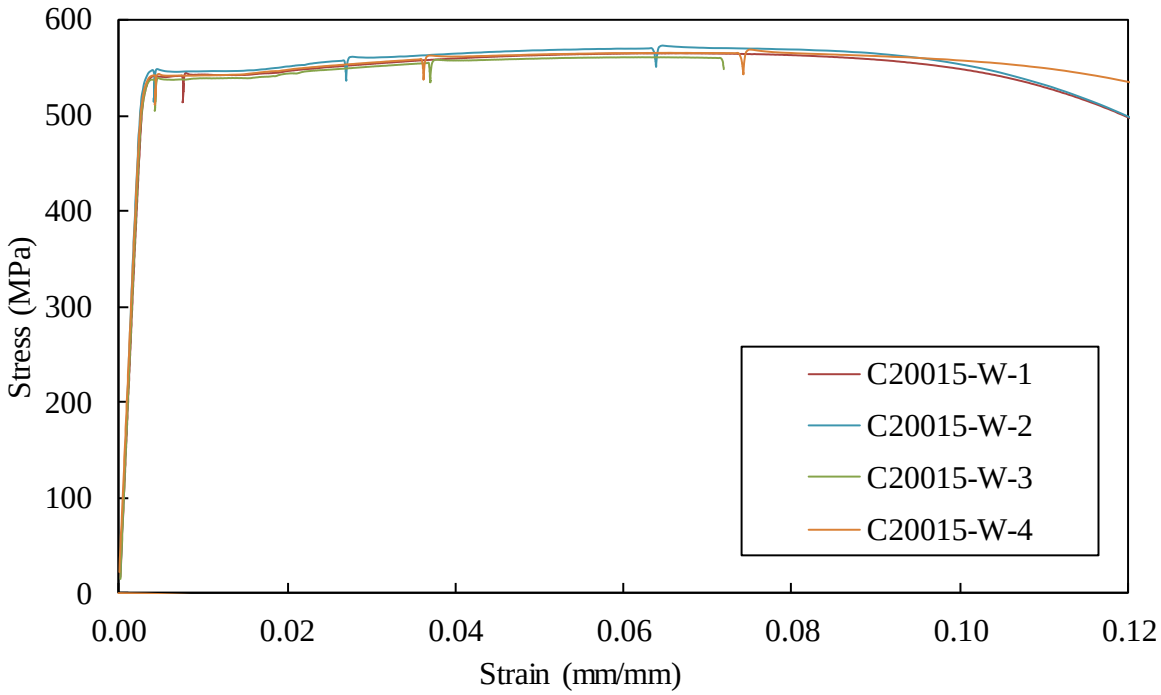

Fig 3.1: Stress-strain curves of 1.5 mm thick material from the tensile coupon tests

3.3 SHEAR TESTS OF COLD-FORMED CHANNEL MEMBERS WITH WEB OPENINGS

All the shear tests in this section were conducted in the dual actuator test rig using two independent servo-controlled hydraulic actuators. Each actuator has a capacity of 253 kN in compression and 162 kN in tension with the stroke travelling range up to 508 mm. Both actuators are controlled simultaneously by an MTS FlexTest controller. During the tests, the movement rates of the two actuators were independently adjusted by using the MPT Procedure Editor.

A total of thirty tests on channel members with web openings in shear were performed. Shear tests of perforated channels with square and rectangular web openings were performed in the first series, whereas the second series focused on circular and slotted holes in the channel webs. Each series included fifteen tests and used the same test rig configuration. The tests for each size of hole were duplicated to ensure the accuracy of the results except for those of square and circular web cut-outs (AR_h = 1.0), which were tested only once for the purpose of calibrating against the previous tests by S.H. Pham [38].

Commercially available plain C-channels with 200 mm web depth, 75 mm flange width, 15 mm lip size was used in all the test series. The depths of holes were designed within a range of 40 to 120 mm, while the chosen aspect ratios of holes (AR_h) were 1.0, 2.0 and 3.0. The web cut-outs become square or circular when the aspect ratio of the elongated holes approaches 1.0. Filleted corners of rectangular holes were cut with a radius of 5 mm to avoid premature fracture in sharp corners. The nominal thickness of all sections was 1.5 mm. The central web openings and the holes with a diameter of 13 mm for bolting in the web were cut out using a water jet cutting machine to ensure accuracy.

3.3.1 Specimen Nomenclature and Dimensions of Channels with Web Openings

The test specimens for the shear tests were labelled to express the type of channel section with nominal web depth, nominal thickness, hole shape, hole dimension and test number. A typical shear test label "C20015-REC-40x80-1" is defined as follows:

- 'C200' indicates channel sections with the web depth of 200 mm
- '15' indicates the nominal thickness times 10 in mm
- 'REC' indicates specimens with rectangular holes (alternatively 'SQR', 'CIR' and 'SLT' indicate specimens with square, circular and slotted web holes respectively)
- '40x80' indicates the web hole size of d_h = 40 mm in depth and L_h = 80 mm in total length
- '1' indicates the test number 1 in the series.

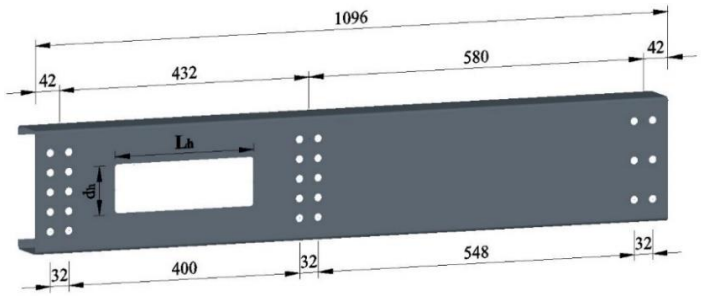

(a) Specimen with a rectangular web opening

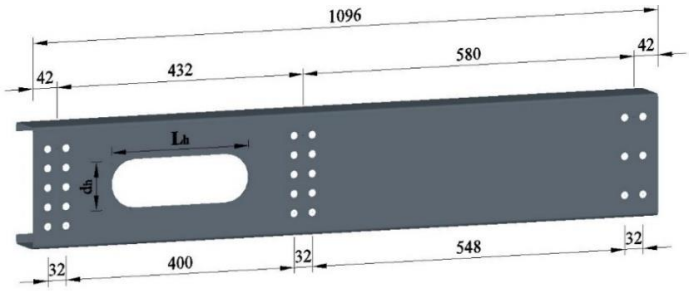

(b) Specimen with a slotted web opening

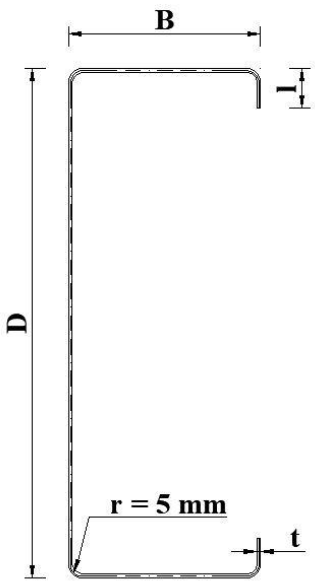

(c) Typical channel section

Fig 3.2: Dimensions of C-channel specimens with web openings in mm

The tests conducted once only were expressed by labels without the test number. The typical channel cross-section and the dimensions of perforated specimens with elongated web openings are shown in **Fig 3.2**. The average measured dimensions of the channel sections are summarised in **Table 3.2**.

Table 3.2: Average measured dimensions of channel sections

	Test Designation	*t* (mm)	*D* (mm)	*B* (mm)	*L* (mm)
	C20015-SQR-40x40	1.53	202.5	76.25	16.85
	C20015-REC-40x80-1	1.52	203.0	76.50	16.50
	C20015-REC-40x80-2	1.52	203.5	76.65	16.45
	C20015-REC-40x120-1	1.52	201.5	76.25	15.85
	C20015-REC-40x120-2	1.52	201.0	76.35	15.80
	C20015-SQR-80x80	1.51	202.5	75.80	16.25
	C20015-REC-80x160-1	1.52	203.5	76.75	16.75
Series 1	C20015-REC-80x160-2	1.52	203.5	76.75	16.80
	C20015-REC-80x240-1	1.54	202.5	76.45	16.55
	C20015-REC-80x240-2	1.54	202.0	76.55	16.55
	C20015-SQR-120x120	1.52	201.5	76.75	16.45
	C20015-REC-120x240-1	1.52	204.5	75.25	16.25
	C20015-REC-120x240-2	1.52	204.0	75.45	16.35
	C20015-REC-120x360-1	1.53	203.0	77.25	16.85
	C20015-REC-120x360-2	1.53	202.5	77.15	16.85
	C20015-CIR-40x40	1.52	202.0	76.45	15.45
	C20015-SLT-40x80-1	1.53	202.5	76.15	15.95
	C20015-SLT-40x80-2	1.53	203.0	76.05	16.15
	C20015-SLT-40x120-1	1.53	201.5	75.85	16.75
	C20015-SLT-40x120-2	1.53	201.5	75.75	16.85
	C20015-CIR-80x80	1.51	202.5	76.45	15.75
	C20015-SLT-80x160-1	1.51	202.0	76.25	16.05
Series 2	C20015-SLT-80x160-2	1.51	202.0	76.35	16.15
	C20015-SLT-80x240-1	1.53	203.0	76.95	16.45
	C20015-SLT-80x240-2	1.53	202.5	77.05	16.45
	C20015-CIR-120x120	1.52	203.5	76.25	16.00
	C20015-SLT-120x240-1	1.52	202.5	76.85	16.25
	C20015-SLT-120x240-2	1.52	203.0	76.75	16.35
	C20015-SLT-120x360-1	1.53	201.5	75.35	15.65
	C20015-SLT-120x360-2	1.53	202.0	75.55	15.85

3.3.2 Test Rig Design

A three-dimensional configuration of the shear tests using the dual actuator test rig is shown in **Fig 3.3**. The shear span with an aspect ratio (*AR*) of 2:1 was chosen with the aim to allow greater lengths of elongated holes. This aspect ratio is appropriate to avoid the significant effects of bending moments which may cause a reduction of shear capacity and change the failure modes when the shear aspect ratio becomes larger.

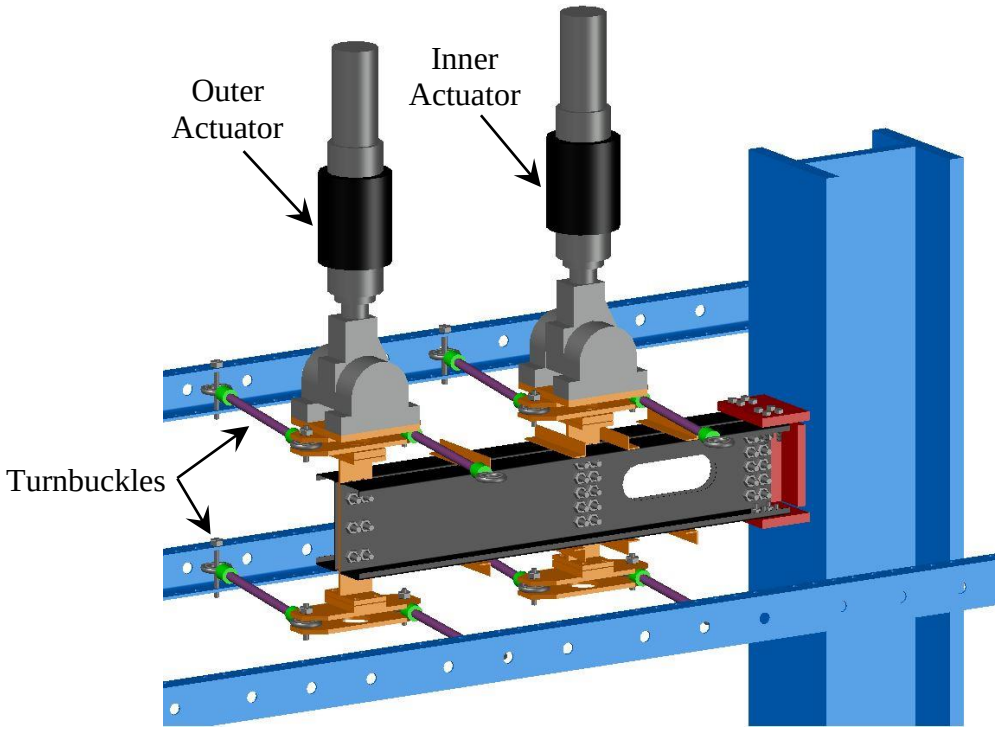

Fig 3.3: Three-dimensional configuration of the shear tests in the dual actuator test rig

In order to approach predominantly shear behaviour and obtain the shear strength close to pure shear capacity, the loads were transferred from the two actuators to the cantilever cold-formed steel beam via loading plates with proper independent movement rates of the actuators so that a pair of equal and opposite sign bending moments at the two ends of the shear span is produced. Bolted connections were used to connect the beam specimens with the loading plates and thick plates welded to a stocky column which is designed to produce a fix support at one end of the cantilever beam specimens. Each test involved two identical channel section specimens bolted back-to-back with flanges facing outwards. Four pairs of straps were screwed to both top and bottom flanges to prevent the distortion of the C-channel flanges.

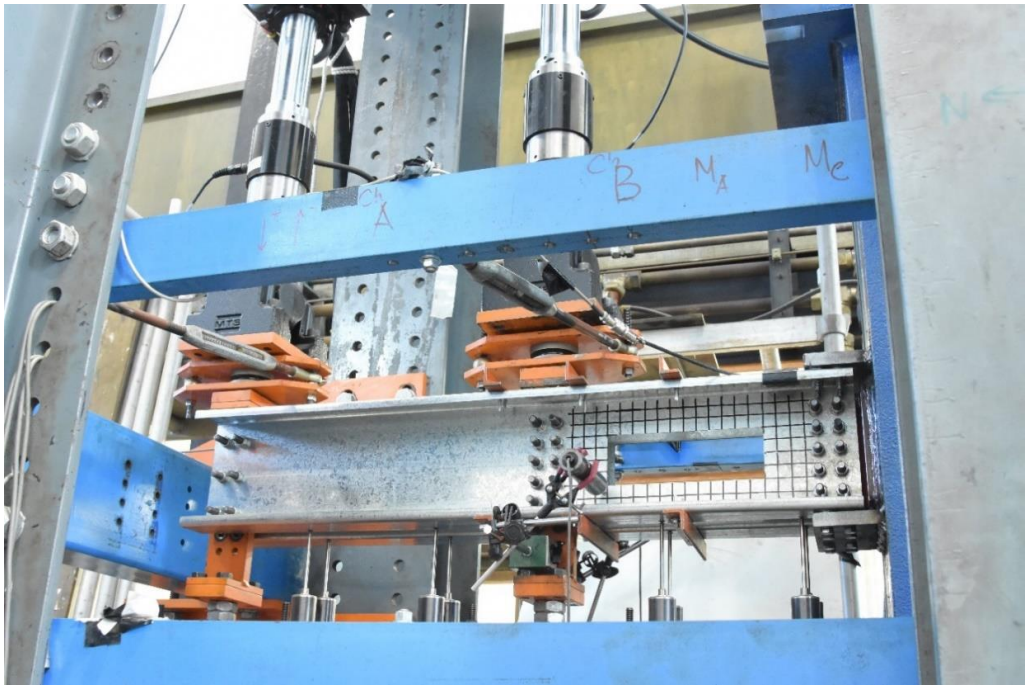

Fig 3.4: Actual shear test set-up

An actual shear test set-up with the dual actuator test rig is shown in **Fig 3.4**. The two servo-controlled hydraulic actuators attached to the loading assemblies by rotary spherical joints transferred the loads to the specimens via 20 mm thick loading plates bolted to the webs using M12 high strength bolts. At the end of the shear span, two vertical rows of five bolts were used to connect the inner loading plate to the webs with the vertical centre to centre distance of 32 mm. The end of the specimens was joined to the outer loading plate by two vertical rows of three bolts arranged with the vertical distance of 64 mm between bolt rows. Bolt connections were also utilised to fasten the specimens to the stocky column through a set of 20 mm thick plates including one T-shaped plate and two horizontal plates. In order to allow full Tension Field Action (TFA) to be developed in the shear span, a group of ten M12 high tensile bolts were used at the beginning of the shear span and arranged similarly to arrays of bolts at the end of the shear span. Groups of four M10 bolts for connections between each flange of the specimens and the horizontal steel plates were used to ensure that the bending moments at two ends of the shear span are carried.

The identical cold-formed steel beams in each test were connected back-to-back to two faces of the loading plates and the T-shaped plate. In order to eliminate large contact areas, a series of M16 bolt nuts were used as spacers between the plates and the specimen webs as shown in **Fig 3.5**. At each position where loads are transferred, four pairs of turnbuckles

connecting with sets of rotating-free plates and the rigid frame performed a role in avoiding lateral displacements and maintaining the verticality of the whole system during the tests. To prevent the flanges from distortion, four pairs of the 30x30x3EA (Equal Angle) straps were screwed to both the top and bottom flanges at the middle of spans and the positions adjacent to the inner loading plate.

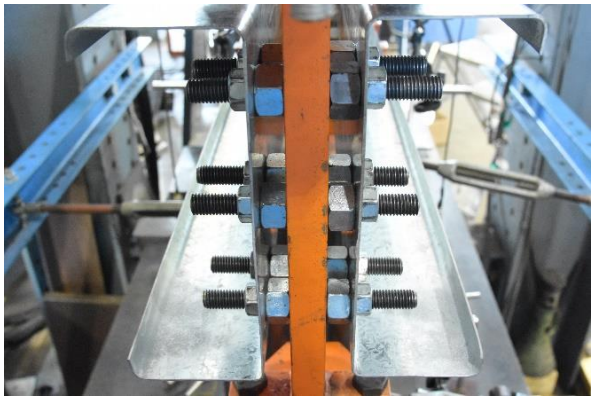

Fig 3.5: M16-bolt-nut spacers

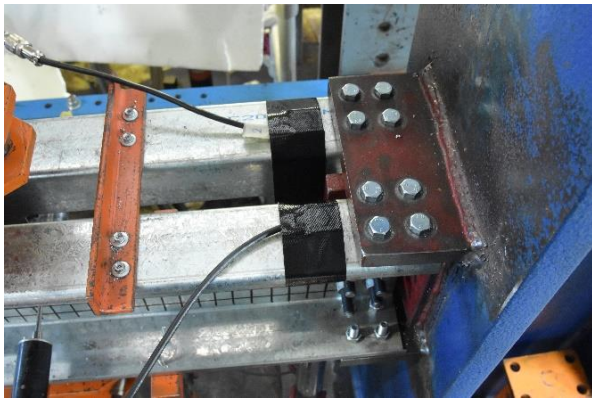

Fig 3.6: Arrangement of inclinometers

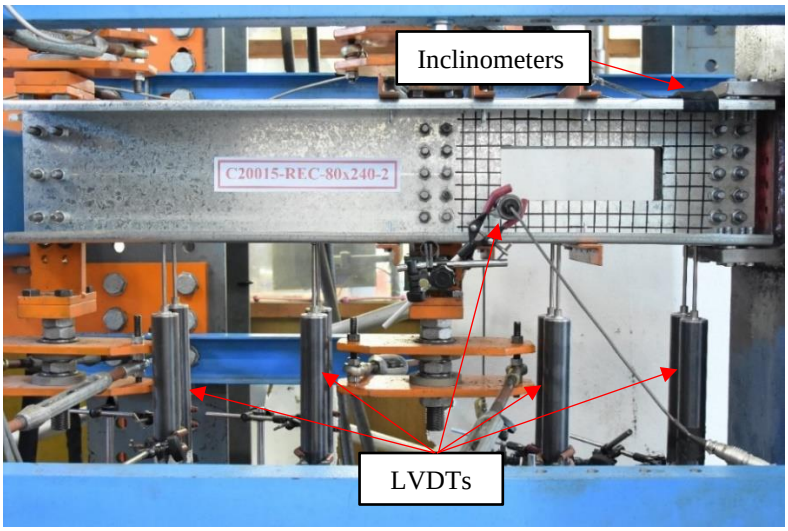

Fig 3.7: Arrangement of LVDTs

A total of ten linear variable displacement transducers (LVDTs) were used to capture deformations and displacements of the specimens during testing. Eight of these were mounted directly to the bottom flanges along the length of the specimens. Two others were mounted to record out-of-plane deformations at the positions close to the filleted corners of the web openings. Two inclinometers, as shown in **Fig 3.6**, were attached to the top flanges to keep

track of the rotational displacements at the begin of the shear span. The arrangement of the LVDTs in the actual shear tests are shown in **Fig 3.7**.

3.3.3 Test Procedure

In order to minimise the effect of bending and obtain a pair of equal and opposite sign bending moments at the two ends of the shear span, the moment ratio (M_C/M_A) of -1.0 was maintained during the tests where M_C and M_A are the bending moments at the beginning and the end of the shear span, respectively. Measured information data from the ten LVDTs, the two inclinometers and the MTS machine including the axial forces and the displacements of the two independent actuators were captured by the data logger. The ratio M_C/M_A and the corresponding shear force (V) were monitored in real time through the Vishay System 5000 StrainSmart software. Once the moment ratio deviated from the required value (-1.0) by 5%, the movement rates (mm/min) of the two actuators were modified properly by pausing the tests and manually changing the rates in the MPT Procedure Editor. This was continuously repeated during the tests until the ultimate shear strengths ($V_{n,test}$) were captured. A schematic internal force diagram is illustrated in **Fig 3.8**.

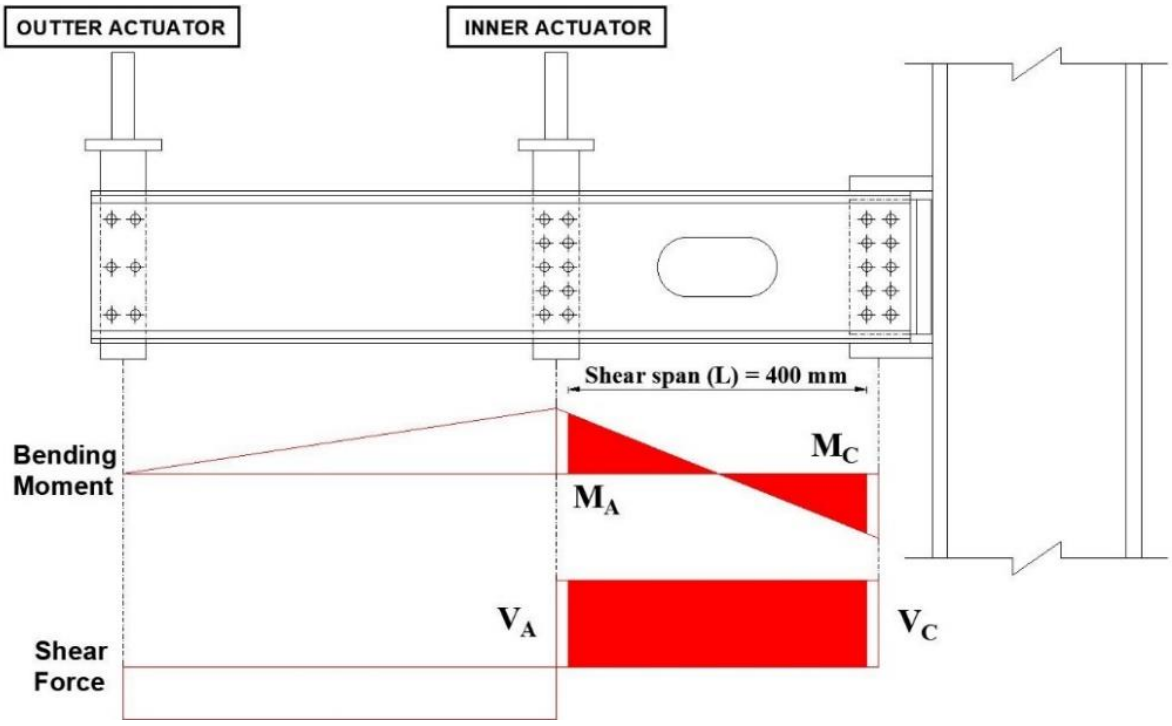

Fig 3.8: Force diagrams in the shear tests

3.4 RESULTS OF SHEAR TESTS AND DISCUSSIONS

3.4.1 Test Results of Channel Members in Shear with Square and Circular Web Openings (AR_h = 1.0)

The shear test results of perforated high strength cold-formed channels with central square and circular web openings (AR_h = 1.0) are summarised in **Table 3.3**. The shear strengths collected from the previous tests with square holes and without holes conducted by S.H. Pham [38] using the same configuration, section, hole size but different material properties are also included in **Table 3.3** for comparison. The shear strength of beams with equivalent circular web holes by S.H. Pham [38] are not mentioned in **Table 3.3** for comparison because of the dissimilarity in circular hole sizes between the two test programs. Due to a difference in the yield stresses of these tests, the ultimate shear strength is normalised to the corresponding yield shear load of unperforated section (V_y). Hole dimensions, hole aspect ratio (AR_h), and ratios of hole depth (d_h) to flat web depth (h) are also included in **Table 3.3**.

Table 3.3: **S**hear test results on specimens with central square and circular web openings

Test Designation	Hole Depth (d_h) (mm)	Hole Length (L_h) (mm)	AR_h	d_h/h	Current Test Series		Tests by S.H. Pham [38]	
					$V_{n,test}$ (kN)	$\frac{V_{n.test}}{V_y}$	$V_{n,test}$ (kN)	$\frac{V_{n.test}}{V_y}$
C20015-No holes							47.60	0.50
C20015-SQR-40x40	40	40	1.0	0.21	43.25	0.45	42.10 42.70	0.44 0.45
C20015-SQR-80x80	80	80	1.0	0.42	29.00	0.30	29.00 28.60	0.31 0.30
C20015-SQR-120x120	120	120	1.0	0.63	15.28	0.16	14.80 15.20	0.15 0.16
C20015-CIR-40x40	40	40	1.0	0.21	44.19			
C20015-CIR-80x80	80	80	1.0	0.42	32.98			
C20015-CIR-120x120	120	120	1.0	0.63	21.55			

(a) C20015-SQR-40x40

(b) C20015-SQR-80x80

(c) C20015-SQR-120x120

(d) C20015-CIR-40x40

(e) C20015-CIR-80x80

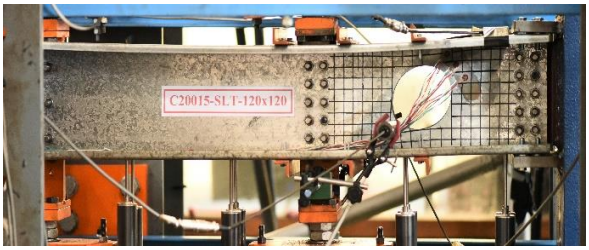

(f) C20015-CIR-120x120

(g) C20015-AR2-S40

(h) C20015-AR2-S80

(i) C20015-AR2-S120

(j) C20015-AR2-C50

(k) C20015-AR2-C120

(l) C20015-AR2-C145

Fig 3.9: Shear failure modes in current study and the tests by S.H. Pham [38]

The failure mode shapes of the shear tests on specimens with central non-elongated web openings are shown in **Fig 3.9**. The failures in shear of channels with square and circular web holes obtained by S.H. Pham [38] are also included in **Fig 3.9 (g-l)** for a comparison. The shapes of failure modes are generally symmetrical about the diagonal axis across the shear span which are similar to those captured in the tests by S.H. Pham [38] on the same test configuration and hole geometry. This demonstrates that the values of equal and opposite sign bending moments at two ends of the shear span were obtained. Therefore, the predominantly shear behaviour and the shear strengths close to pure shear capacity were captured in the tests on channel beams with AR_h = 1.0 in this test program. As can be seen in **Fig 3.9**, with small square and circular web holes (d_h = 40 mm), diagonal shear bands across the web portion of the shear span were formed from two corners of the web openings and spread gradually to two corners of the shear span. More localised curved shear bands were observed when the hole sizes become larger, especially in the tests on beams with substantially large opening (d_h = 120 mm). These outcomes were also achieved in the previous shear tests by S.H. Pham [38] on the same test rig. Further, it can be seen in **Table 3.3** that the close shear test results with the same square hole sizes in both the test programs based on the ratio $V_{n,test}$ /V_y were produced. The facts mentioned above prove that this test program captured well predominantly shear behaviours on beams with central square and circular web openings with shear span aspect ratio (AR) of 2:1 on the basis of the fair agreement of experimental outcomes and results between this test program and the previous tests carried out by S.H. Pham [38]. As a result, the quality and reliability of the test rig and test set-up in this test program are ensured for shear investigation of cold-formed channels with different shapes of holes.

3.4.2 Test Results of Channel Members in Shear with Rectangular and Slotted Web Openings (AR_h > 1.0)

The shear test results of high-strength cold-formed channel sections in shear with rectangular and slotted web openings are summarised in **Table 3.4**. These sorts of cut-out can be regarded as elongated square and circular holes whose opening areas are extended along the length of the web. Included in **Table 3.4** are various hole size dimensions, corresponding hole aspect ratios (AR_h), values of ratio between hole depth and the depth of flat web portion (d_h/h), and the ultimate shear strengths ($V_{n,test}$) produced from the shear tests.

Table 3.4: Results of shear tests on specimens with elongated web openings

	Test Designation	Hole Depth (d_h) (mm)	Hole Length (L_h) (mm)	AR_h	d_h/h	$V_{n,test}$ (kN)
Series 1	C20015-REC-40x80-1	40	80	2.0	0.21	38.05
	C20015-REC-40x80-2	40	80	2.0	0.21	38.55
	C20015-REC-40x120-1	40	120	3.0	0.21	34.58
	C20015-REC-40x120-2	40	120	3.0	0.21	33.62
	C20015-REC-80x160-1	80	160	2.0	0.42	21.41
	C20015-REC-80x160-2	80	160	2.0	0.42	21.21
	C20015-REC-80x240-1	80	240	3.0	0.42	16.13
	C20015-REC-80x240-2	80	240	3.0	0.42	15.69
	C20015-REC-120x240-1	120	240	2.0	0.63	8.76
	C20015-REC-120x240-2	120	240	2.0	0.63	8.77
	C20015-REC-120x360-1	120	360	3.0	0.63	6.08
	C20015-REC-120x360-2	120	360	3.0	0.63	6.00
Series 2	C20015-SLT-40x80-1	40	80	2.0	0.21	41.39
	C20015-SLT-40x80-2	40	80	2.0	0.21	41.44
	C20015-SLT-40x120-1	40	120	3.0	0.21	35.90
	C20015-SLT-40x120-2	40	120	3.0	0.21	36.04
	C20015-SLT-80x160-1	80	160	2.0	0.42	24.21
	C20015-SLT-80x160-2	80	160	2.0	0.42	24.09
	C20015-SLT-80x240-1	80	320	3.0	0.42	18.00
	C20015-SLT-80x240-2	80	320	3.0	0.42	18.00
	C20015-SLT-120x240-1	120	240	2.0	0.63	11.82
	C20015-SLT-120x240-2	120	240	2.0	0.63	11.65
	C20015-SLT-120x360-1	120	360	3.0	0.63	7.59
	C20015-SLT-120x360-2	120	360	3.0	0.63	7.62

The relationships between the sizes of the web cut-outs versus the ultimate shear strengths are produced in **Fig 3.10** where the values of shear strengths are extracted from **Tables 3.3** and **3.4**. The hole aspect ratio of 0.0 refers to a channel without perforations.

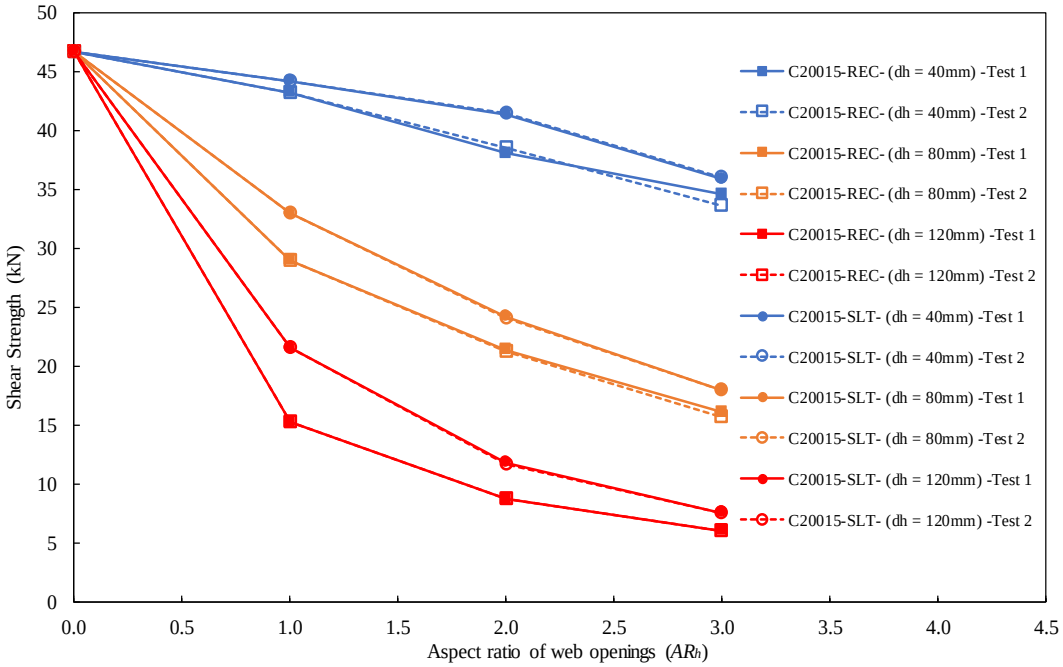

Fig 3.10: Shear strength of channel sections with various sizes of web openings

In general, the presence of openings in the web with all the hole shapes causes a significant reduction in shear capacity. The shear strengths in the Test Series 1 (with rectangular holes) are lower than those of Test Series 2 (with slotted holes) resulting from the larger area of rectangular holes compared to that of slotted openings of the same dimension. It can be seen in **Fig 3.10** that there is a nearly linear reduction in the ultimate shear strengths of channel beams with rectangular holes having the depth of 40 mm and the hole length varying from 40 to 120 mm. However, with the same hole dimension of 40 mm in depth, the shear strength of channel beams with slotted holes reduces more slightly till the hole aspect ratio (AR_h) equals 2.0 and declines more significantly when the hole length is extended up to 120 mm. The close values of shear strengths on beams with circular and square hole size of 40x40 mm are attributable to a small difference in opening areas between these hole shapes. For tests with the hole depth of 80 mm, the shear strength drops more considerably as compared to those with holes of 40 mm in depth due to larger cut-out areas. The reduction in shear strengths with holes of a substantial depth (120 mm) is significant when the hole is elongated to the length of 240 mm (AR_h = 2.0). However, it is noticeable that 12.6 and 16 % of the shear strengths on

channels with rectangular and slotted openings respectively were still retained even though a very large web area in the shear span is taken out when the hole dimension is up to 120x360 mm. This is possibly because the remaining parts of the cross section including the flanges and the lips contribute mainly to the shear resistance of beams with substantially large opening areas when nearly all of the web area is cut out.

(a) C20015-REC-40x80

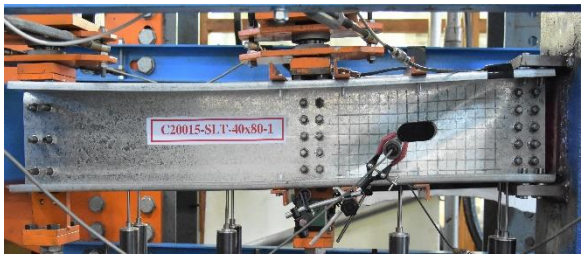

(f) C20015-SLT-40x80

(b) C20015-REC-40x120

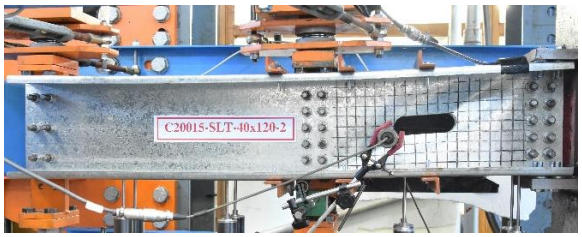

(g) C20015-SLT-40x120

(c) C20015-REC-80x160

(h) C20015-SLT-80x160

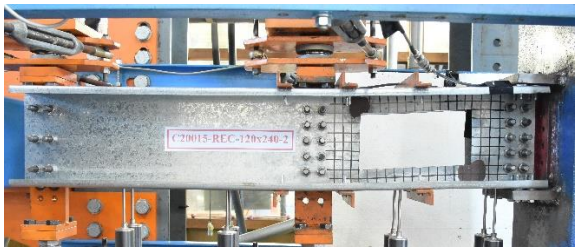

(d) C20015-REC-120x240

(i) C20015-SLT-120x240

(e) C20015-REC-120x360

(j) C20015-SLT-120x360

Fig 3.11: Failure modes in the shear tests with rectangular and slotted web openings

The failure mode shapes of the tests on channel beams in shear with rectangular and slotted holes are shown in **Fig 3.11**. Similar to the failure modes of the shear tests on beams with circular and square holes, shear failure bands with larger aspect ratios of holes (AR_h = 2.0 and 3.0) were still symmetrical around the diagonal axis across the shear span. This demonstrates that the aim of the tests maintaining the moment ratio (M_C/M_A) of -1.0 in the cases of elongated hole lengths was achieved. The shear failure bands spreading from two filleted corners of holes become more localised when the holes are extended along both the length of the shear span and the web depth. This phenomenon is very clearly observed in **Fig 3.12** where the failure shear bands occurred around the areas close to the hole corners in a case of substantially large opening area (d_h = 120 mm, AR_h = 3.0). It is also interesting to note that these failure bands were formed from the intersections of the filleted curves and the hole edges along the shear span to the two flanges instead of the two corners of the shear span as with smaller openings. This indicates that, for beams with large web openings, local effects contribute greatly to the formation of failure shear bands. Even though the filleted corners were designed with a 5 mm internal radius, the shear tests on beams with square and elongated holes suffered fractures propagated from the remaining intersections of the filleted curves and the hole edges along the shear span on web as shown in **Fig 3.12**. It was observed that these fracture lines were perpendicular to the shear bands. However, all the cracks propagated after the ultimate shear loads were reached. These fractures, therefore, did not affect the ultimate test results in shear and they are out of the research scope of this thesis.

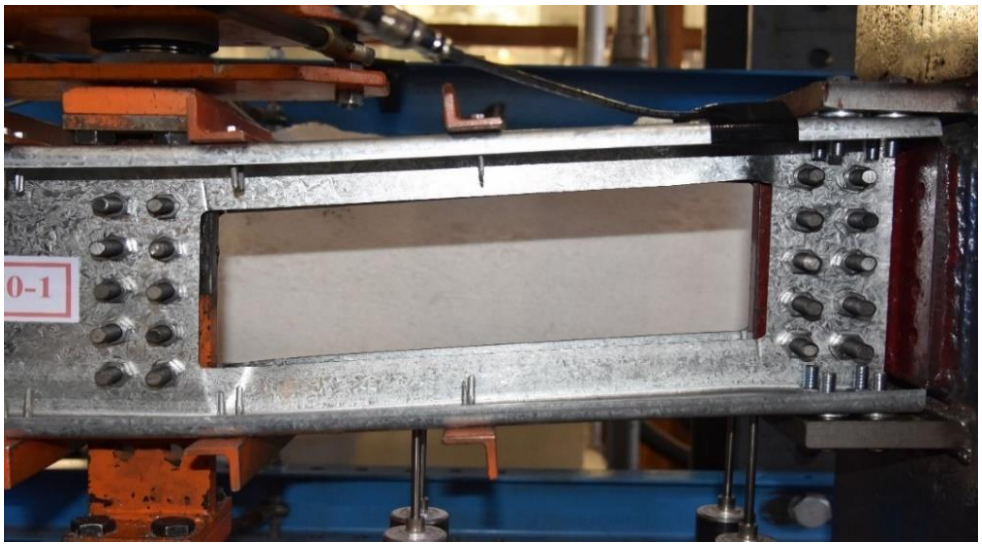

Fig 3.12: Local effects on a specimen with a substantially large opening area

The relationship between the shear loads and the vertical displacements at the end of the shear span with the specimens of 120 mm hole depth are illustrated in **Fig 3.13**. It is of interest to see that the larger length of web cut-out is, the more significant flat plateau was produced around the shear peak load. It is likely that the yielding pattern was formed at the corners of the large holes according to the observation of the failure mode and the ductile behaviour based on the load-displacement diagrams with respect to the hole depth of 120 mm. This was also recognised by S.H. Pham et al. [16] for the cold-formed channels subjected to predominantly shear with substantial large web cut-outs based on the outcomes from the shear tests by C.H. Pham et al. [15]. The load-displacement relationships of members with other hole sizes are shown in **Appendix A**.

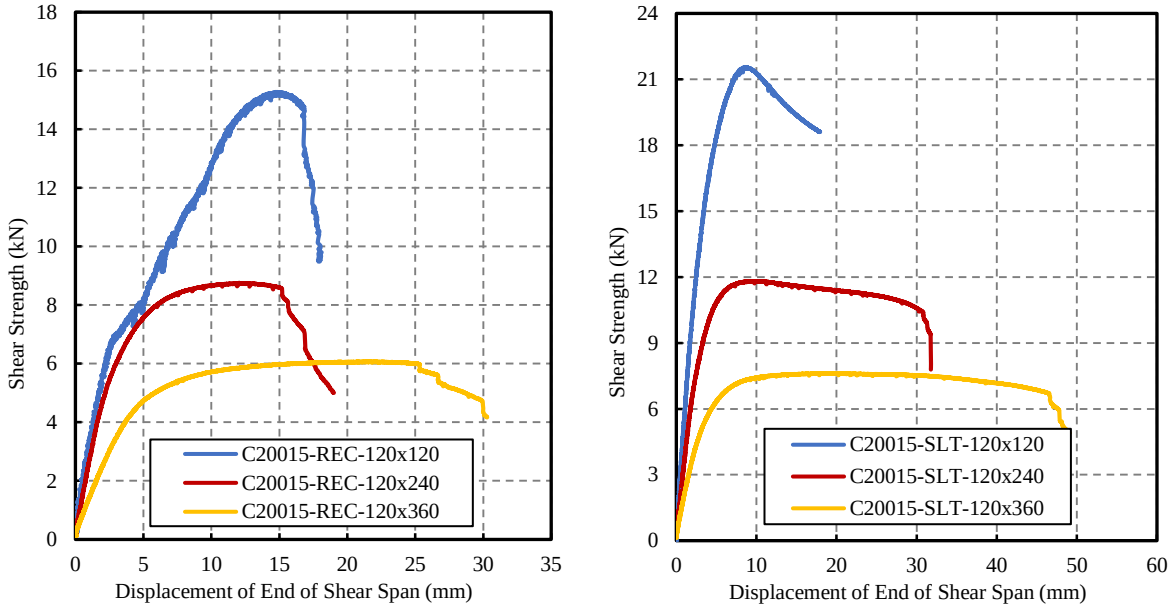

Fig 3.13: Load - displacement relationship of the channels having hole depth of 120 mm

3.5 CHAPTER CONCLUSION

On the basis of the experimental outcomes presented in this chapter, it can be concluded that the predominantly shear behaviour and the shear strengths close to pure shear capacity of cold-formed steel channels with both non-elongated and elongated web holes were obtained in all shear tests by using the dual actuator test rig. Symmetrical shear failure modes were observed in all the shear tests on members with web openings. More localised curved shear bands were observed in the cases of perforated channels with substantially large web holes. The presence of web holes leads to a considerable reduction in shear capacity. The shear strengths of members with slotted web openings are higher than those with rectangular holes because of the difference in cut out areas between the two hole shapes of the same dimension. More than 10 % of the shear strengths on channels with very large elongated holes (120x360 mm) were still retained due to the resistance of flange and lip elements. Based on the observation of the shear failure modes together with the ductile characteristic obtained from the load-displacement curve with respect to members with substantially large openings, the yield patterns were likely to be formed around the hole corners.

Chapter 4
NUMERICAL SIMULATION AND PARAMETRIC STUDY

4.1 CHAPTER INTRODUCTION

This chapter describes numerical non-linear simulations of the shear tests, based on the finite element method (FEM) using the software package ABAQUS/Standard, on high strength cold-formed channel sections subjected to shear with various hole dimensions. The simulations are compared with and calibrated against the test results in Chapter 3 to ensure the accuracy before being utilised to conduct parametric studies to extend the test database and examine the shear behaviour of channel sections with web holes in greater detail.

This chapter also provides a simplified method for shear elastic buckling analysis by using simplified FE models. The buckling results from these models are calibrated against the buckling results of full FE models for actual tests using the *BUCKLE procedure in Abaqus. The shear buckling loads (V_{cr}) are then generated from the simplified models for different cases of stress distributions. The values of shear buckling loads obtained in this chapter are used to determine elastic shear buckling coefficients (k_v) which are for the elastic buckling solutions for the perforated channels in shear with elongated web holes presented in Chapter 5.

On the basis of shear elastic buckling analyses of perforated channels with elongated web holes with a wide range of hole sizes, a dimensional transformation is proposed to transform the dimensions of slotted openings into equivalent sizes of rectangular holes. The applicability of the transformation is also investigated via a parametric study for ultimate shear strength analyses.

4.2 FINITE ELEMENT MODELLING OF ACTUAL TEST RIG AND CHANNEL MEMBERS WITH WEB OPENINGS

4.2.1 Model Details for Ultimate Shear Strength Analysis

Numerical non-linear simulations using the Finite Element Method (FEM) were carried out to undertake geometrically and materially nonlinear inelastic analyses of cold-formed channels with rectangular and slotted web openings. S.H. Pham [38] presented the modelling and ultimate strength analysis of perforated C-channels subjected to pure shear with square and circular web holes using the FEM based on package ABAQUS/Standard. In S.H. Pham [38], the FE models were calibrated successfully against the test outcomes including the ultimate shear loads and the modes of failure. Therefore, the finite element models based on those of S.H. Pham [38] were further developed to investigate the shear behaviour and validate the test results from the experimental study of channel sections with elongated web holes detailed as below.

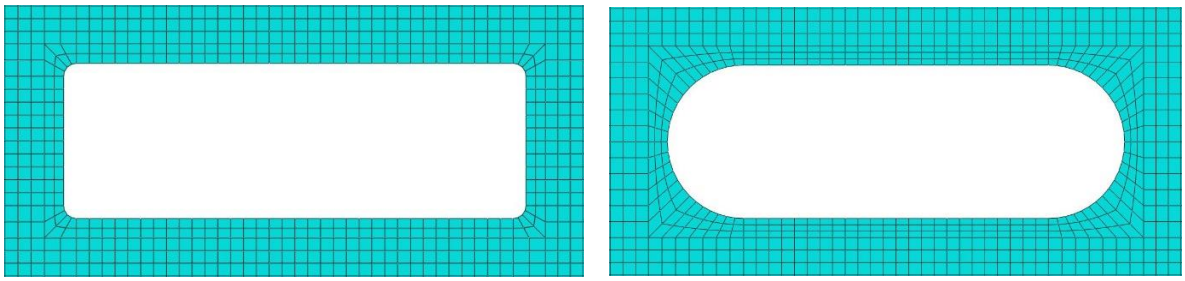

(a) Rectangular web opening (b) Slotted Web Opening

Fig 4.1: Sweep mesh around web openings

The configuration of the FE models in this numerical investigation is similar to that in S.H. Pham [38] except for the type of web openings. The 4-node doubly curved shell element (S4R) with a mesh size of 5 mm was utilised to model the cold-formed channel sections. The reliability of element S4R in capturing the post-buckling behaviour has been proven by Pham & Hancock [56, 57], S.H. Pham et al. [46] and S.H. Pham [38] based on the good agreement between the experimental outcomes and the ABAQUS results. Other components in the dual actuator test rig including the stocky column, the loading plates, the thick plates and the straps were generated using 3D-deformable solid elements with 8-node linear brick elements (C3D8R). The fine mesh size of 5 mm was used for the angle straps and the coarser mesh size

of 10 mm was used for the other parts. The sweep mesh was employed for meshing the area surrounding the web openings as shown in **Fig 4.1**.

Fig 4.2 shows a typical three-dimensional FE model of a shear test with elongated web openings. As can be seen in **Fig 4.2**, only one channel member was modelled instead of the two specimens connected back-to-back via the loading plates and the T-plate as in the actual tests because the two channels are assumed to be bolted symmetrically to both sides of the plates.

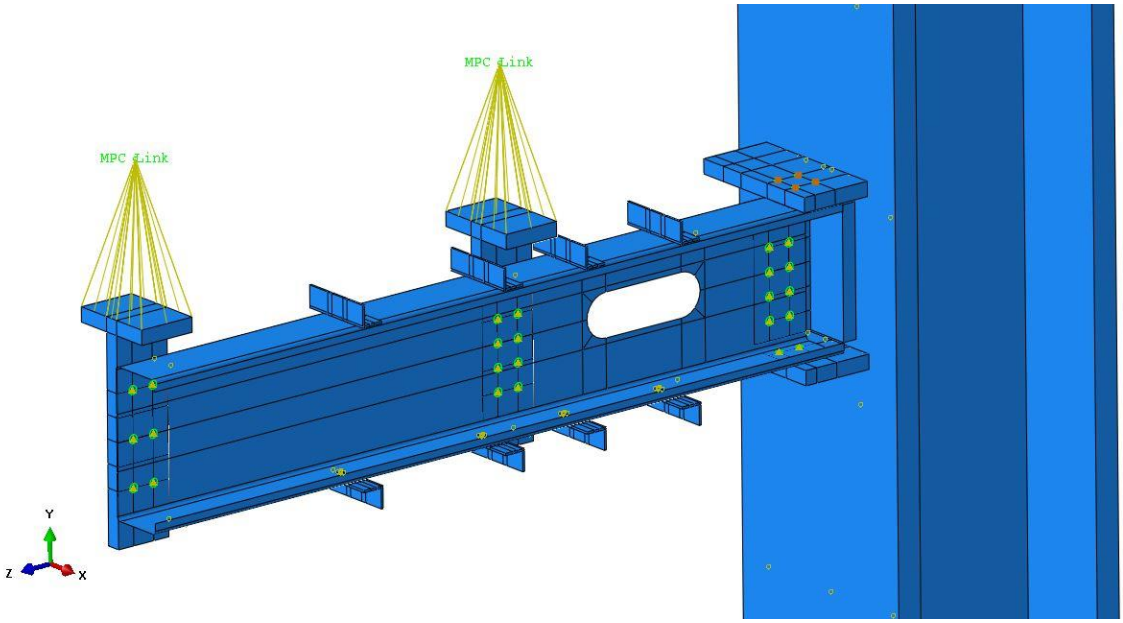

Fig 4.2: Three-dimensional FE model of a shear test with an elongated web opening

For modelling boundary conditions and connections in the FE models, an "ENCASTRE" boundary condition restraining all the degrees of freedom (DoF) was employed to generate a fixity at the column base. In order to produce weld connections between the set of thick plates and the column's surface, a surface-to-surface tie constraint was used to prevent all the translational and rotational movements of the thick plates. This type of constraint was also utilised to model easily the screw connections between the angle straps and the flanges of the channel members. The transference of loads was simulated through displacements applied by the two independent actuators on the loading plates. MPC Link constraints allowing downward movements along the y- direction and rotating movements about the x-axis were generated at the centres of the two rotary spherical joints in the actual tests. The M12 and M10

high strength bolts connecting the channels to the loading plates and the set of thick plates were simulated by discrete fastener elements adopting the generic "cartesian + rotation" connector section. The nonlinear elastic property of this connector was taken from the results of bolted connection tests for cold-formed steel sections by Phan & Rasmussen [59]. The interaction between the plates and elements of the channel were produced by using the surface-to-surface contact.

4.2.2 Material Properties

For nonlinear analysis in Abaqus, true stress (σ_{true}) and true plastic strain (ε_{true}) are required for full stress-strain data. The true stress-strain curve for FE modelling is derived from average engineering stress and strain (σ and ε respectively) obtained from the tensile coupon tests in Chapter 3 as follows:

$$\sigma_{true} = \sigma.(1+\varepsilon) \tag{4.1a}$$

$$\varepsilon_{true} = \ln(1+\varepsilon) - \frac{\sigma_{true}}{E} \tag{4.1b}$$

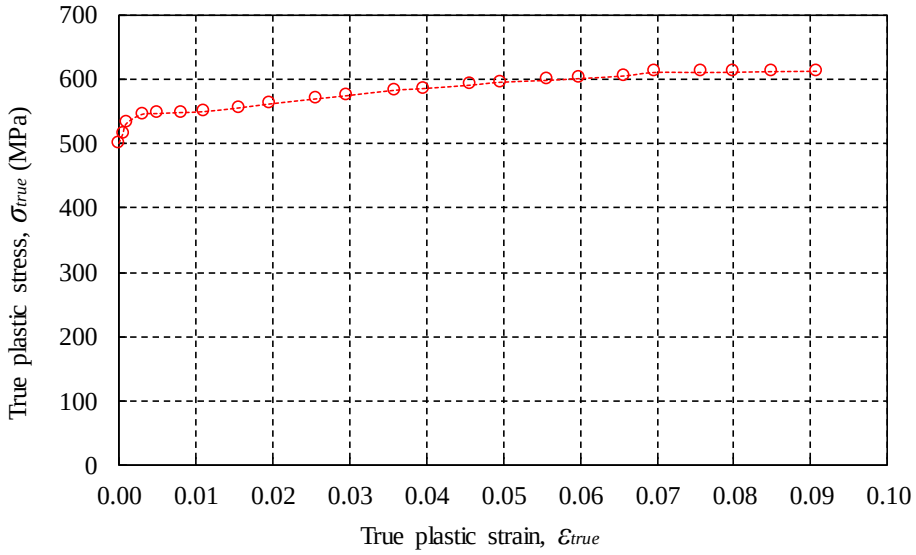

Fig 4.3: True plastic stress-strain curve of G450 steel with thickness of 1.5 mm

Fig 4.3 shows an average plastic true plastic stress-strain curve of 1.5 mm thick coupon specimen taken from the web of the channel members. The values of stress and strain in this curve were input to the plastic material property of channel elements in FE models for shear strength analyses. For the elastic material property of channel sections, the average Young's

modulus of 206228 MPa obtained from the tensile coupon tests, and a typical Poisson's ratio of 0.3 were used.

For material properties of the other hot-rolled components including the stocky column, thick plates, loading plates and straps, Young's modulus of 200000 MPa and Poisson's ratio of 0.3 were used for elasticity. The true stress-strain curve for hot-rolled steel in plastic range which was used by S.H. Pham [38] is shown as **Fig 4.4**.

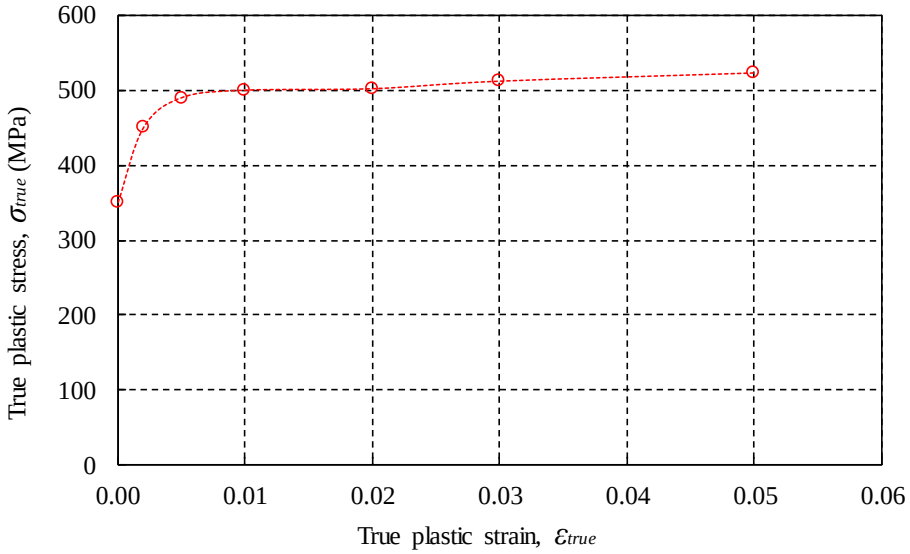

Fig 4.4: True plastic stress-strain curve of hot-rolled components

4.2.3 Solution for Ultimate Shear Strength Analysis

The Riks method or the Arc-Length method developed by Riks [60, 61] is an efficient method in solving non-linear systems of finite element equations. In contrast to the Newton-Method, where the load vector coefficient is given, the Riks method known as the "Modified Riks Method" solves simultaneously variations of the displacements and the load vector coefficient. Therefore, the Riks method copes well in snapping behaviour problems and is implemented in Abaqus. Based on this advantage, The Riks method can be used to solve post-buckling problems both with stable and unstable post-buckling behaviour. This method was also employed in many previous studies by Pham & Hancock [57], Keerthan & Mahendran [26], S.H. Pham [38] due to the solution convergence and reliable predictions of the strength of thin-walled structures. Therefore, the *STATIC, RIKS procedure is used in order to perform post-

buckling analysis and capture the shear strengths of cold-formed channels with web openings in this study.

4.2.4 Finite Element Model Validation of Test Results

A validation of the FE models for shear strength analyses was carried out based on three aspects including the ultimate shear strengths, the failure modes in shear and the relationship between the shear loads and the vertical displacements.

In this study, the sensitivity of the initial geometrical imperfections over the shear outcomes is investigated. There are three methods to define the geometrical imperfections in Abaqus. In the first method, the geometric imperfections can be defined by the linear superposition of buckling eigenmodes. The second method is based on the deformed geometry of a previous static analysis. In the final method, the imperfections can be specified directly from a separate input file which consists of node numbers and imperfection values. In this study, the first method based on eigenmode data was used. This method was also applied by Pham & Hancock [56, 57] and S.H. Pham [38] where the buckling modes with lowest eigenvalue are chosen to incorporate the imperfections into the FE models. The reason for this is that the critical buckling modes are normally the lowest buckling modes. Two scaling factors (*Imp*) of 0.15*t* and 0.64*t* proposed by Silvestre & Camotim [62] and Schafer & Peköz [63] respectively where *t* is the thickness of section were employed as the imperfection magnitudes throughout this investigation. The failure modes observed in the models without the imperfection are exacerbated by the sign of the scaling imperfection factor (positive or negative).

For comparisons of test loads with the finite element modelling, **Table 4.1** summarises both the results of the shear tests and the ultimate shear strength from FEM analyses corresponding to the two imperfection scaling magnitudes of 0.15*t* and 0.64*t*. As can be seen in **Table 4.1**, fair agreement between the ultimate shear loads obtained from the shear tests described in Chapter 3 and the FEM analyses with the maximum absolute variance of 5.37% proves that the sensitivity of the ultimate shear strengths to the initial geometrical imperfections is not significant under shear loading. Further, it can be seen in **Fig 4.5** that the results from

the majority of FE models with imperfection magnitude of 0.64*t* are closer to the shear strengths obtained from the shear tests.

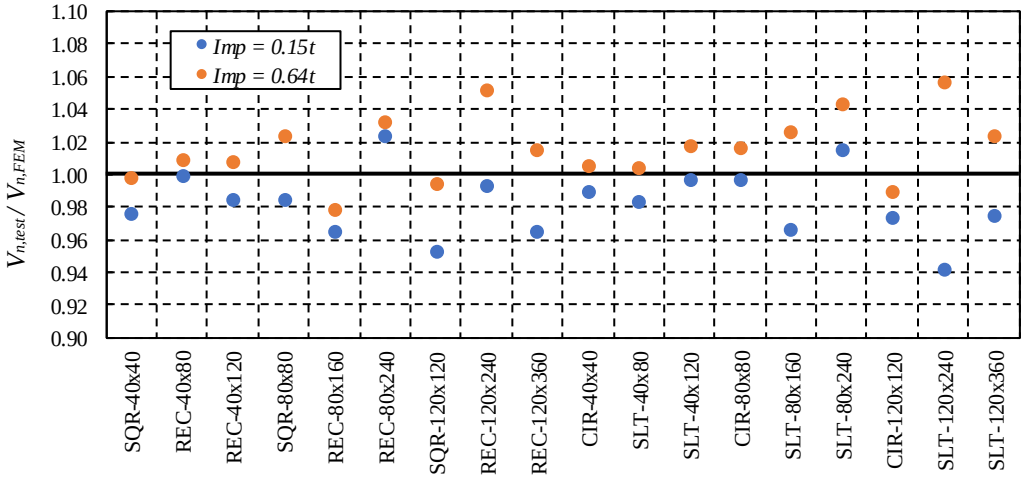

Fig 4.5: Comparison of shear strengths from the tests and FE models including initial geometrical imperfections

Table 4.1: Influence of initial geometrical imperfection to shear strength

Designation	$V_{n,test}$ (kN)	$V_{n,FEM}$ (Imp = 0.15t) (kN)	$V_{n,FEM}$ (Imp = 0.64t) (kN)	Variance (%)
C20015-SQR-40x40	43.25	44.33	43.35	0.23
C20015-REC-40x80	38.25	38.31	37.93	0.16
C20015-REC-40x120	34.10	34.65	33.87	-0.67
C20015-SQR-80x80	29.00	29.48	28.34	1.66
C20015-REC-80x160	21.31	22.11	21.78	2.21
C20015-REC-80x240	15.91	15.55	15.43	-2.26
C20015-SQR-120x120	15.28	16.05	15.38	0.65
C20015-REC-120x240	8.76	8.83	8.33	0.80
C20015-REC-120x360	6.04	6.26	5.95	-1.49
C20015-CIR-40x40	44.19	44.69	43.97	0.50
C20015-SLT-40x80	41.42	42.15	41.28	-0.34
C20015-SLT-40x120	35.97	36.12	35.35	0.42
C20015-CIR-80x80	32.98	33.09	32.47	0.33
C20015-SLT-80x160	24.15	25.02	23.55	-2.48
C20015-SLT-80x240	17.98	17.73	17.24	1.39
C20015-CIR-120x120	21.55	22.16	21.78	1.07
C20015-SLT-120x240	11.74	12.47	11.11	-5.37
C20015-SLT-120x360	7.61	7.81	7.44	-2.23

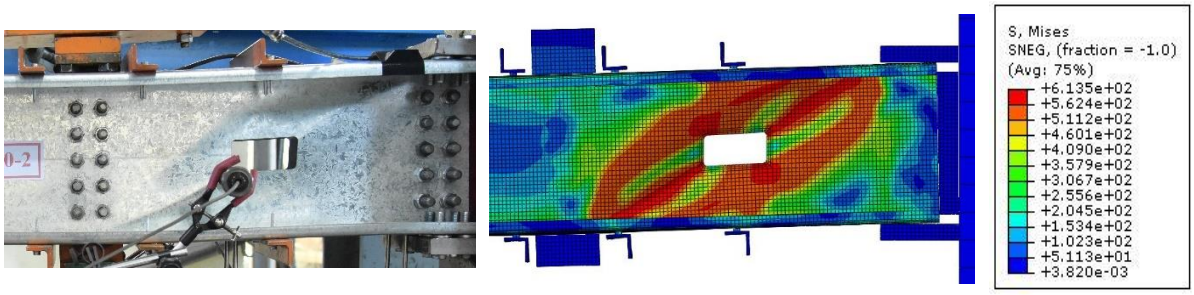

(a) C20015-REC-40x80

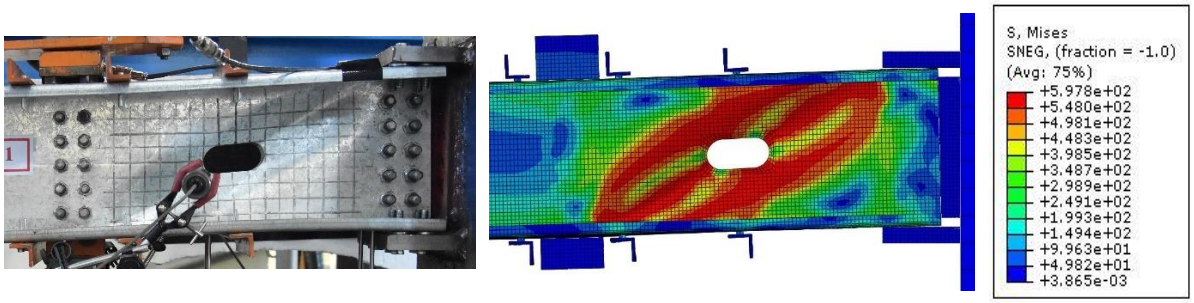

(b) C20015-SLT-40x80

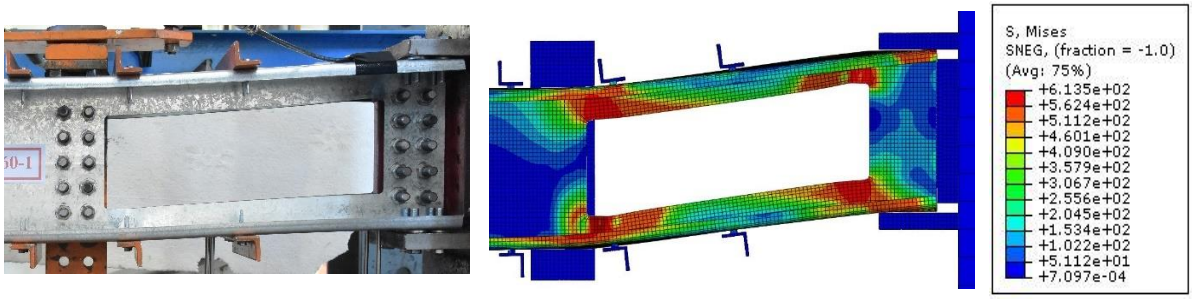

(c) C20015-REC-120x360

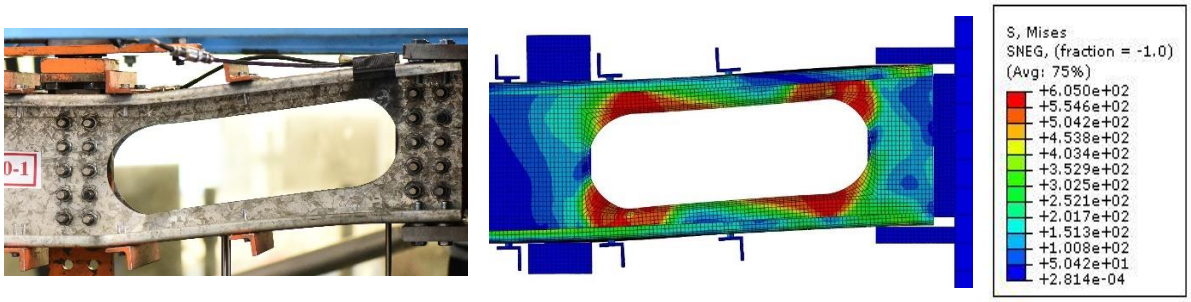

(d) C20015-SLT-120x360

Fig 4.6: Shear failure modes produced by shear tests and FEM analyses

The shear failure modes produced by the FE models with rectangular and slotted web openings are compared to the failure modes in the actual tests in **Fig 4.6**. Obviously, there is a close resemblance between the shear failure modes in the actual tests and those in the FE

models for the cases of both small and very large web holes. Further, the symmetrical failure bands prove that properly simulated movement rates of the actuators were achieved so that the beam failed under close to pure shear.

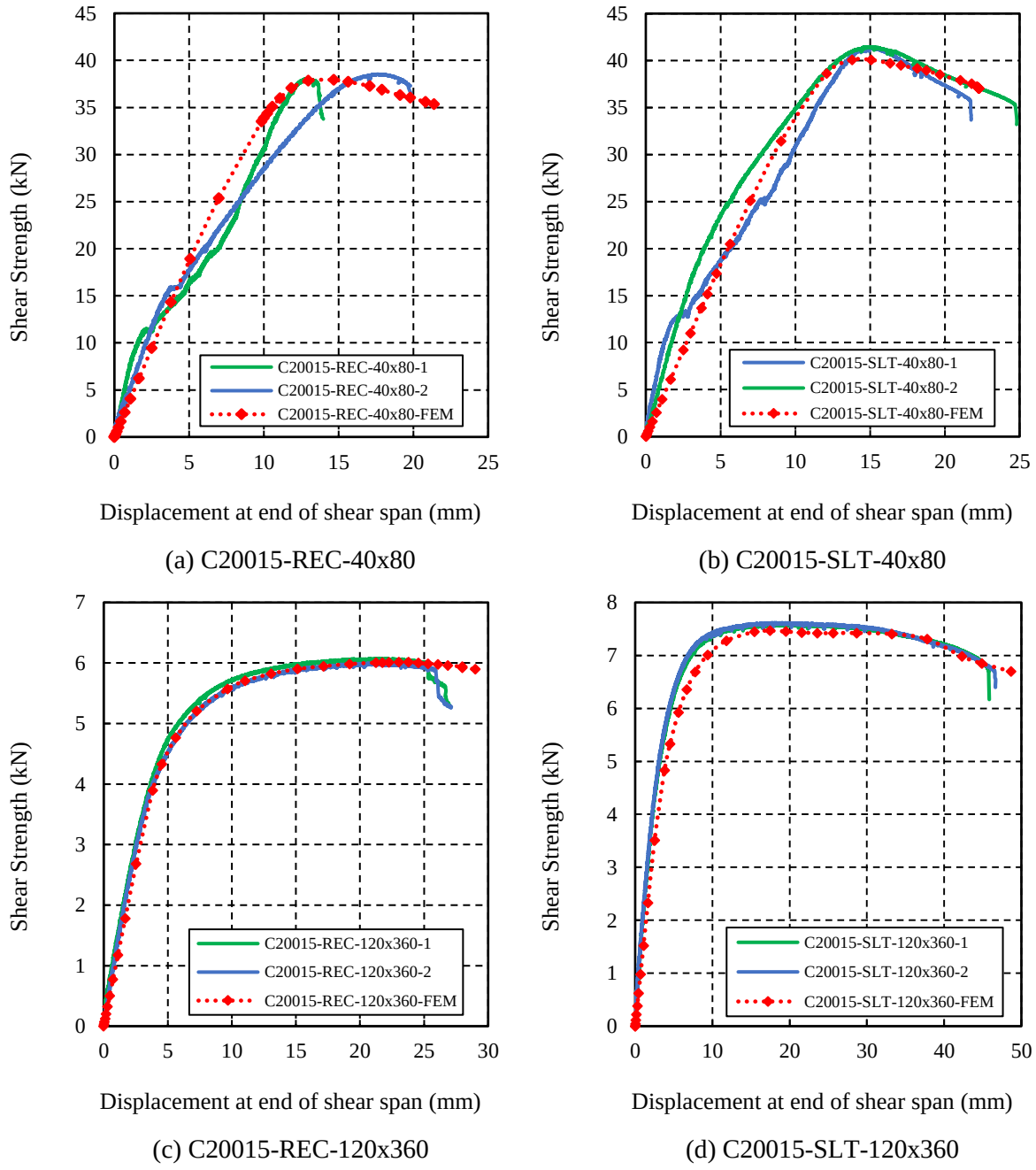

(a) C20015-REC-40x80

(b) C20015-SLT-40x80

(c) C20015-REC-120x360

(d) C20015-SLT-120x360

Fig 4.7: Load-displacement relationship of channels with elongated web holes produced by the shear tests and FE models

Fig 4.7 displays the relationships between the shear loads and the vertical displacements at the end of the shear span with hole sizes of 40x80 and 120x360 mm. For the

case of the smaller hole size (40x80 mm), a minor discrepancy between the vertical displacement of the tests and that of the FE models resulting from the incapability of generating variable movement rates of the two actuators in the FE simulation. Despite a slight mismatch as shown in **Fig 4.7 (a-b)**, the FE simulations still captured well the load-displacement relationship in the actual shear tests. With a very large hole dimension (120x360 mm), the greater consistency of load-displacement curves from the tests and the FE models is attributed to the fact that the movements of the two actuators were maintained properly at the same rate and almost unchanged during testing. The results in **Fig 4.7 (c-d)** also confirm the increased ductility with longer web holes.

4.3 FINITE ELEMENT MODELLING FOR SHEAR ELASTIC BUCKLING ANALYSIS

4.3.1 Simplified Model Details for Shear Elastic Buckling Analysis

Finite element method (FEM) modelling utilising Abaqus/CAE was employed for the elastic buckling analysis of channel sections in shear with rectangular and slotted web openings. The FE models utilised the 4-node doubly curved shell elements (S4R) with a mesh size of 5x5 mm. Poisson's ratio (μ) of 0.3 was chosen as in the AS/NZS 4600:2018 [5], whereas the Young's modulus was taken as the results from the tensile coupon stress-strain curves. For simulation of the simply supported boundary conditions, two ends of each section are restrained in-plane in both the x and y directions to prevent these end sections from deforming in a cross-sectional plane as shown in **Fig 4.8**. A longitudinal restraint was placed on a middle point of the web at one end section to avoid rigid body motion. The span length (L) of each model is 400 mm which equals the length of the shear span in the actual experiments. Dimensions of the channel cross-sections including web depths, lip sizes, flange lengths and dimensions of holes were taken as average measured dimensions in each of the shear tests as shown in **Table 3.2**.

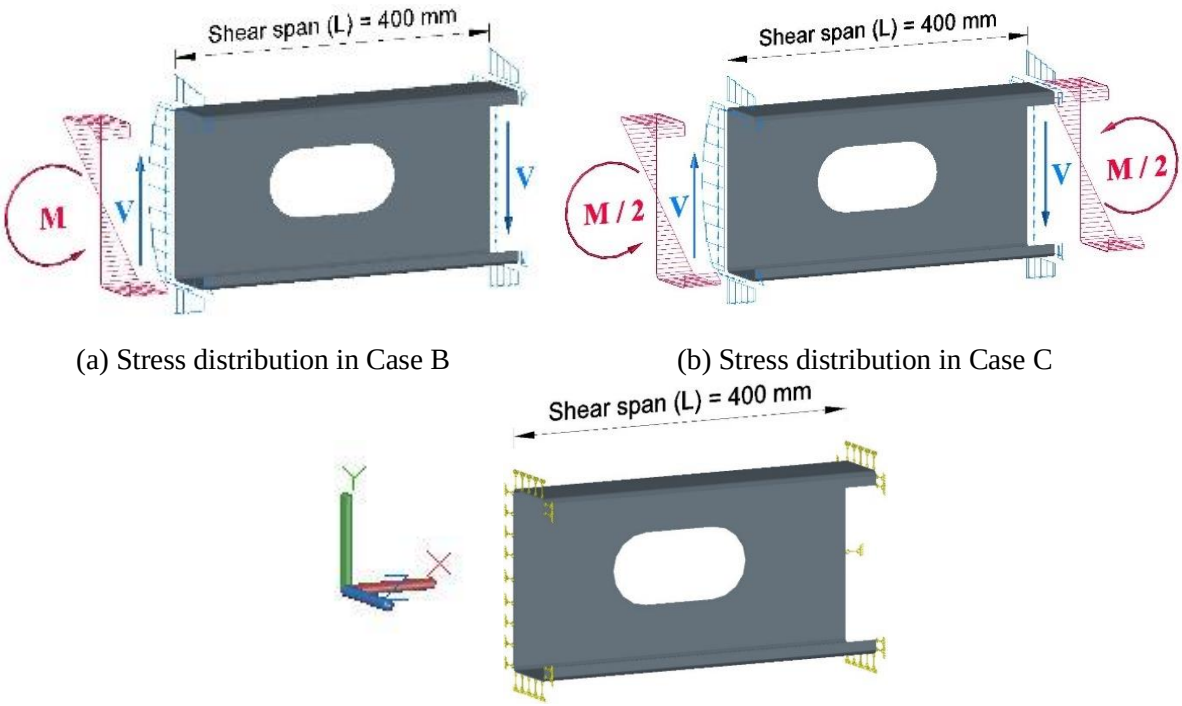

(a) Stress distribution in Case B

(b) Stress distribution in Case C

(c) Boundary Conditions

Fig 4.8: Boundary conditions and stress distributions of lipped channel sections with an elongated web opening

In order to observe the shear buckling behaviour of perforated channels, two cases of stress distribution including Case B and Case C have been developed by C.H. Pham [11] and S.H. Pham [38] as shown in **Fig 4.8**. A pair of bending moments *(M/2 = V.L/2*) is applied at both end sections in Case C in the same direction, whereas the channel is subjected to only one bending moment (*M = V.L*) at one end in Case B to balance with the longitudinal shear stresses resulting from two coupling shear forces. The moment gradients (*M*) generating a uniform shear force (*V*) in FE models are simulated by the distributed line loads in Abaqus. The values of shear elastic buckling loads and shear buckling modes were generated through the *BUCKLE procedure in ABAQUS/Standard.

4.3.2 Finite Element Model Validation by Shear Elastic Buckling Analysis

The reliability of the simplified FE models for shear elastic buckling analyses is validated based on a comparison between the results obtained from the simplified models and those from the full FE models as described in Sections 4.3.1 and 4.2.1 respectively.

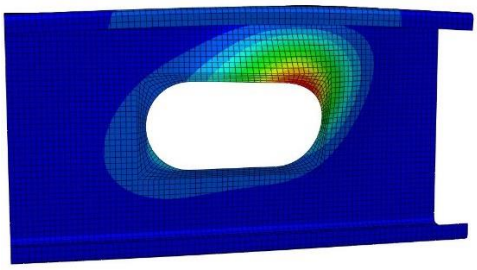

(a) Buckling mode shapes by simplified FE model in Case B

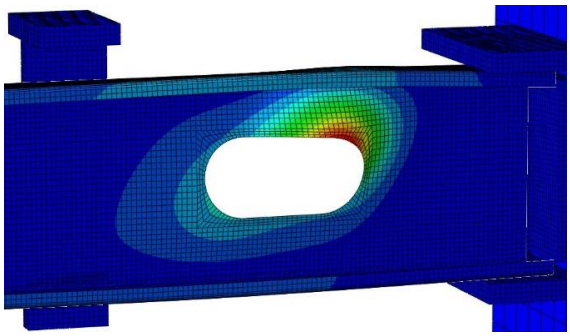

(b) Buckling mode shapes by full FE model in Case B

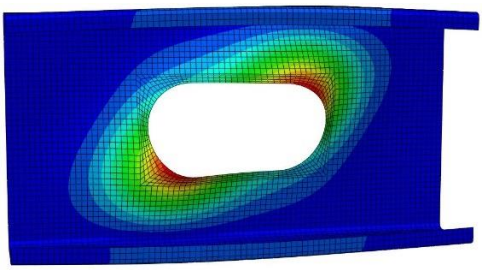

(c) Buckling mode shapes by simplified FE model in Case C

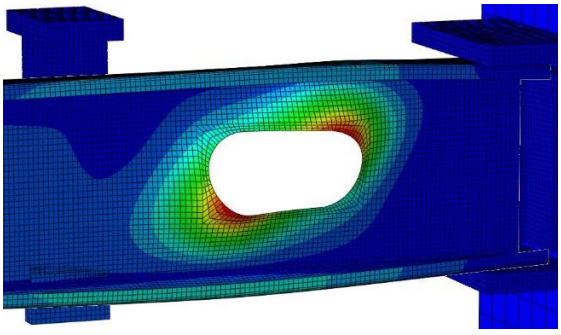

(d) Buckling mode shapes by full FE model in Case C

Fig 4.9: Shear buckling mode shapes of members with a hole size of 80x160 mm

The shear buckling mode shapes in both Case B and Case C from a simplified FE model with a hole size of 80x160 mm were compared with the corresponding outcomes obtained by using a full FE model where all straps at flanges are removed as shown in **Fig 4.9**. In the full FE models for shear elastic buckling analyses, the *RIKS procedure used for ultimate shear strength analyses was replaced by the *BUCKLE procedure. The ratio of movement rates at two independent actuators was adjusted until a pair of equal and opposite sign buckling bending moments was obtained. The shear buckling loads were calculated by a sum of reaction forces at the two actuators. As can be seen in **Fig 4.9**, in both Case B and Case C, both the simplified FE models and the full models produced similar buckling modes. More specifically, in Case C, diagonal shear buckle bands occurred across the shear span due to the pair of moments at two ends of shear span, whereas buckling mode shapes in Case B involved buckling patterns concentrating at one corner of the web hole resulting from the effect of the bending at one end only of the member sections.

Table 4.2: Shear buckling loads by simplified FE models and full FE models

Designation	Case B			Case C		
	$V_{cr,\ simplified}$ (kN)	$V_{cr,\ full}$ (kN)	Variance (%)	$V_{cr,\ simplified}$ (kN)	$V_{cr,\ full}$ (kN)	Variance (%)
C20015-SQR-40x40	17.806	18.36	3.11	18.947	19.56	3.24
C20015-REC-40x80	14.521	14.96	3.02	15.582	16.22	4.09
C20015-REC-40x120	11.852	12.39	4.54	12.936	13.66	5.60
C20015-SQR-80x80	11.611	12.23	5.33	12.658	13.34	5.39
C20015-REC-80x160	7.643	8.12	6.24	8.373	8.73	4.26
C20015-REC-80x240	5.327	5.55	4.19	5.793	6.21	7.20
C20015-SQR-120x120	8.150	8.69	6.63	8.667	9.12	5.23
C20015-REC-120x240	4.634	4.89	5.52	4.854	5.17	6.51
C20015-REC-120x360	2.276	2.44	7.21	2.355	2.53	7.43
C20015-CIR-40x40	18.895	19.26	1.93	20.110	20.87	3.78
C20015-SLT-40x80	15.561	16.03	3.01	16.608	17.05	2.66
C20015-SLT-40x120	12.573	13.22	5.15	13.681	14.26	4.23
C20015-CIR-80x80	13.747	14.35	4.39	14.682	15.31	4.28
C20015-SLT-80x160	8.544	9.06	6.04	9.387	10.06	7.17
C20015-SLT-80x240	5.915	6.27	6.00	6.442	6.77	5.09
C20015-CIR-120x120	9.802	10.32	5.28	10.326	10.85	5.07
C20015-SLT-120x240	5.472	5.86	7.09	5.715	6.04	5.69
C20015-SLT-120x360	2.766	2.89	4.48	2.845	3.02	6.15

Table 4.2 compares the shear buckling loads generated by the simplified FE models ($V_{cr,\ simplified}$) and by the full FE models ($V_{cr,\ full}$) in both Case B and Case C. With a wide range of hole sizes, the two sets of FE models produced very close shear buckling loads (V_{cr}) with a maximum difference of 7.43 %. The slight differences between buckling loads obtained from the two modelling methods are attributed to restraints at the ends of the shear span. In the simplified FE models, simply supported boundary conditions were applied at the end sections. The simplified models always had lower buckling loads as expected. Meanwhile, two ends of the shear span in the full FE models were restrained by rows of five bolts as in the actual test. Further, ideal pure shear loading states were created in the simplified FE models, whereas the shear buckling loads from the full FE models were determined by the moment gradient along the shear span. Generally, on the basis of the comparisons in both buckling mode shapes and shear buckling loads, the simplified FE models for shear elastic buckling analyses were able to capture well the shear buckling behaviour of the perforated channels with both non-elongated and elongated web holes with a shear aspect ratio up to 2.0.

4.4 PARAMETRIC STUDY

4.4.1 Parametric Study for Shear Elastic Buckling Analysis

On the basis of a good agreement between the simplified FE models and full FE models in shear elastic buckling analyses as presented in Section 4.3.2, the simplified FE models are employed in this section to perform a parametric study to create a full range database for buckling analyses. The aim of the parametric study in this section is to provide a deeper understanding of elastic buckling behaviour of cold-formed channel sections in shear with elongated web openings.

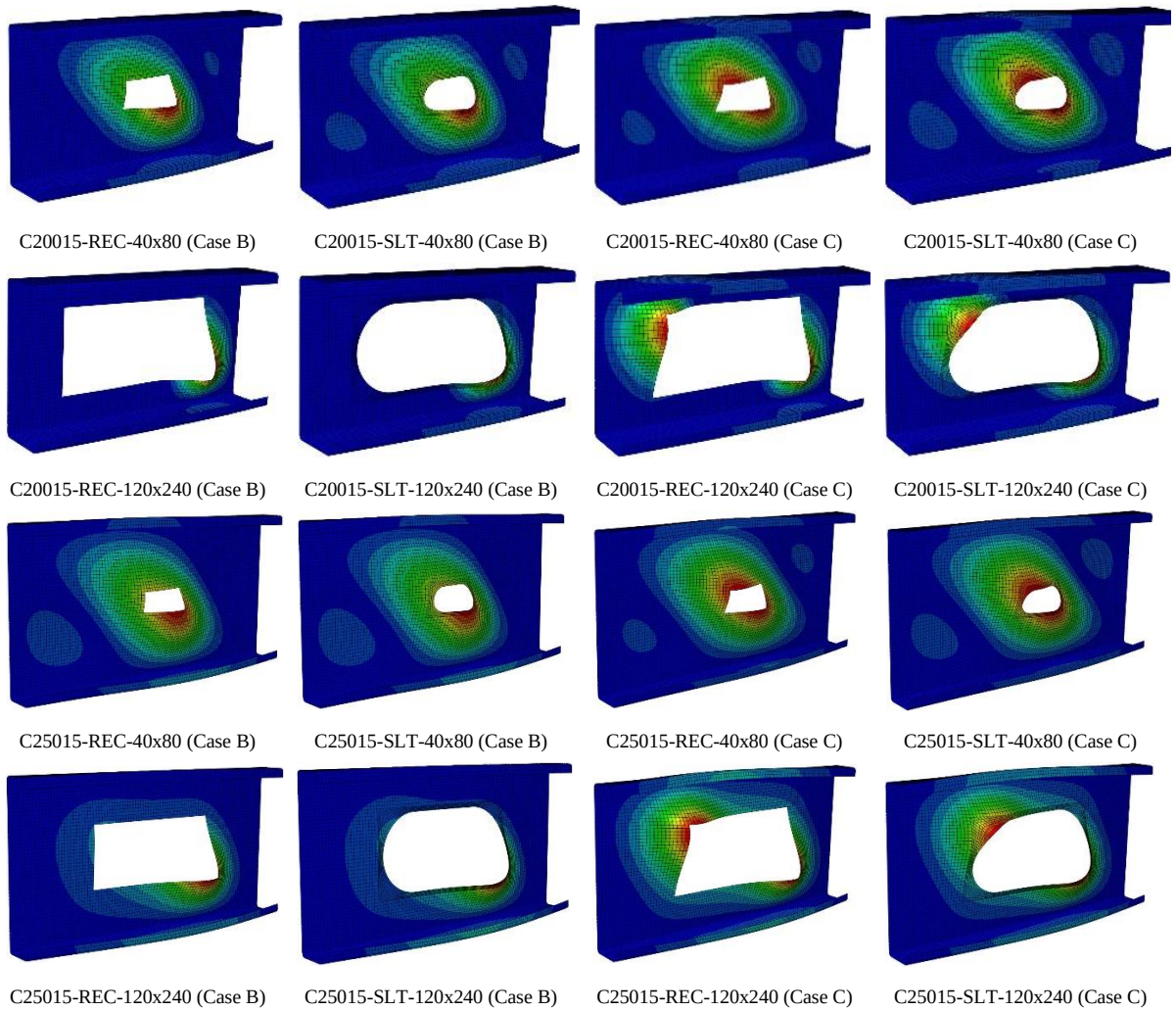

Fig 4.10: Shear buckling mode shapes of perforated members C20015 and C25015

The shear buckling investigations of perforated members were conducted on two plain C-lipped channel sections. The first chosen channel member in shear (C200), which has been

commonly used in Australia and New Zealand, was modelled with a web depth of 200 mm, a flange of 75 mm, and a lip size of 15 mm. The second cold-formed channel (C250), which is popular for members subjected to shear in the US, has a higher web depth of 250 mm and shorter flange width of 50 mm, and the same lip size of 15 mm. The effects of different thicknesses on the buckling behaviour and buckling loads were also investigated. The series of thicknesses chosen includes 1.0, 1.5, 1.9 and 2.4 mm, which are common thicknesses of members in practice.

The shear buckling modes of perforated members C20015 and C25015 (i.e. 200 and 250 mm deep channels with a thickness of 1.5 mm) with small web openings (40x80 mm) and substantial large web holes (120x240 mm) in both Case B and Case C are shown in **Fig 4.10**. The lengths of the channels C20015 and C25015 are 400 and 500 mm respectively (i.e. AR = 2.0). In general, the local buckling mode shapes for Case C are symmetrical about the diagonal axis resulting from a pair of equal moments acting at two end sections in the same direction. When moment is applied at one end in Case B, the shear buckles are more severe at one corner of the holes. Further, in the cases of large openings, the buckling mode shapes become more localised. It is noticeable that, with the same web opening sizes, the buckling shapes were also observed at the flanges of members C25015 due to higher bending as a result of longer shear span (500 mm). In addition, in the cases of substantially large web cut-outs, distortional buckling occurred at the flanges. This phenomenon is attributed to a reduction of the stiffness provided by the net web segments to the flanges.

The shear buckling coefficients (k_v) of the whole channel sections are determined based on the following conventional equation:

$$k_v = \frac{12(1-\mu^2)\left(\frac{h}{t}\right)^2 V_{cr}}{\pi^2 E A_w} \tag{4.2}$$

where V_{cr} is the shear buckling load extracted from the FEM buckling analyses, h is the depth of flat portion of the web, t is the thickness of the web, E is the Young's modulus, μ is the Poisson's ratio, and A_w is the cross-sectional area of web element.

The reduction in the shear buckling coefficients (k_v) of channel members C20015 and C25015 with central web holes resulting from the increase in hole sizes are illustrated in **Fig 4.11** where the values of k_v were back calculated using ***Eq (4.2)***. The ratio d_h/h of 0 refers to a channel without holes.

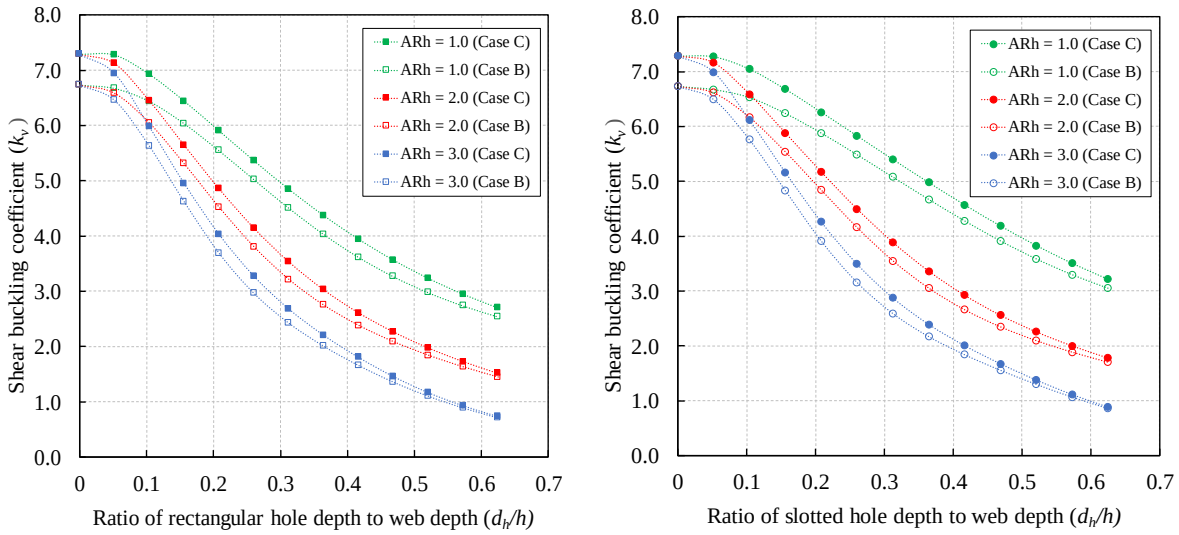

(a) Shear buckling coefficient (k_v) of perforated channel C20015 with various hole sizes

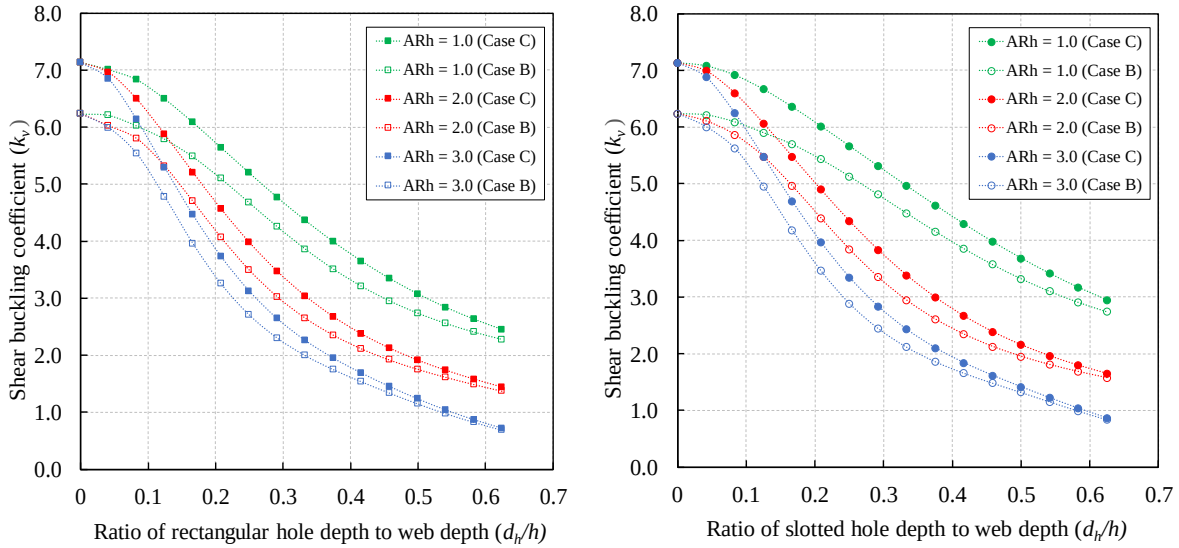

(b) Shear buckling coefficient (k_v) of perforated channel C25015 with various hole sizes

Fig 4.11: The influence of hole sizes on shear buckling coefficient (k_v) of perforated members C20015 and C25015

Overall, the shear buckling coefficients of channels with rectangular holes are lower than those with slotted openings resulting from the larger area of rectangular holes compared

to that of slotted openings of the same overall dimensions. The relationship curves for Case B have the same trend of reduction as those of Case C. The values k_v for Case B are always lower than those for Case C due to the compressive stress in the bottom flange and lip caused by bending moment at one end. Further, the larger the web opening area, the closer are the two relationship curves of Case B and Case C. It can be explained that shear governs the buckle of the whole section and there is no effect of bending at a very low shear buckling coefficient in both Case B and Case C. This was also recognised in the previous studies by C.H. Pham [11] and S.H. Pham [38].

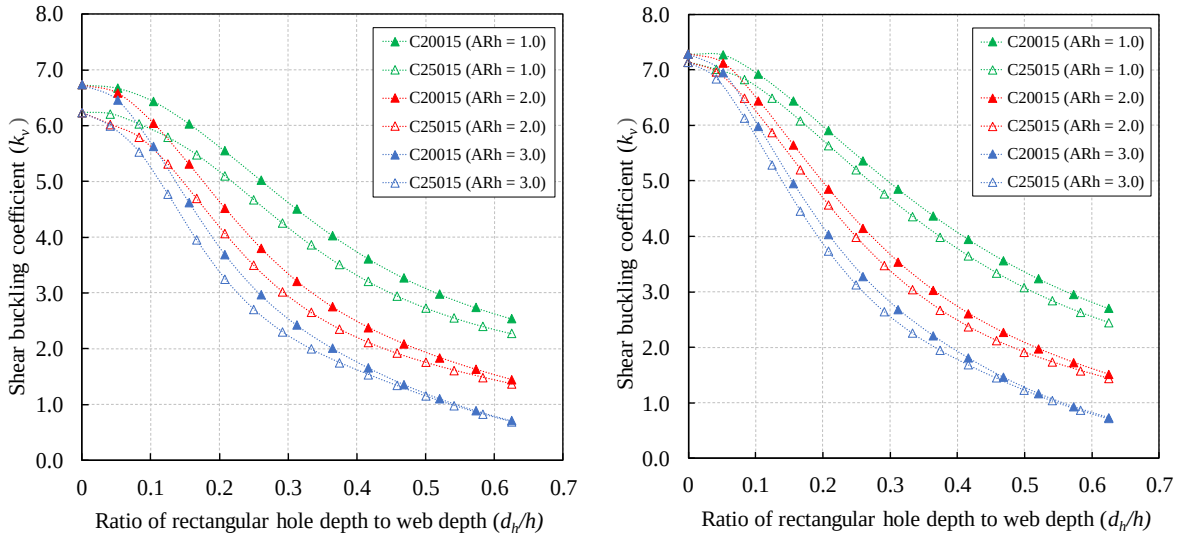

(Case B) (Case C)

Fig 4.12: Comparison of shear buckling coefficient (k_v) of members C20015 and C25015

A comparison of shear buckling coefficient (k_v) of channels C20015 and C25015 in both Case B and Case C is shown in **Fig 4.12**. The values of k_v with respect to C20015 are higher than those of C25015 due to a higher ratio of flange and web depth. However, it can be seen in **Fig 4.10** that flange widths of 75 and 50 mm are wide enough to provide elastic torsional restraint to the web of members C20015 and C25015 respectively. It is also interesting to note that the larger the web is perforated, the closer are the curves of k_v with respect to C20015 and C25015 in both Case B and Case C.

The influence of practical thicknesses on the values of k_v of perforated channel members in two cases $AR_h \geq 1.0$ and $AR_h < 1.0$ was investigated. As can be seen in **Fig 4.13**,

the curve for the thickness of 1.5 mm is almost identical to the curves for three other thickness (1.0, 1.9 and 2.4 mm), as depicted as the dashed curves in both Case B and Case C with the largest difference of 4.2 %. This demonstrates that the sensitivity of the elastic shear buckling coefficient (k_v) to member thickness is not significant under shear loads in different cases of stress distributions. As a result, the elastic shear buckling loads (V_{cr}) of perforated channel members can be determined from the same values of k_v regardless of different thicknesses.

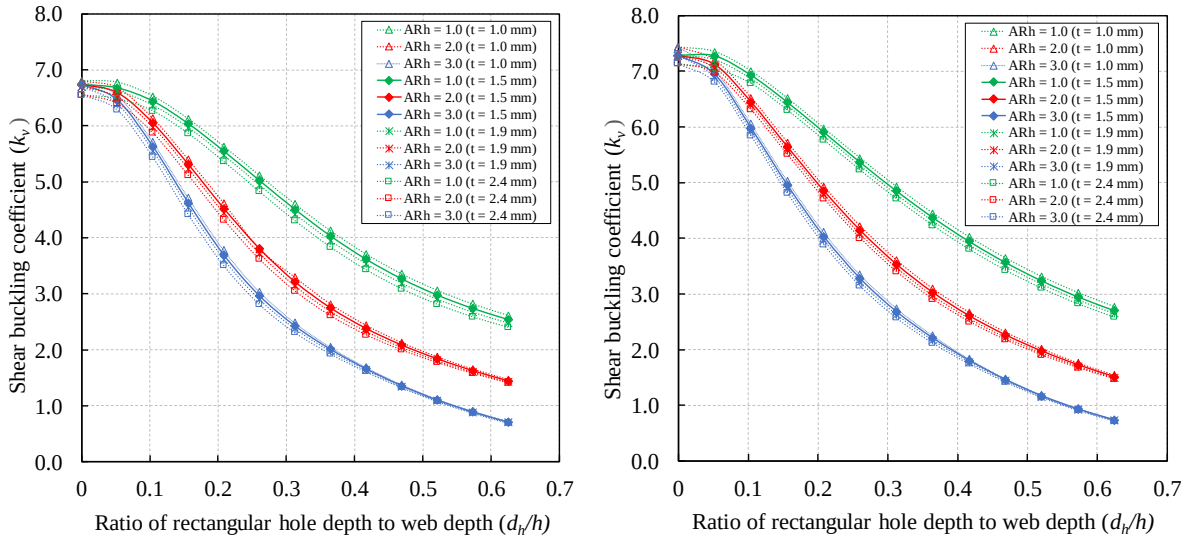

($AR_h \geq 1.0$, Case B) ($AR_h \geq 1.0$, Case C)

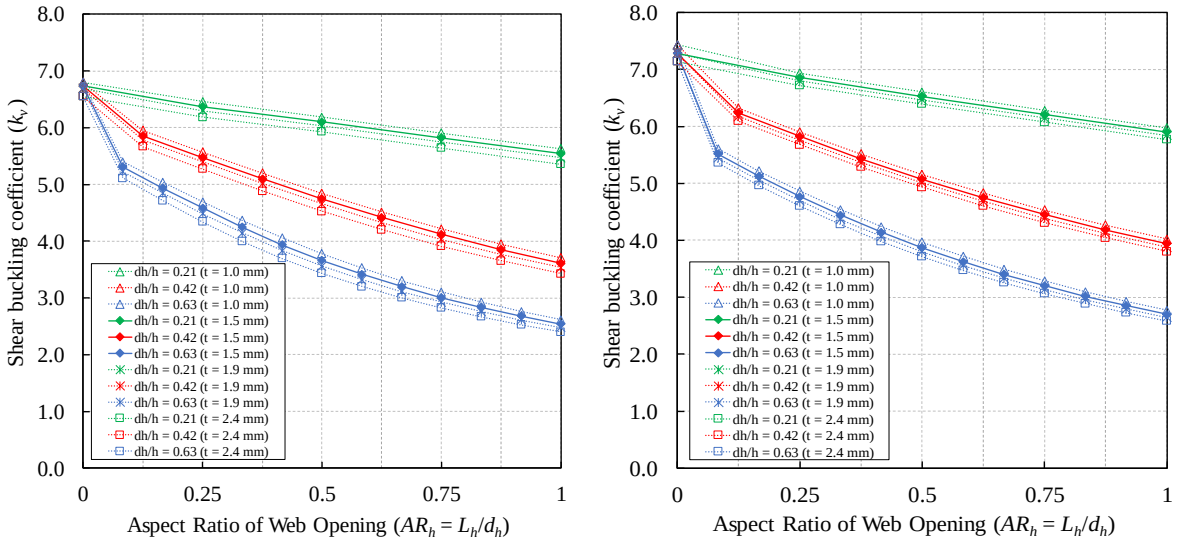

($AR_h \leq 1.0$, Case B) ($AR_h \leq 1.0$, Case C)

Fig 4.13: The influence of thickness on shear buckling coefficient (k_v) of perforated member C200 in both Cases B and C

On the basis of elastic shear buckling analyses of perforated channel members with both horizontally and vertically elongated web holes with a very wide range of holes sizes from a very small size (10x10 mm) to very large dimensions (120x360 and 150x450 mm) in the web of members C20015 and C25015 respectively, a dimensional transformation has been established to transform the dimensions of an actual slotted web opening into the equivalent sizes of a rectangular hole. A series of dimensional transforming equations is expressed as follows:

$$A_{h-eq} = 0.865 A_h \tag{4.3a}$$

With $\frac{L_h}{d_h} \le 1.0$:

$$\begin{cases} L_{h-eq} = \left(0.003 \frac{d_h}{L_h} + 0.822 \right) L_h \\ d_{h-eq} = \frac{A_{h-eq}}{L_{h-eq}} \end{cases} \tag{4.3b}$$

With $\frac{L_h}{d_h} \ge 1.0$:

$$\begin{cases} d_{h-eq} = \left(0.003 \frac{L_h}{d_h} + 0.822 \right) d_h \\ L_{h-eq} = \frac{A_{h-eq}}{d_{h-eq}} \end{cases} \tag{4.3c}$$

where A_h is the original area of a slotted hole, A_{h-eq} is the area of the transformed rectangular hole, L_{h-eq} is the transformed hole length, and d_{h-eq} is the transformed hole depth.

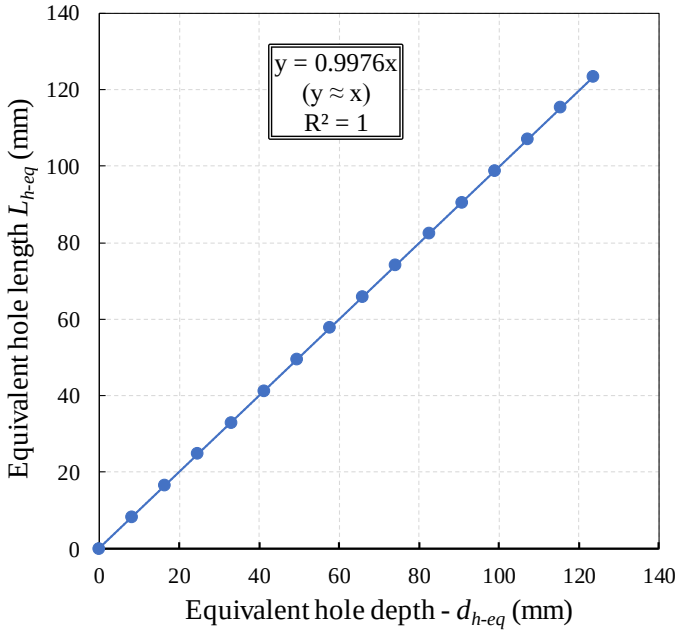

Fig 4.14: Transformed hole depths and lengths with AR_h = 1.0

The equivalent dimensions of holes including the transformed hole depths and lengths with $AR_h = L_h/d_h = 1.0$ determined based on ***Eq (4.3)*** are plotted in **Fig 4.14**. A linear regression line is generated to fit all the calculated points and the linear regression equation ($L_{h-eq} \approx d_{h-eq}$) of the fitting line demonstrates that the transformed hole shape of slotted openings with $AR_h = 1.0$ (circular holes) are squares. Further, when slotted holes become circular shapes, the ratio of the original hole length (L_h) to the original hole depth (d_h) is 1:1. Substituting this hole aspect ratio of 1.0 into ***Eqs (4.3b,c)*** obtains the relations $d_{h-eq} = 0.825 d_h$ and $L_{h-eq} = 0.825 L_h$ respectively. This proves that the transforming expressions for elongated circular web openings in case of $AR_h = 1.0$ are very consistent with the transformation ($d = 0.825\ D$) proposed by S.H. Pham et al. [16] and S.H. Pham [38] for circular and square holes with both shear aspect ratios (AR) of 1.0 and 2.0 where d is the square size and D is the circle diameter.

As can be seen in **Fig 4.15** where the results of shear buckling analyses with various dimensions of slotted web openings and corresponding transformed rectangular holes are illustrated, the shear buckling coefficients of channels with the original web openings are very consistent with the results obtained from models with transformed hole sizes based on ***Eq (4.3)***. It was found that the dimensional transformation produced very close shear buckling coefficients with the largest difference of 3.14 %. It is proven that the values of shear buckling coefficients (k_v) and shear buckling loads (V_{cr}) on the basis of the transforming expressions are capable of being used for the shear buckling analyses with the sizes of slotted web openings under this study. Further, as mentioned above, the member thickness is insensitive to the elastic shear buckling coefficients (k_v). Therefore, the dimensional transformation based on ***Eq (4.3)*** can be used to determine the values k_v and V_{cr} of perforated members with different thicknesses.

In order to generate the shear buckling loads (V_{cr}) of perforated channel members with various hole sizes, the simplified FE models for buckling analyses were constructed using Python code which is used as a script to run the modelling and the eigenvalue analyses to extract the buckling loads and buckling modes. The script is shown in **Appendix G**.

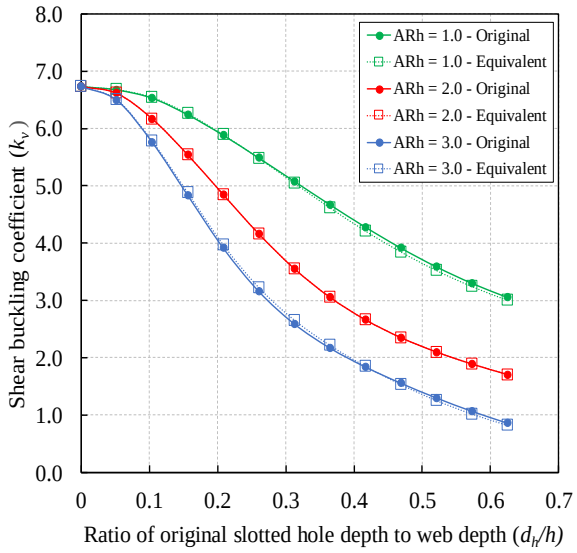

($AR_h \geq 1.0$, Case B)

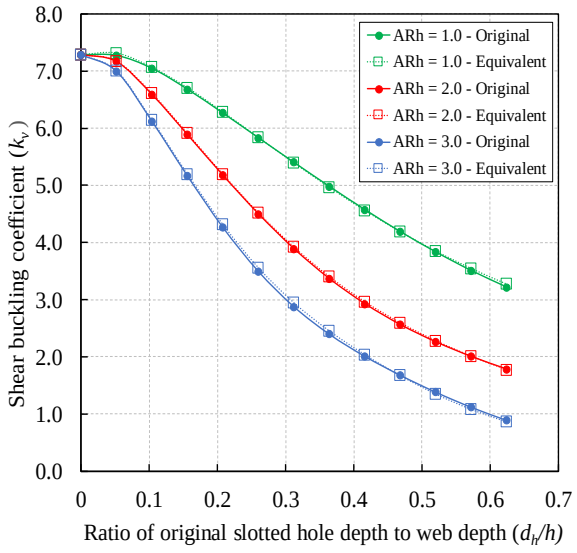

($AR_h \geq 1.0$, Case C)

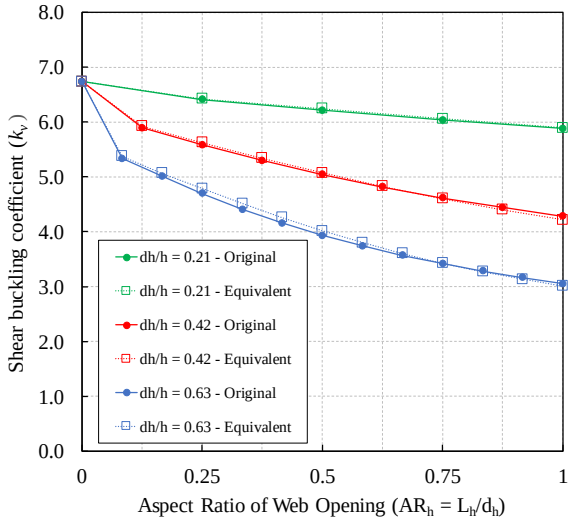

($AR_h \leq 1.0$, Case B)

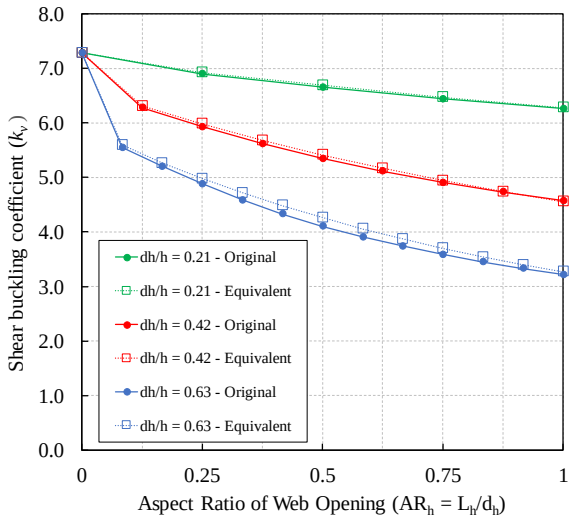

($AR_h \leq 1.0$, Case C)

(a) Shear buckling coefficient (k_v) of channel C20015 with original and transformed slotted holes

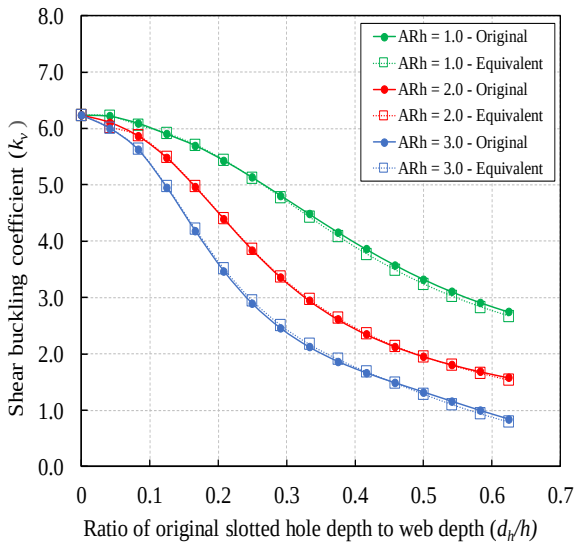

($AR_h \geq 1.0$, Case B)

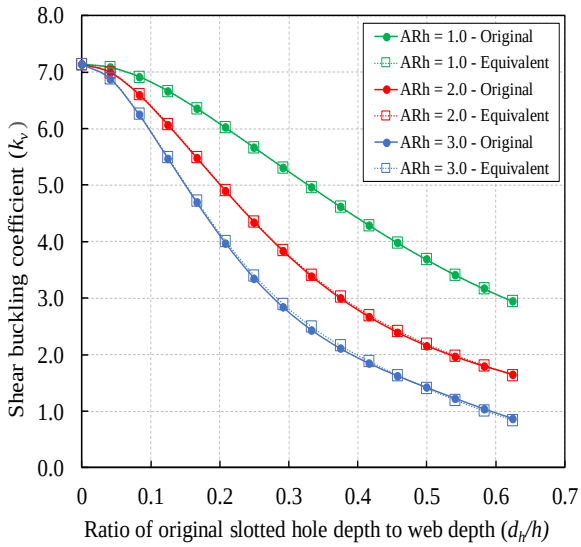

($AR_h \geq 1.0$, Case C)

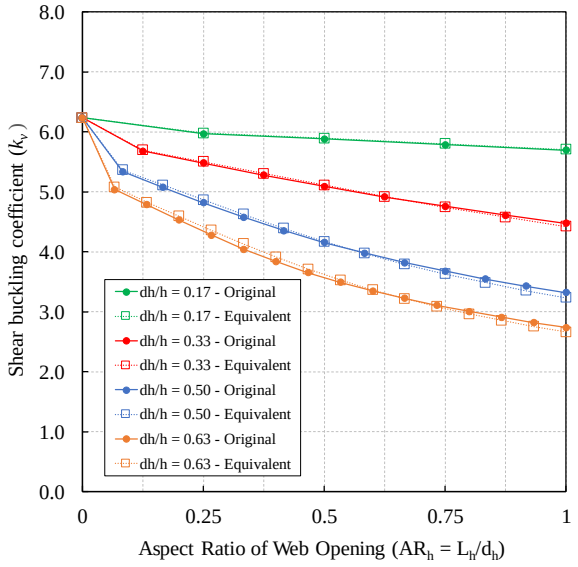

($AR_h \leq 1.0$, Case B)

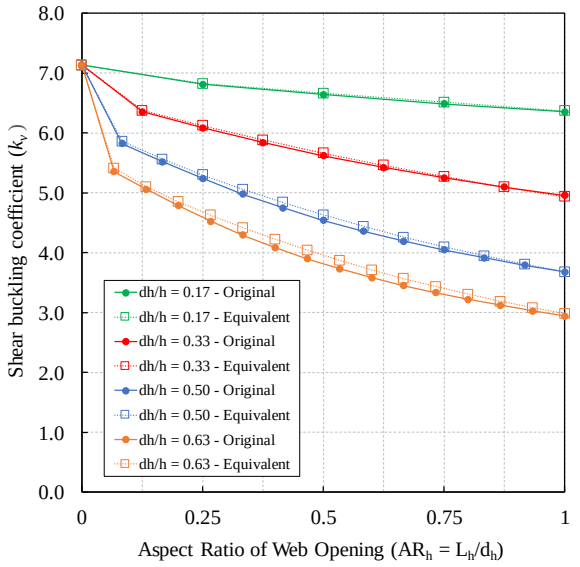

($AR_h \leq 1.0$, Case C)

(b) Shear buckling coefficient (k_v) of channel C25015 with original and transformed slotted holes

Fig 4.15: Shear buckling coefficients of original and transformed slotted holes

4.4.2 Parametric Study for Ultimate Shear Strength Analysis

Due to the accurate calibration of the FEM against the test results, the FE models are further employed to perform an extension of the test database and to evaluate the applicability of the dimensional transformation in terms of ultimate shear strength analysis.

In **Tables 4.3** and **4.4**, where a verification of the dimensional transformation on channels C200 and C250 are shown, typical designations "C20015-40x80" and "C25015-40x80" are defined as follows:

- 'C200' and 'C250' indicate channel sections with the web depths of 200 and 250 mm respectively
- '15' indicates the nominal thickness times 10 in mm (alternatively '10', '19', '24' indicate the nominal thicknesses of 1.0, 1.9 and 2.4 mm respectively)
- '40x80' indicates the original slotted web hole of d_h = 40 mm in depth and L_h = 80 mm in total length

The average yield stress f_y for 1.5 mm thick members is obtained from the tensile coupon tests in this study. The other values of f_y are collected from the tensile coupon tests conducted by C. H. Pham [64]. The ultimate shear strengths ($V_{n\text{-}eq}$) of the channels with transformed web openings are also included. It is noted that the equivalent shear strengths ($V_{n\text{-}eq}$) are extracted from shear strength analyses using FE models with equivalent hole dimensions ($d_{h\text{-}eq}$ and $L_{h\text{-}eq}$).

Table 4.3: Verification of dimensional transformation for shear strength of channel C200 with slotted holes

Designation	t (mm)	d_h (mm)	L_h (mm)	$d_{h\text{-}eq}$ (mm)	$L_{h\text{-}eq}$ (mm)	f_y (MPa)	V_n (kN)	$V_{n\text{-}eq}$ (kN)	Variance (%)
C20010-40x40	1.0	40	40	33.00	32.92	585.11	24.17	24.88	2.94
C20010-40x80	1.0	40	80	33.12	74.59	585.11	21.72	22.56	3.87
C20010-40x120	1.0	40	120	33.24	115.96	585.11	19.49	20.33	4.31
C20010-80x80	1.0	80	80	66.00	65.85	585.11	18.10	18.55	2.49
C20010-80x160	1.0	80	160	66.24	149.18	585.11	13.34	14.22	6.60
C20010-80x240	1.0	80	240	66.48	231.92	585.11	9.99	10.75	7.61
C20010-120x120	1.0	120	120	99.00	98.77	585.11	10.89	11.43	4.96
C20010-120x240	1.0	120	240	99.36	223.77	585.11	6.73	7.32	8.77
C20010-120x360	1.0	120	360	99.72	347.88	585.11	4.28	4.77	11.45
C20015-40x40	1.5	40	40	33.00	32.92	542.87	44.19	44.72	1.20

C20015-40x80	1.5	40	80	33.12	74.59	542.87	41.42	42.32	2.17
C20015-40x120	1.5	40	120	33.24	115.96	542.87	35.97	36.86	2.47
C20015-80x80	1.5	80	80	66.00	65.85	542.87	32.98	33.73	2.27
C20015-80x160	1.5	80	160	66.24	149.18	542.87	24.15	24.71	2.32
C20015-80x240	1.5	80	240	66.48	231.92	542.87	17.98	18.82	4.67
C20015-120x120	1.5	120	120	99.00	98.77	542.87	21.55	22.09	2.51
C20015-120x240	1.5	120	240	99.36	223.77	542.87	11.74	12.32	4.94
C20015-120x360	1.5	120	360	99.72	347.88	542.87	7.61	8.13	6.83
C20019-40x40	1.9	40	40	33.00	32.92	510.48	66.83	68.21	2.06
C20019-40x80	1.9	40	80	33.12	74.59	510.48	58.00	59.88	3.24
C20019-40x120	1.9	40	120	33.24	115.96	510.48	50.67	52.11	2.84
C20019-80x80	1.9	80	80	66.00	65.85	510.48	48.83	50.13	2.66
C20019-80x160	1.9	80	160	66.24	149.18	510.48	34.58	35.88	3.76
C20019-80x240	1.9	80	240	66.48	231.92	510.48	26.12	26.86	2.83
C20019-120x120	1.9	120	120	99.00	98.77	510.48	31.37	32.33	3.06
C20019-120x240	1.9	120	240	99.36	223.77	510.48	17.36	18.02	3.80
C20019-120x360	1.9	120	360	99.72	347.88	510.48	10.86	11.76	4.42
C20024-40x40	2.4	40	40	33.00	32.92	483.49	92.06	94.23	2.36
C20024-40x80	2.4	40	80	33.12	74.59	483.49	84.18	85.11	1.10
C20024-40x120	2.4	40	120	33.24	115.96	483.49	72.01	73.56	2.15
C20024-80x80	2.4	80	80	66.00	65.85	483.49	71.09	72.77	2.36
C20024-80x160	2.4	80	160	66.24	149.18	483.49	48.93	50.12	2.43
C20024-80x240	2.4	80	240	66.48	231.92	483.49	35.79	37.02	3.44
C20024-120x120	2.4	120	120	99.00	98.77	483.49	45.52	46.56	2.28
C20024-120x240	2.4	120	240	99.36	223.77	483.49	23.96	25.36	5.84
C20024-120x360	2.4	120	360	99.72	347.88	483.49	15.32	16.17	5.55

Table 4.4: Verification of dimensional transformation for shear strength of channel C250 with slotted holes

Designation	t (mm)	d_h (mm)	L_h (mm)	$d_{h\text{-}eq}$ (mm)	$L_{h\text{-}eq}$ (mm)	f_y (MPa)	V_n (kN)	$V_{n\text{-}eq}$ (kN)	Variance (%)
C25010-40x40	1.0	40	40	33.00	32.92	585.11	26.92	27.06	0.52
C25010-40x80	1.0	40	80	33.12	74.59	585.11	23.62	24.77	4.87
C25010-40x120	1.0	40	120	33.24	115.96	585.11	20.99	22.13	5.43
C25010-80x80	1.0	80	80	66.00	65.85	585.11	19.61	21.05	7.34
C25010-80x160	1.0	80	160	66.24	149.18	585.11	15.63	16.02	2.50
C25010-80x240	1.0	80	240	66.48	231.92	585.11	12.74	13.32	4.55
C25010-120x120	1.0	120	120	99.00	98.77	585.11	14.23	15.16	6.54
C25010-120x240	1.0	120	240	99.36	223.77	585.11	9.85	10.78	9.44
C25010-120x360	1.0	120	360	99.72	347.88	585.11	7.22	7.56	4.71
C25010-150x150	1.0	150	150	123.75	123.46	585.11	10.56	11.48	8.71
C25010-150x300	1.0	150	300	124.20	279.72	585.11	6.34	7.11	12.15
C25010-150x450	1.0	150	450	124.65	434.84	585.11	4.31	4.91	13.92
C25015-40x40	1.5	40	40	33.00	32.92	542.87	50.12	50.31	0.38
C25015-40x80	1.5	40	80	33.12	74.59	542.87	47.47	48.36	1.87

C25015-40x120	1.5	40	120	33.24	115.96	542.87	42.43	42.45	0.05
C25015-80x80	1.5	80	80	66.00	65.85	542.87	40.14	40.49	0.87
C25015-80x160	1.5	80	160	66.24	149.18	542.87	32.50	33.84	4.12
C25015-80x240	1.5	80	240	66.48	231.92	542.87	26.15	26.62	1.80
C25015-120x120	1.5	120	120	99.00	98.77	542.87	29.38	30.87	5.07
C25015-120x240	1.5	120	240	99.36	223.77	542.87	19.75	20.67	4.66
C25015-120x360	1.5	120	360	99.72	347.88	542.87	14.00	15.28	9.14
C25015-150x150	1.5	150	150	123.75	123.46	542.87	21.79	22.97	5.42
C25015-150x300	1.5	150	300	124.20	279.72	542.87	12.38	13.25	7.03
C25015-150x450	1.5	150	450	124.65	434.84	542.87	8.09	8.77	8.41
C25019-40x40	1.9	40	40	33.00	32.92	510.48	73.14	73.56	0.57
C25019-40x80	1.9	40	80	33.12	74.59	510.48	67.37	68.02	0.96
C25019-40x120	1.9	40	120	33.24	115.96	510.48	62.12	62.98	1.38
C25019-80x80	1.9	80	80	66.00	65.85	510.48	61.46	63.12	2.70
C25019-80x160	1.9	80	160	66.24	149.18	510.48	46.02	47.00	2.13
C25019-80x240	1.9	80	240	66.48	231.92	510.48	36.24	37.11	2.40
C25019-120x120	1.9	120	120	99.00	98.77	510.48	42.75	43.76	2.36
C25019-120x240	1.9	120	240	99.36	223.77	510.48	27.67	28.55	3.18
C25019-120x360	1.9	120	360	99.72	347.88	510.48	19.19	20.22	5.37
C25019-150x150	1.9	150	150	123.75	123.46	510.48	31.91	32.76	2.66
C25019-150x300	1.9	150	300	124.20	279.72	510.48	17.28	18.33	6.08
C25019-150x450	1.9	150	450	124.65	434.84	510.48	11.14	12.02	7.90
C25024-40x40	2.4	40	40	33.00	32.92	483.49	105.83	107.66	1.73
C25024-40x80	2.4	40	80	33.12	74.59	483.49	97.78	99.03	1.28
C25024-40x120	2.4	40	120	33.24	115.96	483.49	88.76	89.55	0.89
C25024-80x80	2.4	80	80	66.00	65.85	483.49	86.98	88.65	1.92
C25024-80x160	2.4	80	160	66.24	149.18	483.49	67.70	68.39	1.02
C25024-80x240	2.4	80	240	66.48	231.92	483.49	50.38	51.56	2.34
C25024-120x120	2.4	120	120	99.00	98.77	483.49	65.50	66.78	1.95
C25024-120x240	2.4	120	240	99.36	223.77	483.49	38.89	39.65	1.95
C25024-120x360	2.4	120	360	99.72	347.88	483.49	26.21	27.12	3.47
C25024-150x150	2.4	150	150	123.75	123.46	483.49	46.43	47.98	3.34
C25024-150x300	2.4	150	300	124.20	279.72	483.49	23.97	25.29	5.51
C25024-150x450	2.4	150	450	124.65	434.84	483.49	15.13	16.16	6.81

In **Tables 4.3** and **4.4**, the verifications of dimensional transformation for shear strength of channels C200 and C250 with a wide range of hole aspect ratios (AR_h) from 1.0 up to 3.0 are conducted. The shear strengths (V_n) of channels with original slotted web openings are compared to those with equivalent holes ($V_{n\text{-}eq}$). The shear strengths (V_n) used in this section are collected from the results of shear tests ($V_{n,test}$) and extended database using FE models for shear strength analyses ($V_{n,FEM}$). The equivalent hole dimensions are calculated using ***Eq (4.3)*** which is proposed based on the parametric study of elastic shear buckling analysis. It can be seen in **Tables 4.3** and **4.4** that the shear strengths ($V_{n\text{-}eq}$) with respect to transformed holes are

generally close to those of channels with original slotted holes, even in the cases of greatly elongated openings (AR_h = 3.0). It is also interesting to observe that the dimensional transformation works well with all the different practical member thicknesses from 1.0 to 2.4 mm. Although the highest variance obtained from the verifications is up to 13.92 % for a slotted hole with an AR_h = 3.0, this error is acceptable for Direct Strength Method (DSM) design as verified later in Chapter 5.

4.5 CHAPTER CONCLUSION

On the basis of the finite element model validation of test results as presented in Section 4.2.4, it can be concluded that the FE models developed in this study are able to capture the shear behaviour of cold-formed channel sections with web elongated holes. Therefore, all the shear strengths extracted from the numerical non-linear simulations are close to pure shear capacity. Further, it is found that the effect of the initial geometrical imperfections on the shear failure modes and shear strengths of cold-formed channels with web holes is insignificant.

Based on the comparisons between the simplified FE models and the full FE models in terms of shear buckling modes and shear buckling loads, it is proven that the simplified models are able to capture the shear buckling behaviour of cold-formed channel sections with web elongated holes. Thus, the shear buckling coefficient (k_v) calculated from the shear buckling loads (V_{cr}) of the simplified FE models are reliable.

The dimensional transformation for slotted holes suggested in this chapter are validated based on both the elastic shear buckling and ultimate shear strength analyses of different channel sections (C200 and C250) with practical thicknesses. As a consequence of the accurate predictions of both the buckling loads and shear strengths of the transformed sections, the transformation in dimensions of slotted and circular holes is further used for the Direct Strength Method (DSM) of design for channel sections in shear with non-elongated and elongated web holes. The applicability of the dimensional transformation proposed in this chapter to the DSM design for shear is further evaluated in Chapter 5.

Chapter 5

DIRECT STRENGTH METHOD FOR COLD-FORMED MEMBERS IN SHEAR WITH ELONGATED WEB OPENINGS

5.1 CHAPTER INTRODUCTION

This chapter summarises the Direct Strength Method (DSM) for cold-formed sections in shear with web openings on the basis of previous proposals including a suggestion based on net web area model and Vierendeel model by Unabia B. [14] and S.H. Pham et al. [16] respectively.

A comparison of Direct Strength Method (DSM) design loads for shear with predominantly shear tests of channel sections with rectangular and slotted web holes is conducted to evaluate the applicability of the previous proposals by Unabia B. [14] and S.H. Pham et al. [16] to the presence of elongated web openings. In order to reveal the limitations of the previous suggestions, the results from the shear tests presented in Chapter 3 are plotted against the current DSM shear curves with and without Tension Field Action (TFA) where the yield shear loads (V_y) are determined based on net web area model and Vierendeel model for the DSM of design for channel members in shear with square and circular web cut-outs. The shear elastic buckling loads (V_{cr}) used in the DSM are extracted from the elastic buckling analyses using the Finite Element Method (FEM) as presented in Chapter 4.

On the basis of the limitations of the previous proposals when applied to elongated holes, a new strategy for the determination of the shear yield loads together with the Vierendeel mechanism approach are presented in this chapter to propose a modified DSM design for perforated channels with both elongated and non-elongated web openings. The results from the shear tests and parametric studies presented in Chapters 3 and 4 including $V_{n,test}$, $V_{n,FEM}$, and V_{cr} are further used to verify the new DSM design of channels in shear with elongated web holes. Due to the good predictions of the transformation in both buckling loads and shear strengths as proven in Chapter 4, the same transformation is also used throughout this chapter.

5.2 DIRECT STRENGTH METHOD FOR COLD-FORMED CHANNELS IN SHEAR

5.2.1 DSM Design Rules for Unperforated Channel Members in Shear

The nominal shear strength (V_n) of channels without holes in the web and without web stiffeners excluding Tension Field Action (TFA) is determined from Section G2.1 in AISI S100-16 [4] as follows:

For $\lambda_v \le 0.815$: $V_n = V_y$ (5.1a)

For $0.815 < \lambda_v \le 1.227$: $V_n = 0.815\sqrt{V_{cr}.V_y}$ (5.1b)

For $\lambda_v > 1.227$: $V_n = V_{cr}$ (5.1c)

The nondimensional slenderness (λ_v), the yield shear load (V_y) of the web based on an average shear yield stress of 0.6 f_y, and the elastic shear buckling load of the whole section (V_{cr}) are computed respectively by:

$$\lambda_v = \sqrt{V_y / V_{cr}} \tag{5.2}$$

$$V_y = 0.6\, A_w f_y \tag{5.3}$$

$$V_{cr} = \frac{k_v \pi^2 E A_w}{12(1-\mu^2)\left(\frac{h}{t}\right)^2} \tag{5.4}$$

where k_v is the shear buckling coefficient for the whole section based on the results of shear buckling analyses by formula or FEM, h is the depth of the flat portion of the web; t is the thickness of the web, E is Young's modulus, μ is Poisson's ratio, A_w is the cross-sectional area of web element, and f_y is the design yield stress.

The nominal shear strength (V_n) of unperforated channels including Tension Field Action (TFA) is specified in Section G2.2 in AISI S100-16 [4] as follows:

For $\lambda_v \le 0.776$: $V_n = V_y$ (5.5a)

For $\lambda_v > 0.776$: $V_n = \left[1 - 0.15\left(\frac{V_{cr}}{V_y}\right)^{0.4}\right]\left(\frac{V_{cr}}{V_y}\right)^{0.4} V_y$ (5.5b)

where V_y and V_{cr} are given above in ***Eqs (5.3)*** and ***(5.4)*** respectively

5.2.2 DSM Design Rules for Perforated Channel Members in Shear with Square and Circular Web Holes

5.2.2.1 Proposal Based on Net Web Area Model

The DSM design for cold-formed channel sections with square and circular holes were proposed by Unabia B. [14] where the conventional shear yield load (V_y) is replaced by the proposed shear yield load based on net web area referred as $V_{y,net}$. This proposal is formulated by the following expression:

$$V_{y,net} = 0.6\left(h - d_h\right) f_y.t \tag{5.6}$$

where h is the depth of the web plate, d_h is the depth of the hole, t is the thickness of the web, and f_y is the design yield stress.

5.2.2.2 Proposal Based on Vierendeel Model

The DSM design for cold-formed channel sections with square and circular holes was proposed by S.H. Pham et al. [16] where the conventional shear yield load (V_y) is replaced by the proposed shear yield load based on the practical model referred as V_{yh}. This proposal has been recently recommended by S.H. Pham [13] for shear aspect ratios (AR) up to 2:1 and formulated by the following expressions:

$$\text{when } 0 < \frac{d_h}{h} \le 0.10, \qquad V_{yh} = V_y \tag{5.7a}$$

$$\text{when } 0.10 < \frac{d_h}{h} < 0.60, \qquad V_{yh} = V_y - 2\left(\frac{d_h}{h} - 0.1\right)\left(V_y - V_{vrd,0.6}\right) \tag{5.7b}$$

$$\text{when } 0.60 \le \frac{d_h}{h}, \qquad V_{yh} = V_{vrd} \tag{5.7c}$$

where d_h is the depth of the hole, h is the depth of the web plate. The shear load (V_{vrd}) of perforated sections with substantially large openings based on the Vierendeel mechanism is computed by:

$$V_{vrd} = \frac{4M_{pv}}{L_h} \tag{5.8}$$

where M_{pv} is the plastic bending capacity of the top (or bottom) segment above (or below) the opening, including the flanges and lips provided that the hole is centrally located, and L_h is the

length of the hole. $V_{vrd,0.6}$ is the value of V_{vrd} that is computed for the perforated section with the ratio d_h/h = 0.6.

5.3 COMPARISON OF DIRECT STRENGTH METHOD (DSM) DESIGN LOADS FOR SHEAR WITH PREDOMINANTLY SHEAR TESTS OF CHANNEL SECTIONS WITH RECTANGULAR AND SLOTTED WEB OPENINGS

5.3.1 Comparison Based on Net Web Area Model

The predominantly shear test results of lipped channel sections with central circular, square and elongated web openings with the aspect ratio (*AR*) of 2.0 in this study are plotted in **Fig 5.1** against both the current DSM design curves for shear without Tension Field Actions (TFA) and with TFA where the yield shear loads are taken as the yield loads based on the net web areas ($V_{y,net}$) by Unabia B. [14].

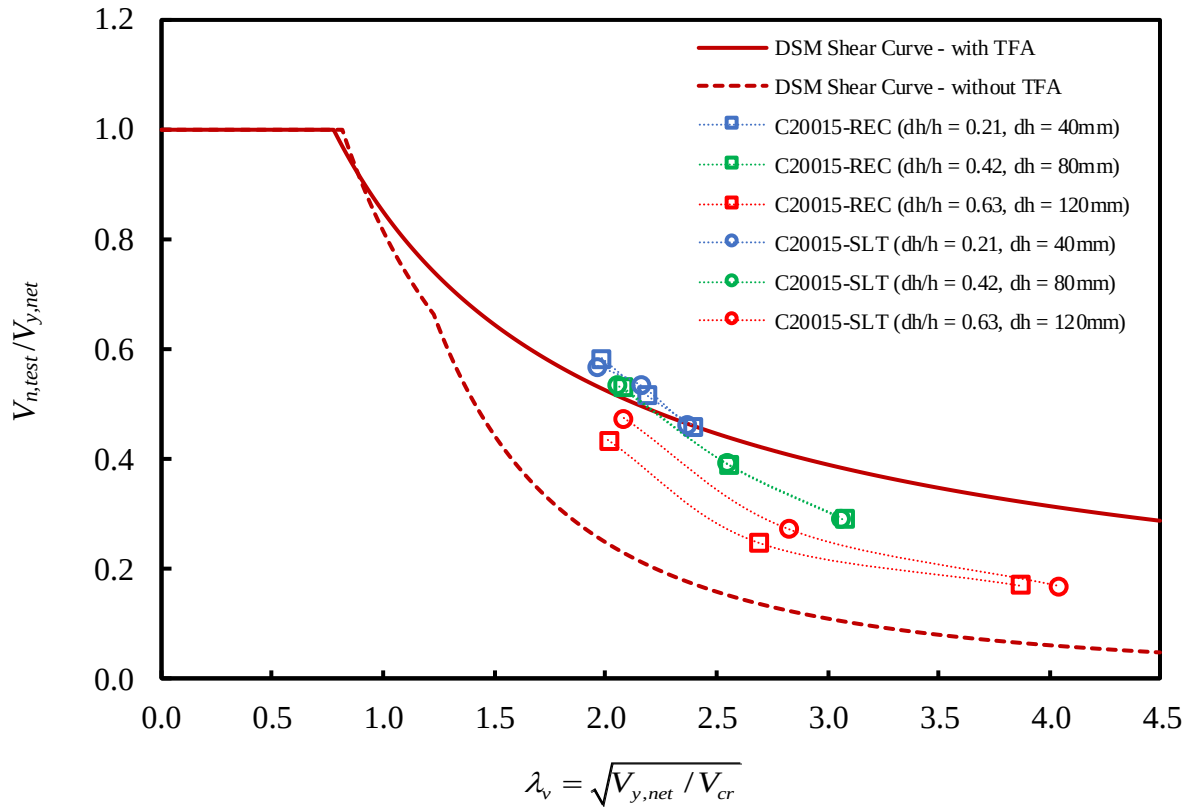

Fig 5.1: Shear test results based on $V_{y,net}$ versus DSM shear curves

The resulting points are classified into three groups according to the hole depths. The openings with the depths of 40, 80, and 120 mm are assigned separately to the blue, green, and

red dashed curves. The dotted and square points represent the results on channels with slotted and rectangular web openings respectively. The elastic shear buckling loads (V_{cr}) used in the DSM for shear in this section are extracted from the shear buckling analyses of the FE models including the web holes. The dimensions of the channel sections for determination of V_{cr} were taken from **Table 3.2**. The transformation in dimensions of slotted holes based on ***Eq (4.3)*** is applied to determine both the elastic shear buckling loads (V_{cr}) and the yield shear loads ($V_{y,net}$) of the channels with circular and slotted web openings. The determination of the test points plotted in **Fig 5.1** are shown in **Appendix B**.

It is very clear to see that there are the same trends occurring for all the groups which show that the resulting points are shifted down and horizontally to the right when the hole lengths increase. It can be explained by the reduction in the values of the elastic shear buckling loads (V_{cr}) and the shear strengths ($V_{n,test}$) resulting from extending the lengths of web openings together with the unchanged values of $V_{y,net}$ due to the same net sections in each group which causes an increase in the nondimensional slenderness (λ_v) and a decrease in the ratio of $V_{n,test}$ to $V_{y,net}$. All shear test points of the perforated sections with small hole sizes (the group of 40mm hole depth) lie on the DSM shear curve with TFA. It is interesting to note that while the test points with square and circular openings in the group of 80 mm hole depth are still very close to the DSM shear curve with TFA, the results with respect to extended hole lengths (L_h = 160 and 240 mm) deviate significantly from the DSM curve for shear with TFA and lie below this curve. The reason for this is a considerable drop in shear strengths of beams with larger web cut-outs (80x160 mm and 80x240 mm) as shown in **Fig 3.10**. In terms of channels with a very large hole depth (d_h = 120 mm), all the results are located well away from the DSM shear curve with TFA because of the dramatic reduction in shear strengths with substantial large openings resulting from large web cut-out areas. While the resulting points corresponding to the hole dimension of 120x120 mm are relatively equidistant from the two DSM shear curves, the resulting points for the perforated sections with larger hole aspect ratios (120x240 mm and 120x360 mm) lie closer to the DSM curve in shear without TFA. However, in comparison with the two groups having hole depths of 40 and 80 mm, there is not a sharp drop in the results for the channels with 120 mm hole depth when the hole lengths are elongated from 240 mm (AR_h = 2.0) to 360 mm (AR_h = 3.0). This is possibly because the shear resistance is still retained when the hole dimension is up to 120x360 mm according to the previous explanation based on

Fig 3.13. On the basis of characteristics observed from the comparison between the current DSM design for shear and the test results on channel sections with rectangular and slotted holes in this section where the yield shear loads are determined as the yield loads on the net web portion ($V_{y,net}$), the DSM shear curve with TFA may be applicable for design of channel sections with a certain range of hole dimensions. More specifically, with small hole depths of 40 mm, the DSM curve for shear with TFA can be utilised with hole aspect ratios up to 3.0. For larger hole depth (d_h = 80 mm), the adoption of the DSM shear curve with TFA can be acceptable for cases of AR_h up to 2.0. For very large hole depth ($d_h \geq$ 120 mm), the use of the DSM shear curve without TFA can be recommended because the channel members with large openings do not mobilise the Tension Field Action.

5.3.2 Comparison Based on Vierendeel Model

The changes in shear yield loads determined by ***Eqs (5.6)*** and ***(5.7)*** for perforated channels with various sizes of holes are illustrated on **Fig 5.2** where the values of $V_{y,net}$ and V_{yh} are represented respectively by the dashed line and coloured dotted solid curves. It is noted that the values of $V_{vrd,0.6}$ used for the determination of V_{yh} are the values of V_{vrd} computed for the perforated sections when $d_h = 0.6h$. The value of L_h for $V_{vrd,0.6}$ in ***Eq (5.8)*** is replaced by the product of the hole depth $d_h = 0.6h$ by the aspect ratio of the hole (AR_h) under consideration.

The predominantly shear tests and FEM results of lipped channel sections with central circular, square and elongated web openings with the shear span aspect ratio (AR) of 2.0 in this study where the yield shear loads are determined using V_{yh} in ***Eq (5.7)*** proposed by S.H. Pham [13] are plotted against the current DSM design curves for shear with and without Tension Field Actions (TFA) in **Fig 5.3**. The illustrations in **Fig 5.3** are similar to those in **Fig 5.1** with regard to the classification of resulting points. The elastic shear buckling loads (V_{cr}) in this section are extracted from results of shear buckling analyses on FEM models in Abaqus. The dimensions of the circular and slotted web openings used for the determination of both the elastic shear buckling loads (V_{cr}) and the yield shear loads based on V_{yh} are transformed into equivalent sizes calculated by ***Eq (4.3)***. The determination of the resulting points plotted in **Fig 5.3** are given in **Appendix C**.

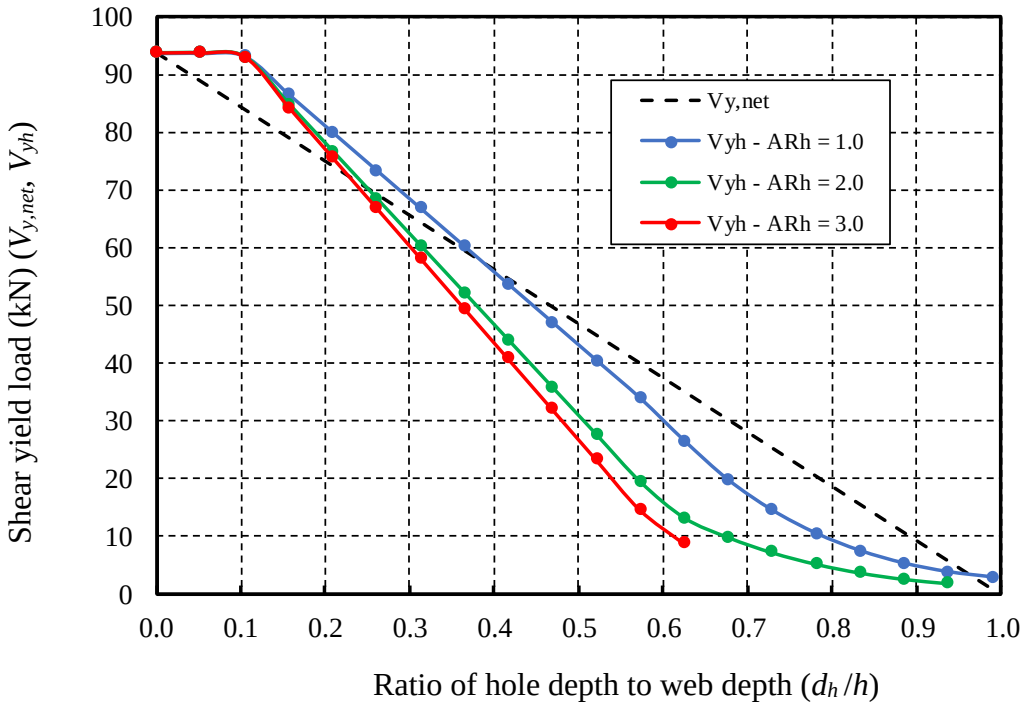

Fig 5.2: Shear yield loads based on the net web area model by Unabia B. [14] and Vierendeel model by S.H. Pham [13]

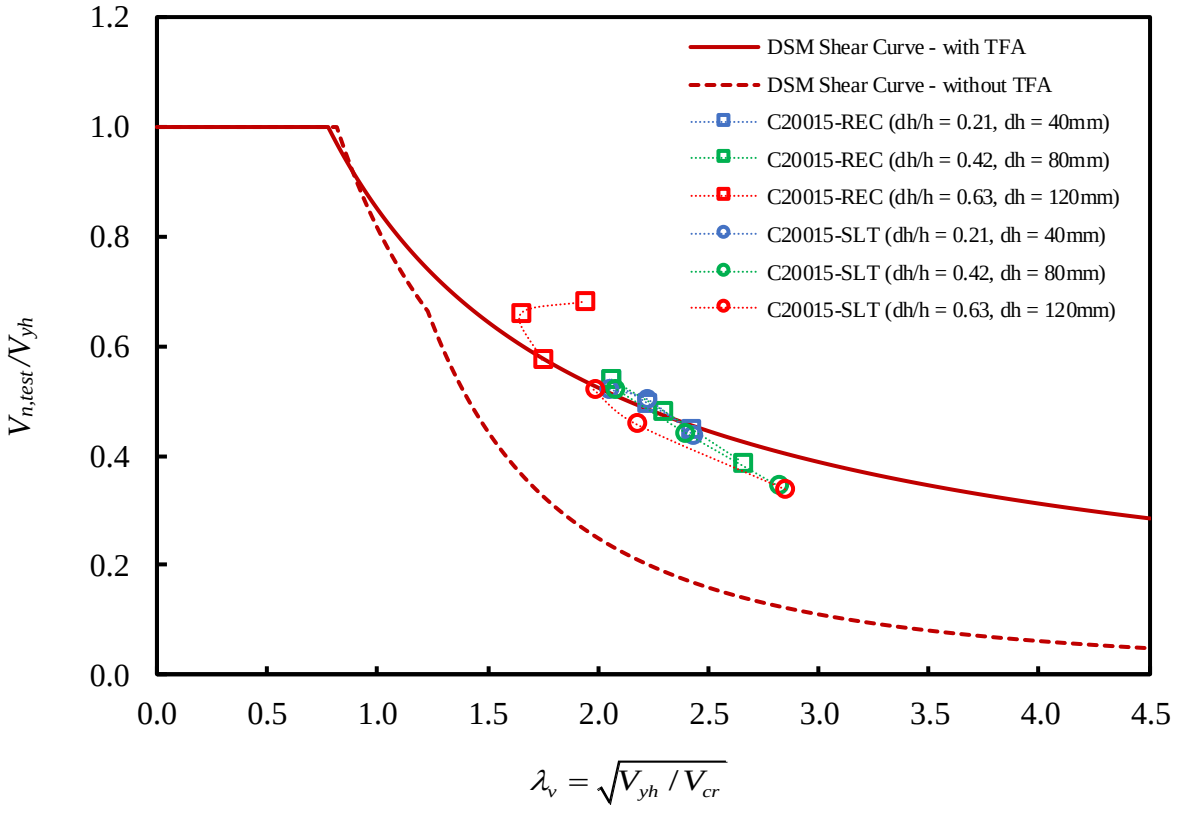

Fig 5.3: Shear test results based on V_{yh} versus DSM shear curves

As can be seen in **Fig 5.3**, nearly all the resulting points lie close to the DSM shear curve with TFA. This proves that the use of V_{yh} instead of $V_{y,net}$ produces a significant improvement in the predictions of the shear strengths of perforated sections with elongated web openings. In spite of a slight shift down to the right compared to the results based on $V_{y,net}$ on the same hole sizes, the positions of the resulting points with small cut-outs (40 mm in depth) are still very close to the DSM shear curve with TFA as for those based on $V_{y,net}$. This can be understood on the basis of a small change in the values of the shear yield loads with a hole depth of 40 mm (d_h /h = 0.2) as shown in **Fig 5.2**. It is also observed in **Fig 5.2** that there is an intersection of the black dashed line ($V_{y,net}$) and the blue dotted curve which displays the values of V_{yh} of perforated channels with AR_h = 1.0 around the ratio d_h /h of 0.4. As a result, the resulting points for the perforated channels with a hole dimension of 80x80 mm stay almost at the same positions as those determined based on $V_{y,net}$. Further, for elongated web cut-outs with the depth of 80 mm, the values of V_{yh} are lower than the those of $V_{y,net}$ as shown in **Fig 5.2**. This leads to left-upward movements of points for hole dimensions of 80x160 and 80x240 mm. It is also interesting to note in **Fig 5.3** that the resulting points for channels with equivalent slotted holes 120 mm in depth are also shifted up very significantly and horizontally to the left close to the DSM shear curve with TFA due to a dramatic decrease in yield shear load based on V_{yh}. For perforated sections with a very large hole depth (d_h = 120 mm) where the yield shear loads are determined based on the Vierendeel mechanism (V_{vrd}), the points for the channel with square web opening (AR_h = 1.0) lies on the DSM curve for shear with TFA, whereas this curve underestimates the shear test results of beams with the elongated holes (120x240 and 120x360 mm). On the basis of the comparison performed in this section, the DSM shear curve with TFA together with the yield shear loads (V_{yh}) by S.H. Pham [13] have applicability to the design of perforated channels with a wider range of elongated hole dimensions. This curve predicts well the shear strength of the member with an opening size up to 80x240 mm (AR_h = 3.0). For channels with larger and longer hole sizes, however, the results deviate from the DSM shear curve with TFA. While the design curve overestimates the ultimate shear strength of perforated members with slotted hole dimensions including 120x240 and 120x360 mm, the resulting points regarding rectangular hole sizes of 120x240 and 120x360 mm are located in the upper region of the DSM shear curve with TFA.

5.4 NEW METHOD FOR DETERMINATION OF SHEAR YIELD LOADS AND NEW PROPOSAL FOR DSM DESIGN FOR CHANNEL MEMBERS IN SHEAR WITH ELONGATED WEB OPENINGS

5.4.1 Motivation and New Strategy for Determination of Shear Yield Loads

It can be seen in **Fig 5.4** showing close-up views of the yielding pattern formed over perforated sections with substantial rectangular hole dimensions of 120x240 and 120x360 mm whose ductile behaviour in shear are explained based on the load-displacement relationships in **Fig 3.13**, plastic hinges have likely occurred locally in the vicinity of the hole corners. Based on the outcomes observed from the shear tests such as a parallelogram of web holes under pure shear and the formation of plastic hinges in regions of high shear, it can be asserted that the shear behaviour of the channels with large elongated web openings is governed by the Vierendeel action also recognised by S.H. Pham et al. [16] in the cases of large square and circular web openings. However, it is very interesting to note that the positions of the plastic hinges were not precisely at the two edge-sections of the cut-outs. This is a primary motivation for a new strategy to determine the shear yield loads of perforated members with elongated web holes as detailed below.

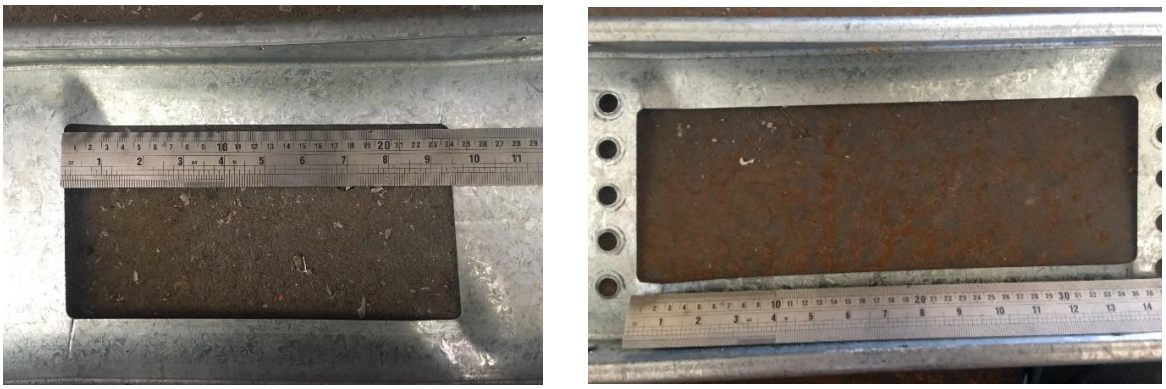

(a) C20015-REC-120x240 (b) C20015-REC-120x360

Fig 5.4: Close-up view of the yielding pattern formed over perforated sections with very large rectangular web openings

Due to the limited applicability of the proposals aforementioned to the prediction of shear strengths for channels with elongated web openings, a new strategy based on non-linear simulations using the FEM has been developed to determine shear yield loads ($V_{y,FEM}$) for the cases of elongated holes. The FE models for the determination of $V_{y,FEM}$ were constructed

similarly to the simulations by S.H. Pham [13] except for the hole shapes. The material properties of the cold-formed channels in the models were defined using stress-strain curves derived from the engineering stress-strain curves obtained from the coupon tests. The dimensions of the channel cross-sections in each of the models in this section were taken as average measured dimensions as shown in **Table 3.2**. In order to obtain the value of $V_{y,FEM}$ close to the theoretical shear yield load (i.e. the channels failing in yielding alone), the elements in the web and the lips in the FE models are laterally restrained to prevent the occurrence of any instability before the shear strengths of the beams reached the peak loads. The angle straps were retained to minimise the distortional deformation of the flanges. The values of $V_{y,FEM}$ are used to estimate the performance of the Vierendeel mechanism for each of hole size. Thereafter, a formulation of the proposed shear yield loads is carried out based on the shear loads derived from the Vierendeel action which is presented in the following sections.

5.4.2 Vierendeel Mechanism Approach

The Vierendeel mechanism has been well-known as a critical structural behaviour in perforated steel beams with single large web openings. When a perforated steel member is subjected to shear, two sectional segments above and below the perforated section carry a combination of forces including the applied global shear, the primary (global or convectional) moment and the secondary moment (the Vierendeel moment) due to the shear force acting over the length of the web holes. Thus, the Vierendeel mechanism is directly influenced by the length of the web openings. This was also stated by Chung et al. [65] and Tsavdaridis & D'Mello [66].

Fig 5.5 shows an examination of the stress distributions in the channels with rectangular hole dimensions of 120x240 and 120x360 mm at both first yield and failure conditions. It is very clearly observed that a symmetrical yielding pattern about the centre of the cut-out and the formation of plastic hinges occurs which are developed fully around the hole corners and spread out to the flanges and lips. This demonstrates that the channels failed in yielding under a pair of equal shear forces and bending moments at the two ends of the shear span. Further, the plastic hinges spread more towards the middle of the shear span. According to Tsavdaridis & D'Mello [66], the exact positions of the plastic hinges around the corners of the web openings are determined via a term (φ_p) which is an angle taken from the low moment side (LMS) and the vertical centre-line of the web opening. The critical opening length (L_h') (i.e.

the distance between plastic hinges along the span length) is then determined from φ_p. However, this approach is not adopted in this study because of the difference in the member sections, the material properties, and the test configurations. A scheme describing the Vierendeel mechanism in the case where the member is subjected to a pure shear and where the plastic hinges are located in two sections 1'-1' and 2'-2' is shown in **Fig 5.6**.

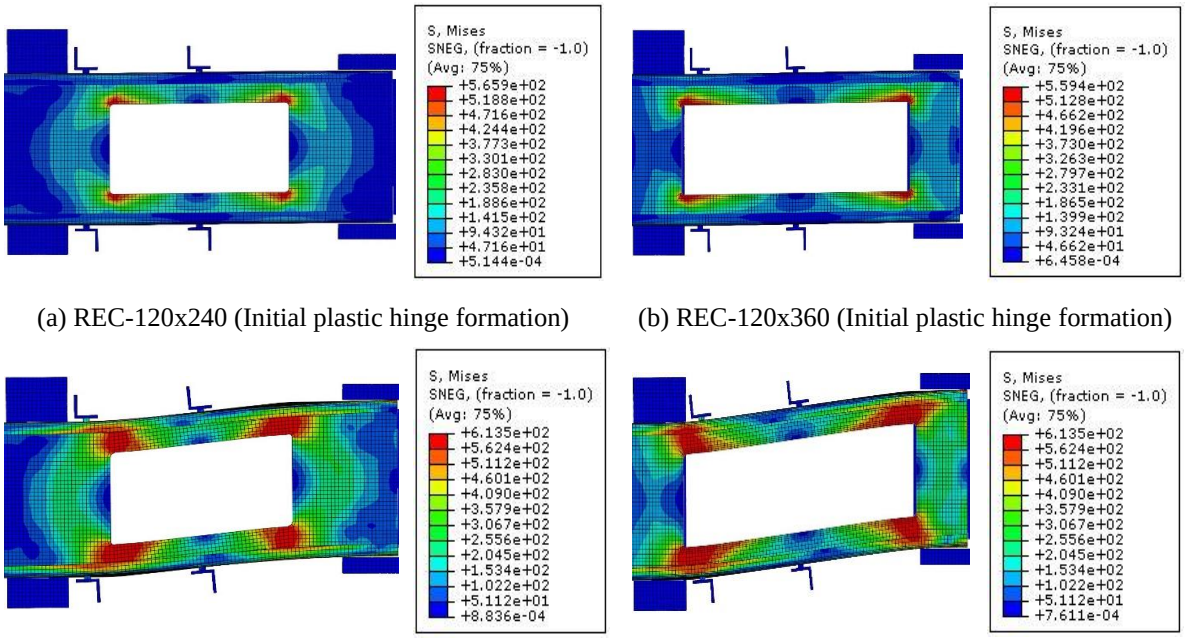

(a) REC-120x240 (Initial plastic hinge formation) (b) REC-120x360 (Initial plastic hinge formation)

(c) REC-120x240 (Yielding pattern at failure) (d) REC-120x360 (Yielding pattern at failure)

Fig 5.5: Close-up view of the yielding pattern formed over perforated sections with very large rectangular web openings

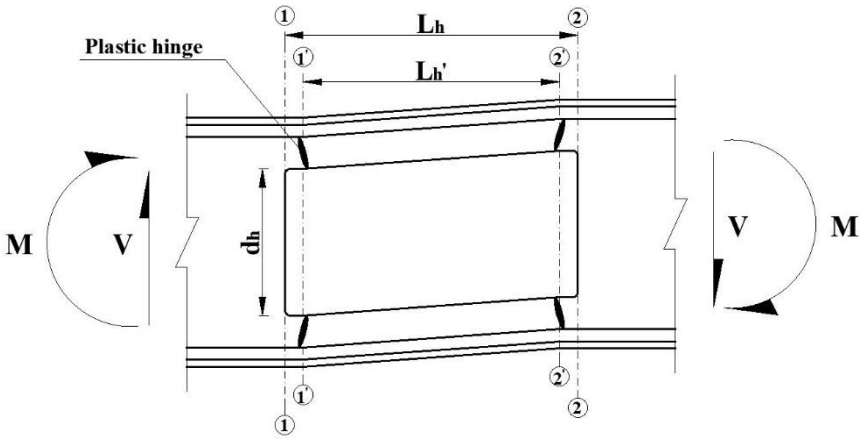

Fig 5.6: Vierendeel mechanism and location of plastic hinges for C-channels in shear with elongated holes

The value of L_h' can be determined by investigating an indicative parameter (v_i) called the 'Vierendeel parameter' which was proposed by Chung et al. [65] and applied by Tsavdaridis & D'Mello [66] to estimate the performance of the Vierendeel mechanism in perforated sections. The value of v_i is determined by the following expression:

$$v_i = \frac{V_{y,FEM}}{V_{vrd}} \tag{5.9}$$

where $V_{y,FEM}$ is the peak load extracted from the FE models with lateral restraints in the web and the lips, and V_{vrd} is the shear yield loads based on the Vierendeel mechanism determined by ***Eq (5.8)***.

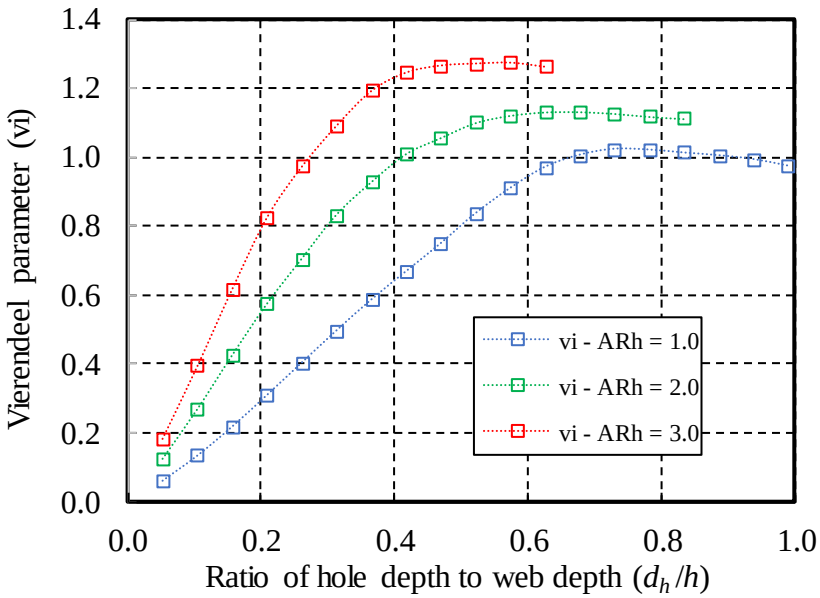

Fig 5.7: Performance of the Vierendeel mechanism in perforated sections

The Vierendeel parameter (v_i) is plotted in **Fig 5.7** against the ratio of d_h/h. The values of v_i become more than 1.0 when the d_h/h ratios become larger than 0.40 and 0.25 for the cases of AR_h = 2.0 and 3.0 respectively. The reason for this is that the hole length (L_h) which is used to determine V_{vrd} is larger than the actual horizontal distance between the plastic hinges (L_h') (i.e. the plastic hinges lie inside the region of hole length). For determination of the critical hole dimensions where the Vierendeel failure mechanism is triggered, plots of the shear yield loads ($V_{y,FEM}$ and $V_{vrd}.v_i$) against the ratio d_h/h are shown in **Fig 5.8** where the value of v_i is

based on both the hole length (L_h) and the hole depth (d_h) using the following quadratic relationship:

$$v_i = 0.745 + 0.28.\left(\frac{L_h}{d_h}\right) - 0.025.\left(\frac{L_h}{d_h}\right)^2 \tag{5.10}$$

From the graph shown in **Fig 5.8**, the transition points where the shear yield load curves start fitting the Vierendeel curves factored by v_i correspond to the critical hole dimensions. Hence, the critical length of the web openings (L_h'), when the Vierendeel mechanism occurs, are inversely proportional to the total length of the web holes (L_h) as follows:

$$L_h' = \frac{L_h}{v_i} \tag{5.11}$$

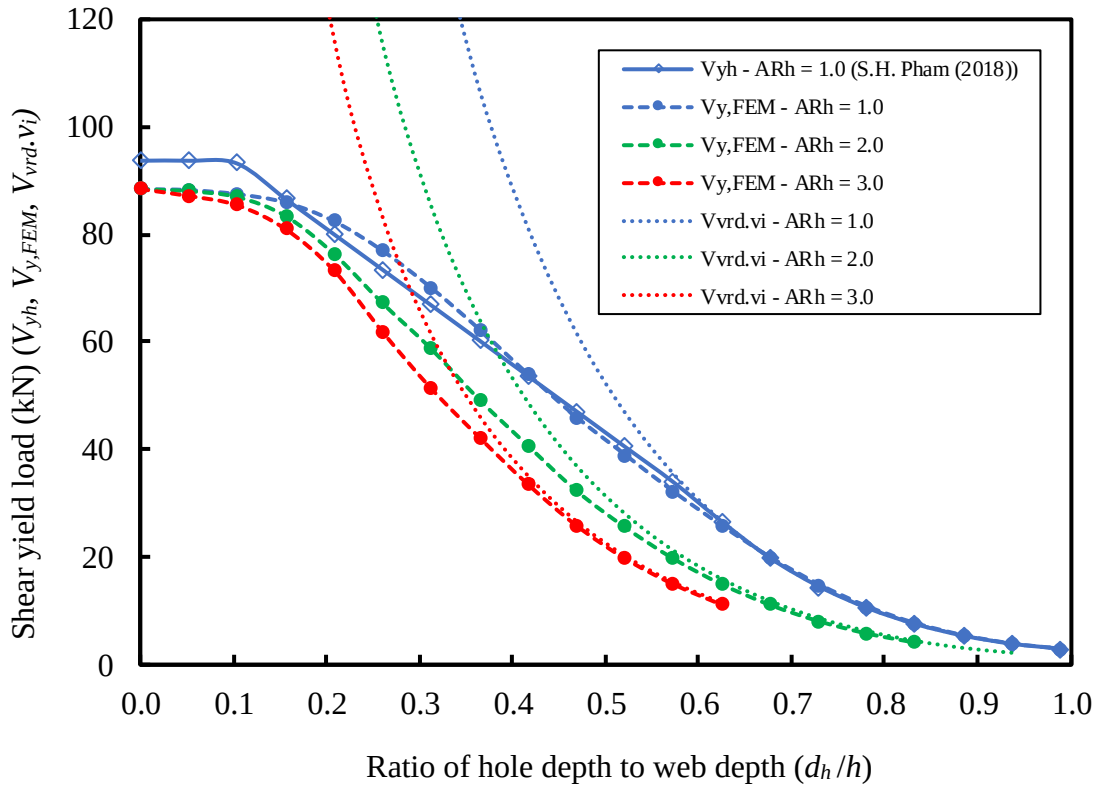

Fig 5.8: Combination of shear yield loads (V_{yh}, $V_{y,FEM}$, $V_{vrd}.v_i$)

It can be seen in **Fig 5.8** that there is a difference between the values of of $V_{y,FEM}$ and V_{yh} when the d_h/h ratios are in the range of 0.0 to 0.1 because of the use of $V_y = 0.6\, A_w\, f_y$ and the hypothesis of unchanged shear yield loads with small web holes ($d_h/h \leq 0.1$). This has also been explained by S.H. Pham et al. [16]. It is interesting to see that the blue dotted curve

presenting the values of $V_{y,FEM}$ with AR_h = 1.0 nearly fits the curve of V_{yh} when $d_h/h \geq 0.1$. This demonstrates that the FE models for the determination of the shear yield loads in this study have produced the same results as those proposed by S.H. Pham et al. [16], despite the difference in model configuration and strategy in capturing the shear yield loads.

5.4.3 New Proposal for DSM Design for Shear with Elongated Web Openings

On the basis of the new strategy presented above, a modified shear yield load ($V_{y,proposed}$) is proposed for the DSM design for channel sections in shear with elongated web openings as below:

When $0 < \frac{d_h}{h} \leq 0.10$, $V_{y,proposed} = V_y$ (5.12a)

When $0.10 < \frac{d_h}{h} < m$, $V_{y,proposed} = V_y - \left(\frac{1}{m-0.1}\right)\left(\frac{d_h}{h} - 0.1\right)\left(V_y - V_{vrd,m}.v_i\right)$ (5.12b)

When $m \leq \frac{d_h}{h}$ $V_{y,proposed} = V_{vrd}.v_i$ (5.12c)

where $m = 0.715 - 0.125.\left(\frac{L_h}{d_h}\right) + 0.01.\left(\frac{L_h}{d_h}\right)^2$ (5.12d)

The parameter v_i is determined by ***Eq (5.10)***. The dimensions for the calculation of $V_{vrd,m}$ are determined as follows:

$$d_{h,m} = m\ .h \quad (5.13a)$$

$$L_{h,m} = \frac{d_{h,m}}{d_h} L_h \quad (5.13b)$$

where $d_{h,m}$ and $L_{h,m}$ are the hole depth and hole length respectively when $d_h/h = m$. For circular and slotted holes, d_h and L_h are respectively replaced by $d_{h\text{-}eq}$ and $L_{h\text{-}eq}$ determined using ***Eq (4.3)***.

It can be seen in ***Eq (5.12)*** that there are close similarities between the proposal by S.H. Pham [13] for the cases of members having *AR* up to 2.0 with square and circular holes and the new proposal in this study when substituting the ratio L_h/d_h by 1.0 (i.e. square or circular holes). Therefore, this new proposal is an extension of the previous formulation for the

determination of shear yield loads of perforated members with AR_h = 1.0 and applies up to AR_h = 3.0.

The predominantly shear test results of perforated channel sections in this study are plotted against the current DSM shear curves for shear in **Fig 5.9** where the shear yield loads are determined using the new proposal. The equivalent dimensions of the slotted web openings are determined by ***Eq (4.3)***. The determination of the testing points plotted in **Fig 5.9** are shown in **Appendix D**. As can be seen in **Fig 5.9**, all the resulting points lie very close to the DSM design curve for shear with TFA. This proves that the current DSM design curve for shear with TFA together with the new proposal predict more accurately the shear strengths of perforated channels with web openings up to 120x360 mm compared to the previous proposals by Unabia B. [14] and S.H. Pham [13]. Further, on the basis of the significant improvement in the shear strength estimation provided by $V_{y,proposed}$, not only is the dimensional transformation based on ***Eq (4.3)*** capable of being used for the shear buckling analysis but also for predicting the ultimate shear strength.

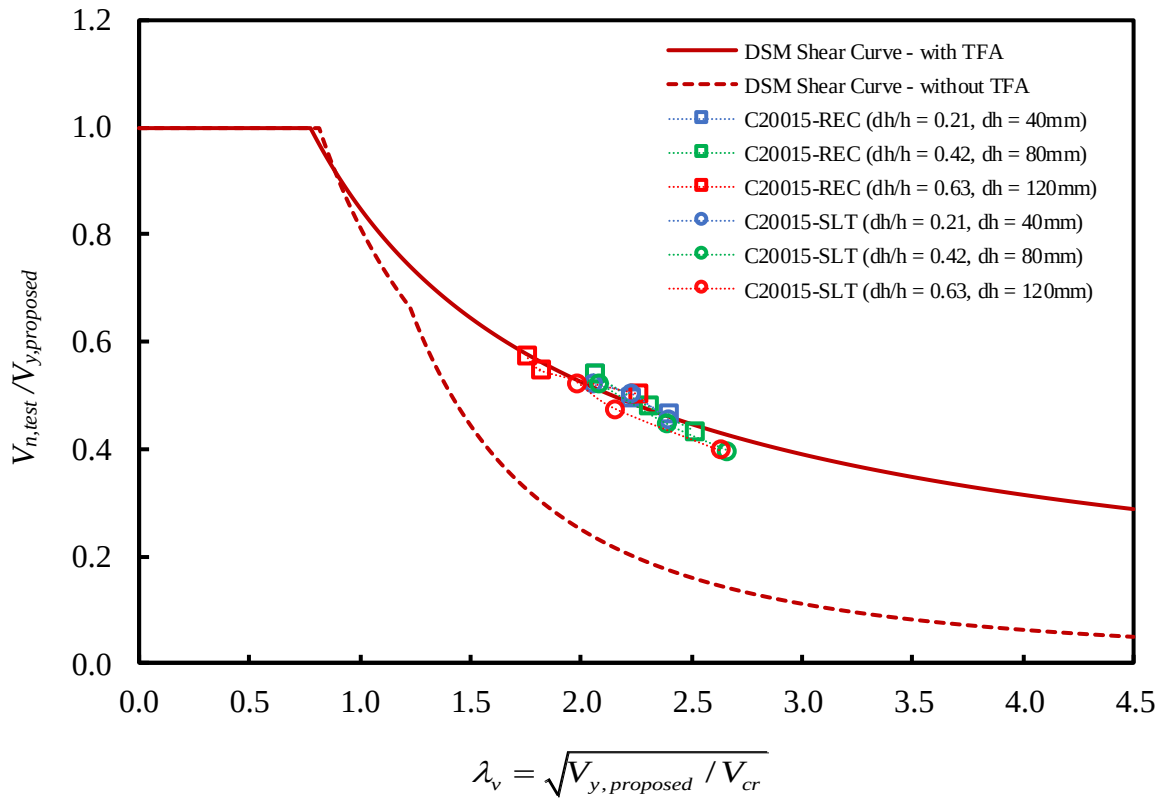

Fig 5.9: Shear test results based on $V_{y,proposed}$ versus DSM shear curves

5.5 VERIFICATION OF NEW PROPOSAL FOR DSM DESIGN FOR SHEAR WITH WEB OPENINGS

The shear buckling loads (V_{cr}) and the ultimate shear strengths ($V_{n,test}$ and $V_{n,FEM}$) obtained from the parametric studies in Chapter 4 are employed to verify the proposed shear yield load ($V_{y,proposed}$) in the DSM design formulae for shear as per ***Eq (5.12)*** on 200 and 250 mm deep channel members with a wide range of thicknesses from 1.0 to 2.4 mm. The opening sizes taken out in the web of channels C200 range from 40x40 to 120x360 mm. For members C250, the biggest hole size is up to 150x450 mm. The values of V_{cr} and $V_{y,proposed}$ corresponding to members with slotted holes are determined based on equivalent hole dimensions using ***Eq (4.3)***. On the basis of the observation of testing points as discussed above, full Tension Field Action (TFA) is deemed to be reached. Hence, the DSM curve without TFA is disregarded in the following graphs in this section.

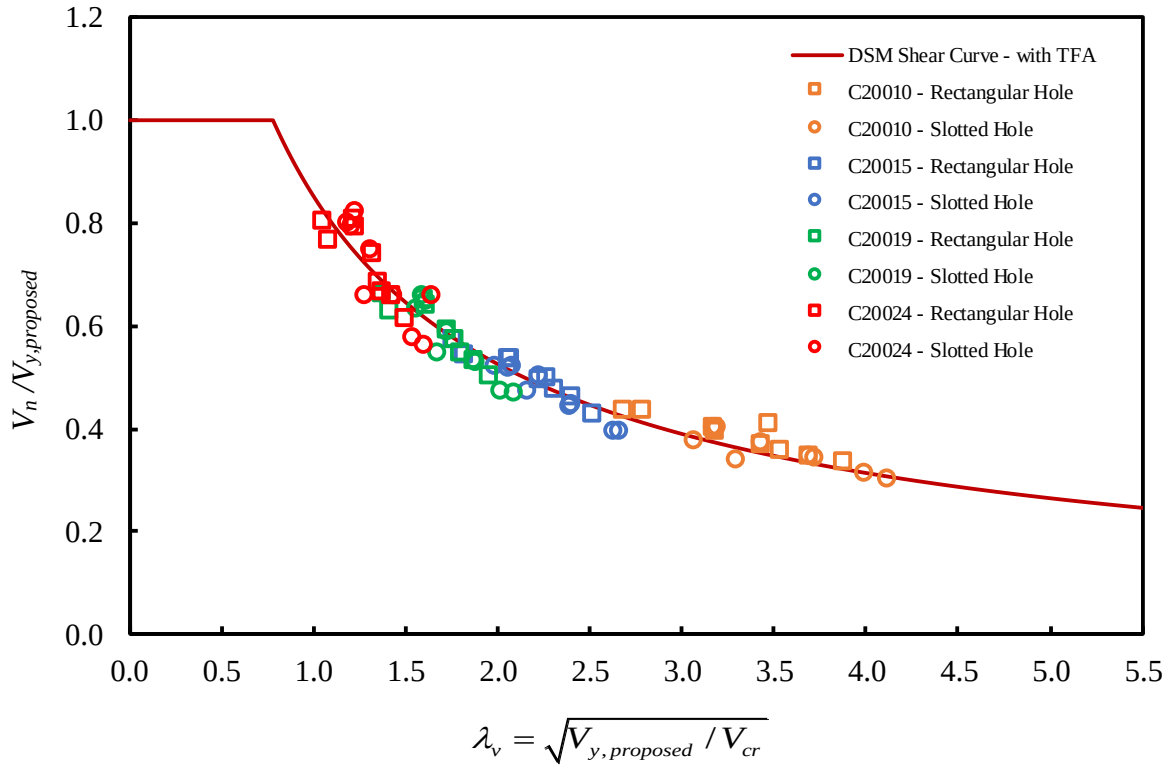

Fig 5.10: Verification of $V_{y,proposed}$ with C200 channel members

As can be seen in **Figs 5.10** and **5.11** where the resulting points of C200 and C250 are plotted respectively against the current DSM shear curve with TFA, the data follows well the

DSM design curve, even when the web holes are substantial. It is very interesting to note that resulting points corresponding to thicker members (1.9 and 2.4 mm) tend left upward, whereas the points with respect to thinner channels (1.0 and 1.5 mm) are shifted down and horizontally right but still lie close to the DSM design curve. This is attributed to significant changes in the nondimensional slenderness and the ratio of shear strength (V_n) to shear yield load ($V_{y,proposed}$) which depend on thicknesses. Indeed, in the cases of increasing thickness, the critical buckling loads (V_{cr}) become higher and the ratio $V_n/V_{y,proposed}$ gets closer to 1.0 (i.e. the thick members tend to fail in yielding). This leads to left-upward movements of points with respect to members C20019, C20024, C25019 and C25024. On the contrary, the failure of thinner channels is rather governed by the shear buckle. As a result, there are a significant decrease in the normalised ratio $V_n/V_{y,proposed}$ and an increase in the nondimensional slenderness (λ_v).

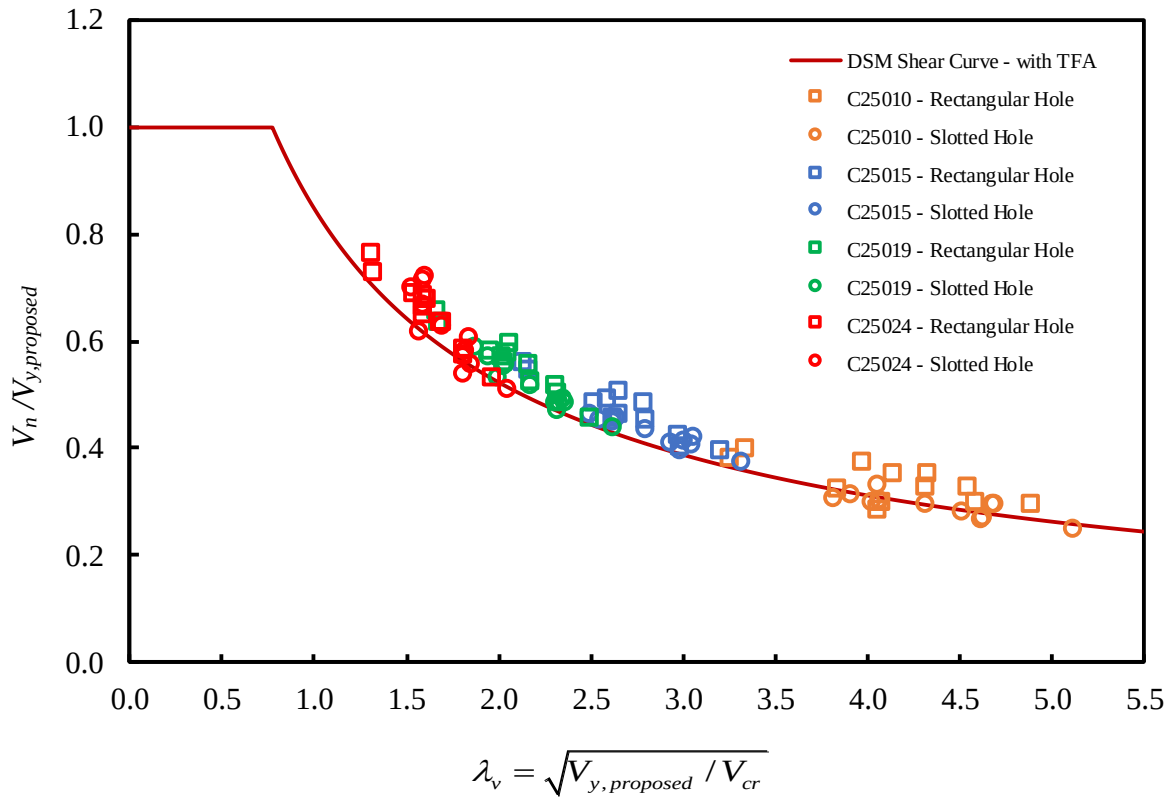

Fig 5.11: Verification of $V_{y,proposed}$ with C250 channel members

All the resulting points with respect to members C250 tend right downward compared to those of C200. It can be explained that the lower flange-to-web ratio of C250 caused an increase in the nondimensional slenderness (λ_v) which is also influenced by section slenderness.

The calculations of resulting points plotted in **Figs 5.10** and **5.11** are detailed in **Appendices E.1** and **E.2** respectively.

Further, based on the associated coefficient of variations (*CoV*) of 5.34% and 5.43% and the average $P_{m,avg}$ ratio ($V_n / V_{n,DSM}$) of 1.01 and 1.06 as computed from the results of members C200 and C250 respectively, it is obviously evident that the proposed model to compute shear yield loads is able to predict well the ultimate shear strength of perforated channels with elongated web openings.

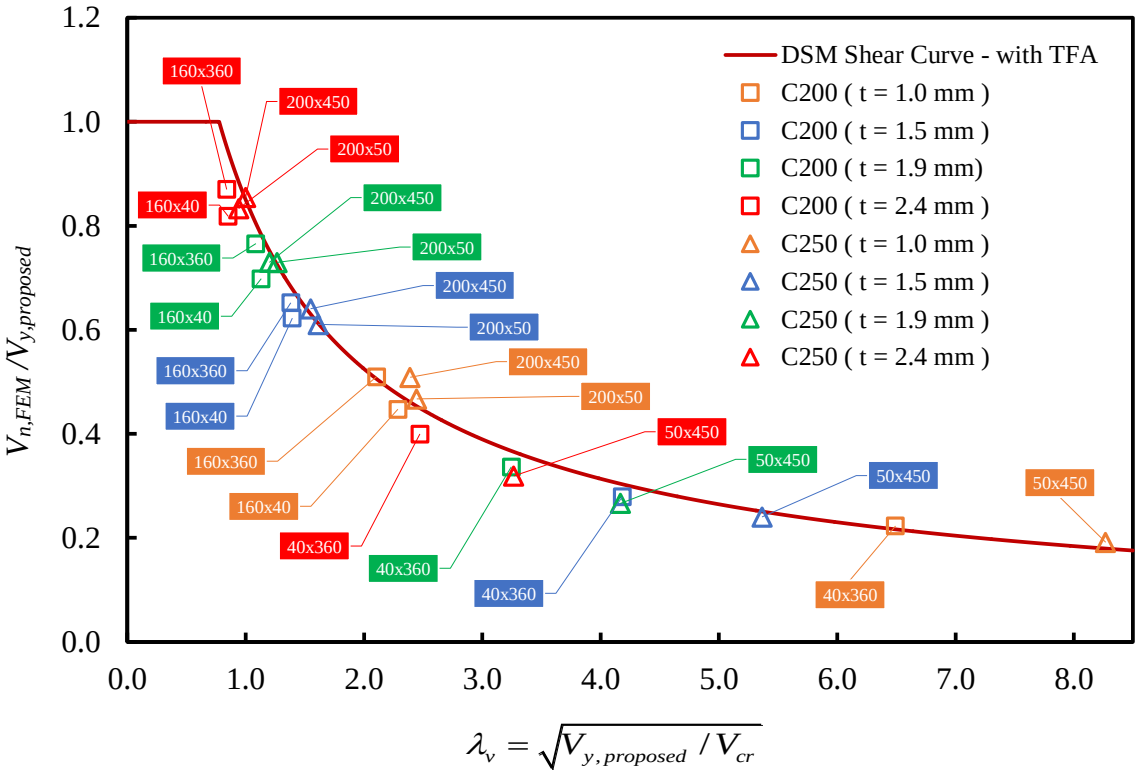

Fig 5.12: Verification of $V_{y,proposed}$ with critical opening sizes on channels C200 and C250

Fig 5.12 shows a verification of $V_{y,proposed}$ with critical hole sizes on 200 and 250 mm deep sections. The critical web cut-outs which are investigated include long horizontally elongated openings (hole sizes of 40x360 and 50x450 mm in the webs of channels C200 and C250 respectively, AR_h = 9.0, d_h/h = 0.2, L_h/L = 0.9), long vertically elongated openings (hole sizes of 160x40 and 200x50 mm in the webs of channels C200 and C250 respectively, AR_h = 0.25, d_h/h = 0.8, L_h/L = 0.1), and extremely large openings (hole sizes of 160x360 and 200x450 mm in the webs of channels C200 and C250 respectively, AR_h = 2.25, d_h/h = 0.8, L_h/L = 0.9).

It can be seen in **Fig 5.12** that the DSM curve with TFA is also able to predict well the shear strength of channel sections with critical web openings, even with very large opening areas. Although some resulting points are located at the region under the DSM curve (i.e. predicted values are higher than shear strengths), these points still lie very close to the prediction curve. The calculations of resulting points plotted in **Fig 5.12** are detailed in **Appendix F**.

On the basis of the verifications of $V_{y,proposed}$ with cold-formed channel members C200 and C250 with a full range of hole size and with different practical member thicknesses, the limitations on the applicability of the modified DSM design for cold-formed members in shear can be stated as follows:

(i) $1.0 \le \frac{L}{h} \le 2.0$

(ii) $d_h \le 0.8h$

(iii) $L_h \le 0.9L$

where L_h is the overall length of web hole taken along the member, d_h is the overall depth of web hole, h is the depth of flat portion of web measured along plane of web, L is the length of the shear span, ratio L/h is understood of the shear aspect ratio (AR). It is noted that the holes are centred at mid-depth of the web and mid-length of the shear span.

5.6 CHAPTER CONCLUSION

On the basis of the Vierendeel mechanism approach presented in this Chapter, a modification of the shear yield loads is introduced to account for the presence of non-elongated and elongated web holes (square, circular, rectangular and slotted openings) perforated in the web of cold-formed channel sections with shear aspect ratio (*AR*) up to 2.0. Two new terms including '*m*' and 'v_i' are added to the new proposal for shear yield load ($V_{y,proposed}$). The term 'v_i' is defined as an indicative parameter or Vierendeel parameter to estimate the performance of the Vierendeel mechanism in channel sections in high shear with web openings. While the shear yield loads with respect to members with web holes under the condition $0.1 < d_h/h < m$ are determined based on the factor 'v_i' and the values of $V_{vrd,m}$ (the yield shear loads based on the Vierendeel mechanism corresponding to the perforated sections when $d_h/h = m$) , the shear yield loads of channels with web openings having the ratio d_h/h which is higher than '*m*' are the shear strength of the perforated members without instability which is modified by the Vierendeel parameter (v_i). The introduction of the indicative parameter 'v_i' in the new proposal is due to the changes in the distance between plastic hinges along the span length (critical hole length) when the web opening is elongated. Further, because the Vierendeel mechanism is influenced by the overall hole size including the overall length and depth of the web opening, non-dimensional parameters '*m*' and '*vi*' depend on the aspect ratio of the hole (L_h/d_h). This is the basis for the formulation of '*m*' and '*vi*' in this thesis.

In order to verify the applicability of the new proposal for different cases of channel sections with various hole sizes, the resulting points determined based on the experiments and the parametric studies using FE models presented respectively in Chapters 3 and 4 are plotted against the DSM shear curve with TFA. It was observed that all the points lie around and close to the prediction curve. This demonstrates that the current DSM curve with TFA is able to capture well the shear strengths of cold-formed steel channel sections with different dimensions and with a very wide range of hole sizes. Further, by observing the locations of the resulting points, the behaviour of channel members in shear with different practical thicknesses is performed via three shear loads including the shear buckling load, shear yield load and ultimate shear strength.

In addition, the applicability of the new proposal to the cases of critical web openings is also investigated. On the basis of a verification of $V_{y,proposed}$ with critical opening sizes (i.e. extremely elongated holes and very large holes) on 200 and 250 mm deep sections, the limits of shear span aspect ratio (*AR*) and web opening dimensions are established.

Chapter 6
CONCLUSIONS AND RECOMMENDATIONS

6.1 SUMMARY OF RESEARCH AND CONCLUSIONS

The study in this thesis broadens the understanding of the shear behaviour of high strength cold-formed steel sections, particularly for channel members with elongated web openings including rectangular and slotted holes, and also thin-walled structures with large shear spans. On the basis of experimental and numerical investigations, a new Direct Strength Method (DSM) of design for perforated members in shear is proposed to estimate the shear capacity of cold-formed channels with both non-elongated and elongated web openings.

Due to much simpler and faster assembly compared to the Basler test rig used in earlier research to achieve high shear with low moment, the dual actuator test rig developed at the University of Sydney was further employed in an experimental investigation of cold-formed channel sections in shear with various hole sizes, and with a shear span aspect ratio of 2.0. A total of thirty shear tests divided into two test series were performed on standard plain C-channels with the web depth of 200 mm, the flange width of 75 mm, and the lip size of 15 mm. The chosen aspect ratios of hole length (L_h) to hole depth (d_h) were 1.0, 2.0 and 3.0. Based on the experimental outcomes presented in Chapter 3, it can be concluded that pure shear behaviour of channels with both non-elongated and elongated web openings were captured by using the dual actuator test rig which is able to isolate the shear failure mode and minimise the bending at both ends of the shear span. Further, in the case of substantially large holes in the web, significant shear strengths together with ductile behaviour were observed from the load-displacement curves affirming the contribution of the flanges and lips to the shear resistance and the formation of yield patterns or plastic hinges around the corners of the web openings.

Numerical non-linear simulations of shear tests using the Finite Element Method (FEM) were performed in Chapter 4 to compare and calibrate against the test results in Chapter 3. The validation of the FE models for shear strength analyses was performed by the comparisons of the shear capacities, shear failure modes and load-displacement relationships.

On the basis of the good agreement between the ultimate shear strengths from the actual shear tests and those obtained from FEM analyses with two imperfection scaling factors of 0.15*t* and 0.64*t* where *t* is the member thickness, it is concluded that the sensitivity of the initial geometrical imperfections over the shear capacity of cold-formed channel sections is not significant. In addition, because the shear failure modes and load-displacement curves extracted from the FE models are consistent with the shear test results, more FE simulations were used for the parametric studies. In order to investigate elastic shear buckling behaviour of cold-formed channels with holes perforated in the web, a simplified FE model was introduced. The reliability of these models was validated against the full FE models which were used to calibrate against the shear test results. Based on the good agreement in the shear buckling analyses by using the simplified and full FE models as proven in Chapter 4, the simplified FE model was able to capture well the elastic buckling of channels in shear and then was used to create a full range database for buckling analyses. On the basis of the parametric investigation of shear buckling analyses on perforated channels with both cases $AR_h \leq 1.0$ and $AR_h \geq 1.0$, a dimensional transformation was proposed to transform the dimensions of an actual slotted web opening into the equivalent sizes of a rectangular hole. Moreover, this transformation is also validated based on shear strength analyses and used for calculations in the Direct Strength Method (DSM). It is proven that the dimensional transformation is able to be applied to different plain C-lipped sections including 200 and 250 mm deep channels with various practical thicknesses of 1.0, 1.5, 1.9 and 2.4 mm.

On the basis of comparisons of the Direct Strength Method (DSM) design loads for shear with predominantly shear tests of cold-formed channels with elongated web openings, it is proven that the use of previous proposals for shear yield loads $V_{y,net}$ and V_{yh} by Unabia B. [14] and S.H. Pham [38] respectively are unable to predict well the expected shear strengths of some substantially large openings. Therefore, more accurate practical models of yield shear load together with the Vierendeel mechanism approach were proposed and studied to suggest a modified design for perforated sections in shear with all cases of web openings including circular, square, rectangular and slotted holes. The underlying idea of the new proposal is based on the changes in the distance between the plastic hinges along the span length (critical hole length) when the web hole is elongated. This leads to the introduction of an indicative parameter 'v_i' which is also called the Vierendeel parameter. This factor serves a role in

evaluating the performance of the Vierendeel mechanism in the cases of substantially large web openings. A non-dimensional parameter '*m*' is also added in the new proposal as discussed in Chapter 5 to reflect the influence of hole depths on shear yield loads ($V_{y,proposed}$). The applicability of the new proposal to different cases of cold-formed channel sections with different member dimensions and thicknesses, and with different hole sizes is validated against the current DSM curve in shear with Tension Field Action (TFA). Further, based on the resulting test points of channels in shear with extremely elongated openings and very large openings, the limits of web opening dimensions are also now specified.

6.2 RECOMMENDATIONS FOR FUTURE STUDIES

Despite the originality of this research which was to develop a Direct Strength Method of design for cold-formed members in shear with elongated web openings has been solved, there are several problems needing to be addressed.

All the shear buckling coefficients (k_v) in this study are generated from the FE models. Although FE models used for shear buckling analyses are simplified, they are still very complex to the users. S.H. Pham [38] suggested a simple expression to determine the shear buckling coefficients based on the artificial neutral network. However, this proposal is only able to be used for the cases of square and circular web holes. Hence, the work of determining the shear buckling coefficients (k_v) for elongated holes requires more work.

Further, more experiments with aspect ratios (*AR*) larger than 2.0 should be carried out to investigate the influence of combined bending and shear on perforated channels with web openings. In conjunction with combined actions on perforated members, it is also important to study the effects of the hole location on the ultimate strengths of the beams.

REFERENCES

[1] G. Winter, *Cold-formed, light-gage steel construction.* Journal of Structural Engineering, 1959. 85: p. 151-171.

[2] W.-W. Yu, *Cold-formed steel design*. 2000: John Wiley & Sons.

[3] G.J. Hancock, *Design of Cold-formed Steel Structures: To Australian/New Zealand Standard AS/NZS 4600: 2005*. 2007: Australian steel institute.

[4] AISI S100-16, *North American specification for the design of cold-formed steel structural members*, in *AISI S100-16*. AISI-2016: Washington, DC, U.S.A.

[5] AS/NZS 4600:2018, *AS 4600 Cold-formed Steel Structures*. Standards Australia, 2018: Standards Australia / Standards New Zealand.

[6] C.H. Pham and G.J. Hancock, *Shear buckling of thin-walled channel sections.* Journal of Constructional Steel Research, 2009. 65(3): p. 578-585.

[7] C.H. Pham and G.J. Hancock, *Direct strength design of cold-formed C-sections for shear and combined actions.* Journal of Structural Engineering, 2012. 138(6): p. 759-768.

[8] S.C.W. Lau and G.J. Hancock, *Buckling of thin flat-walled structures by a spline finite strip method.* Thin-walled structures, 1986. 4(4): p. 269-294.

[9] G.J. Hancock and C.H. Pham, *Shear buckling of channel sections with simply supported ends using the semi-analytical finite strip method.* Thin-Walled Structures, 2013. 71: p. 72-80.

[10] C.H. Pham. *Buckling studies of thin-walled C-sections with square holes in shear using the spline finite strip method*. in *Proc., 8th Int. Conf. on Advances in Steel Structure, Univ. of Lisbon, Lisbon, Portugal*. 2015.

[11] C.H. Pham, *Shear buckling of plates and thin-walled channel sections with holes.* Journal of Constructional Steel Research, 2017. 128: p. 800-811.

[12] G. Eccher, *Isoparametric spline finite strip analysis of perforated thin-walled steel structures*. 2007, School of Civil Engineering, Faculty of Engineering and Information, The University of Sydney.

[13] S.H. Pham, *Design of Cold-Formed Steel Beams with Holes and Transverse Stiffeners in Shear*. 2018, PhD Thesis, School of Civil Engineering, The University of Sydney, 2018.

[14] Unabia B., *Numerical Simulation of Plain Cold-formed Steel C-sections with Square Holes subjected to Shear*, in *School of Civil Engineering*. 2013, the University of Sydney.

[15] C.H. Pham, A. Pelosi, T. Earls, and G.J. Hancock, *Experimental investigation of cold-formed C-sections with central square holes in shear*, in *23rd International Specialty Conference on Cold-formed Steel Structures*. 2016: Baltimore, U.S.A.

[16] S.H. Pham, C.H. Pham, and G.J. Hancock, *Direct strength method of design for channel sections in shear with square and circular web holes.* Journal of Structural Engineering, 2017. 143(6): p. 04017017.

[17] C.D. Moen, *Direct strength design of cold-formed steel members with perforations*. 2008, Johns Hopkins University: Baltimore, the U.S.A.

[18] C.D. Moen and B.W. Schafer, *Direct strength method for design of cold-formed steel columns with holes.* Journal of Structural Engineering, 2010. 137(5): p. 559-570.

[19] C.D. Moen and B.W. Schafer. *Extending direct strength design to cold-formed steel beams with holes*. in *20th International Specialty Conference Cold-formed Steel Beams with Holes*. 2010. Missouri University of Science and Technology, Rolla, MO.

[20] AISI S100-12, *North American specification for the design of cold-formed steel structural members*, in *AISI S100-12*. AISI-2012: Washington, DC, U.S.A.

[21] C.H. Pham, Y.H. Chin, P. Boutros, and G.J. Hancock, *The behaviour of cold-formed C-sections with square holes in shear*, in *22nd International Specialty Conference on Cold-formed Steel Structures* 2014: St. Louis, Missouri, U.S.A. p. 311-327.

[22] P. Keerthan and M. Mahendran, *Experimental studies of the shear behaviour and strength of lipped channel beams with web openings.* Thin-Walled Structures, 2013. 73: p. 131-144.

[23] M.-Y. Shan, R.A. LaBoube, and W.-w. Yu, *Behavior of web elements with openings subjected to bending, shear and the combination of bending and shear*. 1994: University of Missouri-Rolla. Rolla, Missouri.

[24] R. Schuster, C. Rogers, and A. Celli, *Research into cold formed steel perforated C-sections in shear*. Program Rep. No. 1 Phase I CSSBI/IRAP Project, 1995.

[25] M.R. Eiler, R.A. LaBoube, and W.W. Yu, *Behavior of web elements with openings subjected to linearly varying shear*. 1997: University of Missouri-Rolla.

[26] P. Keerthan and M. Mahendran, *Improved shear design rules for lipped channel beams with web openings*. Journal of Constructional Steel Research, 2014. 97: p. 127-142.

[27] S.H. Pham, C.H. Pham, C.A. Rogers, and G.J. Hancock, *Experimental validation of the Direct Strength Method for shear spans with high aspect ratios*. Journal of Constructional Steel Research, 2019. 157: p. 143-150.

[28] ABAQUS 6.14-2, *Abaqus/CAE User's Manual (2014)*. 2014, Dassault Systèmes Simulia Corp., Providence, RI, USA.

[29] S.P. Timosenko and J.M. Gere, *Theory of Elastic Stability*. McGraw-Hill Book Inc. 1961, New York.

[30] H.G. Allen and P. Bulson, *Background to Buckling*. McGraw-Hill Book Inc. 1980.

[31] H. Bleich, *Buckling Strength of Metal Structures*. MCGraw-hill Book Inc. 1952, New York.

[32] P.S. Bulson, *Stability of Flat Plates*. Chatto & Windus Ltd. 1970, London W.C.2.

[33] K. Rockey, R. Anderson, and Y. Cheung. *The behaviour of square shear webs having a circular hole*. in *Symposium on Thin-Walled Steel Structures, University College of Swansea*. 1967.

[34] R. Narayanan and N. Der Avanessian, *Elastic buckling of perforated plates under shear*. Thin-Walled Structures, 1984. 2(1): p. 51-73.

[35] C.H. Pham and G.J. Hancock, *Elastic buckling of cold-formed channel sections in shear*. Thin-Walled Structures, 2012. 61: p. 22-26.

[36] P. Keerthan and M. Mahendran, *Shear buckling characteristics of cold-formed steel channel beams.* International Journal of Steel Structures, 2013. 13(3): p. 385-399.

[37] S.H. Pham, C.H. Pham, and G.J. Hancock. *07.12: On the design of cold-formed steel beams with holes in shear using the direct strength method*. in *ce/papers*. 2017.

[38] S.H. Pham, *Design of Cold-Formed Steel Beams with Holes and Transverse Stiffeners in Shear*, in *School of Civil Engineering*. 2018, Ph.D Thesis, The University of Sydney.

[39] K. Basler, *Strength of plate girders in shear*. Journal of the Structural Division, 1961. 87(7): p. 151-180.

[40] T. Hoglund. *Strength of thin plate girders with circular or rectangular web holes without web stiffeners*. in *Proceedings of the Colloquium of the International Association of Bridge and Structural Engineering, London*. 1971.

[41] C. Marsh, *Theoretical model for collapse of shear webs.* Journal of the Engineering Mechanics Division, 1982. 108(5): p. 819-832.

[42] T. Höglund, *Shear buckling resistance of steel and aluminium plate girders.* Thin-walled structures, 1997. 29(1-4): p. 13-30.

[43] A. Davies, D. Griffith, T. Hoglund, and E. 3, *SHEAR STRENGTH OF STEEL PLATE GIRDERS.* Proceedings of the Institution of Civil Engineers-Structures and Buildings, 1999. 134(2): p. 147-157.

[44] B. ANSI, *AISC 360-16, Specification for Structural Steel Buildings.* Chicago, IL: American Institute of Steel Construction, 2016.

[45] R.D. Ziemian, *Guide to stability design criteria for metal structures*. 2010: John Wiley & Sons.

[46] S.H. Pham, C.H. Pham, and G.J. Hancock, *Experimental study of shear strength of cold-formed channels with an aspect ratio of 2.0.* Journal of Constructional Steel Research, 2018. 149: p. 141-152.

[47] C.H. Pham and G.J. Hancock, *Experimental investigation of high strength cold-formed C-sections in combined bending and shear.* Journal of structural engineering, 2009. 136(7): p. 866-878.

[48] S.H. Pham, C.H. Pham, C.A. Rogers, and G.J. Hancock, *Experimental Studies of Cold-formed Beams under Uniformed Shear Forces with Minimal Bending Moments*, in *The 8th International Conference in Thin-walled Structures, ICTW2018*. 2018: Lisbon, Portugal.

[49] K. Chung, T. Liu, and A. Ko, *Investigation on Vierendeel mechanism in steel beams with circular web openings.* Journal of Constructional Steel Research, 2001. 57(5): p. 467-490.

[50] K. Chung, T. Liu, and A. Ko, *Steel beams with large web openings of various shapes and sizes: an empirical design method using a generalised moment-shear interaction curve.* Journal of Constructional Steel Research, 2003. 59(9): p. 1177-1200.

[51] K. Basler, B. Yen, J. Mueller, and B. Thurlimann, *Web buckling tests on welded plate girders*. 1960: Fritz Engineering Laboratory, Lehigh University.

[52] R. LaBoube and W. Yu, *Cold-formed steel beam webs subjected primarily to shear.* Research Rep, 1978. 1.

[53] P. Keerthan and M. Mahendran, *Shear behaviour and strength of LiteSteel beams with web openings.* Advances in Structural Engineering, 2012. 15(2): p. 171-184.

[54] V. Nguyen, G. Hancock, and C. Pham. *Development of the THIN-WALL-2 program for buckling analysis of thin-walled sections under generalised loading*. in *Eighth International Conference on Advances in Steel Structures, Lisbon, Portugal*. 2015.

[55] Z. Li and B.W. Schafer, *Buckling analysis of cold-formed steel members with general boundary conditions using CUFSM conventional and constrained finite strip methods.* 2010.

[56] C.H. Pham and G.J. Hancock, *Numerical investigation of longitudinally stiffened web channels predominantly in shear.* Thin-Walled Structures, 2015. 86: p. 47-55.

[57] C.H. Pham and G.J. Hancock, *Numerical simulation of high strength cold-formed purlins in combined bending and shear*. Journal of Constructional Steel Research, 2010. 66(10): p. 1205-1217.

[58] AS1391-2005, *"Tensile Testing at Ambient Temperature"*, in *AS1391-2005*. AS-2005: Standards Australia, Sydney, Australia.

[59] D.K. Phan and K. Rasmussen, *Cold-formed Steel Bolted and Screw-fastened Connections in Shear*, in *Eight International Conference on Thin-Walled Structures*. 2018: Lisbon, Portugal.

[60] E. Riks, *The application of Newton's method to the problem of elastic stability.* Journal of Applied Mechanics, 1972. 39(4): p. 1060-1065.

[61] E. Riks, *An incremental approach to the solution of snapping and buckling problems.* International journal of solids and structures, 1979. 15(7): p. 529-551.

[62] N. Silvestre and D. Camotim, *GBT-based analysis of the distortional post-buckling behaviour of cold-formed steel Z-section columns and beams.* Thin-walled structures: Advances in research, design and manufacturing technology (Ictws 2004-Loughborough, 22-24/6), Institute of Physics Publishing, Bristol, 2004: p. 243-250.

[63] B. Schafer and T. Peköz, *Computational modeling of cold-formed steel: characterizing geometric imperfections and residual stresses.* Journal of constructional steel research, 1998. 47(3): p. 193-210.

[64] C. H. Pham, *Direct Strength Method (DSM) of Design of Cold-formed Sections in Shear, and Combined Bending and Shear*, in *School of Civil Engineering*. 2010, Ph.D Thesis, The University of Sydney.

[65] K. Chung, C. Liu, and A. Ko, *Steel beams with large web openings of various shapes and sizes: an empirical design method using a generalised moment-shear interaction curve.* Journal of Constructional Steel Research, 2003. 59(9): p. 1177-1200.

[66] K.D. Tsavdaridis and C. D'Mello, *Vierendeel bending study of perforated steel beams with various novel web opening shapes through nonlinear finite-element analyses.* Journal of Structural Engineering, 2012. 138(10): p. 1214-1230.

APPENDICES

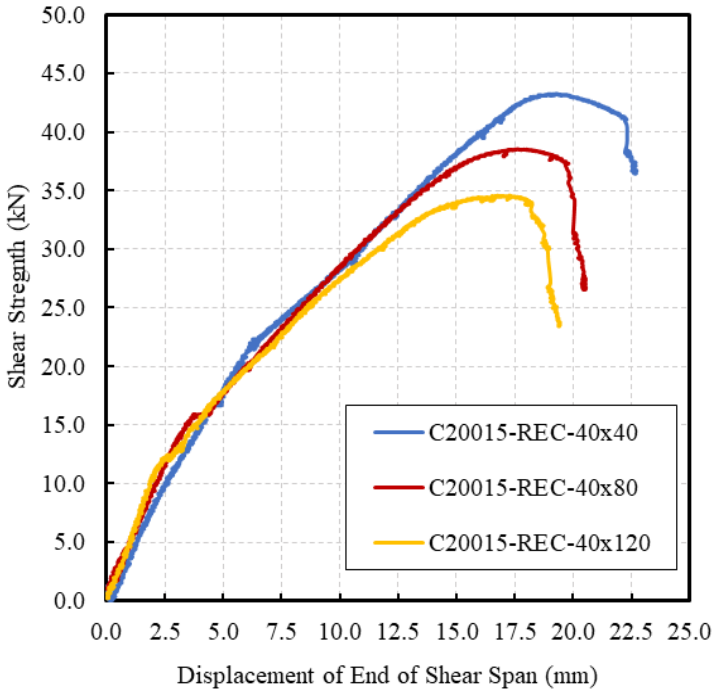

Appendix A.1: Load - displacement relationship of cold-formed channels with rectangular hole with d_h = 40 mm

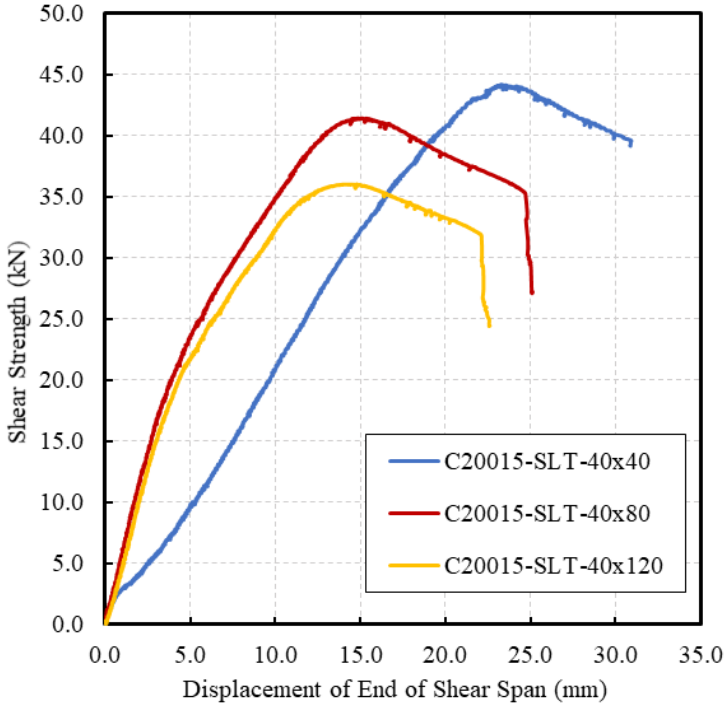

Appendix A.2: Load - displacement relationship of cold-formed channels with slotted hole with d_h = 40 mm

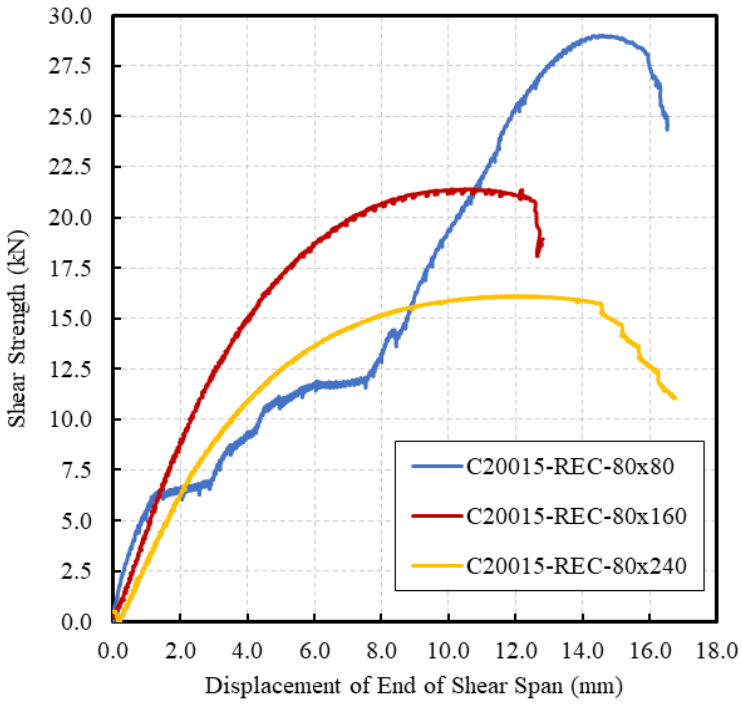

Appendix A.3: Load - displacement relationship of cold-formed channels with rectangular hole with d_h = 80 mm

Appendix B: Shear test results based on $V_{y,net}$ versus DSM shear curves

Designation	L_h (mm)	d_h (mm)	d_h / h	L_{h-eq} (mm)	d_{h-eq} (mm)	d_{h-eq} / h	k_v	V_{cr} (kN)	$V_{y,net}$ (kN)	$V_{n,test}$ (kN)	$\lambda_v = \sqrt{V_{y,net} / V_{cr}}$	$V_{n,test} / V_{y,net}$
C20015-SQR-40x40	40.00	40.00	0.21	40.00	40.00	0.21	5.90	18.95	74.26	43.25	1.98	0.58
C20015-REC-40x80-1	80.00	40.00	0.21	80.00	40.00	0.21	4.85	15.58	74.26	38.05	2.18	0.51
C20015-REC-40x80-2	80.00	40.00	0.21	80.00	40.00	0.21	4.85	15.58	74.26	38.55	2.18	0.52
C20015-REC-40x120-1	120.00	40.00	0.21	120.00	40.00	0.21	4.03	12.94	74.26	34.58	2.40	0.47
C20015-REC-40x120-2	120.00	40.00	0.21	120.00	40.00	0.21	4.03	12.94	74.26	33.62	2.40	0.47
C20015-SQR-80x80	80.00	80.00	0.42	80.00	80.00	0.42	3.94	12.66	54.72	29.00	2.08	0.53
C20015-REC-80x160-1	160.00	80.00	0.42	160.00	80.00	0.42	2.61	8.37	54.72	21.41	2.56	0.39
C20015-REC-80x160-2	160.00	80.00	0.42	160.00	80.00	0.42	2.61	8.37	54.72	21.21	2.56	0.39
C20015-REC-80x240-1	240.00	80.00	0.42	240.00	80.00	0.42	1.80	5.79	54.72	16.13	3.07	0.29
C20015-REC-80x240-2	240.00	80.00	0.42	240.00	80.00	0.42	1.80	5.79	54.72	15.69	3.07	0.29
C20015-SQR-120x120	120.00	120.00	0.63	120.00	120.00	0.63	2.70	8.67	35.18	15.28	2.01	0.43
C20015-REC-120x240-1	240.00	120.00	0.63	240.00	120.00	0.63	1.51	4.85	35.18	8.76	2.69	0.25
C20015-REC-120x240-2	240.00	120.00	0.63	240.00	120.00	0.63	1.51	4.85	35.18	8.77	2.69	0.25
C20015-REC-120x360-1	360.00	120.00	0.63	360.00	120.00	0.63	0.73	2.36	35.18	6.08	3.86	0.17
C20015-REC-120x360-2	360.00	120.00	0.63	360.00	120.00	0.63	0.73	2.36	35.18	6.00	3.86	0.17
C20015-CIR-40x40	40.00	40.00	0.21	32.92	33.00	0.17	6.28	20.17	77.68	44.20	1.96	0.57
C20015-SLT-40x80-1	80.00	40.00	0.21	74.59	33.12	0.17	5.19	16.67	77.68	41.39	2.16	0.53
C20015-SLT-40x80-2	80.00	40.00	0.21	74.59	33.12	0.17	5.19	16.67	77.68	41.44	2.16	0.53
C20015-SLT-40x120-1	120.00	40.00	0.21	115.96	33.24	0.17	4.31	13.85	77.68	35.90	2.37	0.46
C20015-SLT-40x120-2	120.00	40.00	0.21	115.96	33.24	0.17	4.31	13.85	77.68	36.04	2.37	0.46
C20015-CIR-80x80	80.00	80.00	0.42	65.85	66.00	0.34	4.56	14.63	61.56	32.98	2.05	0.54
C20015-SLT-80x160-1	160.00	80.00	0.42	149.18	66.24	0.35	2.96	9.50	61.44	24.21	2.54	0.39
C20015-SLT-80x160-2	160.00	80.00	0.42	149.18	66.24	0.35	2.96	9.50	61.44	24.09	2.54	0.39
C20015-SLT-80x240-1	240.00	80.00	0.42	231.92	66.48	0.35	2.04	6.54	61.33	18.00	3.06	0.29
C20015-SLT-80x240-2	240.00	80.00	0.42	231.92	66.48	0.35	2.04	6.54	61.33	18.00	3.06	0.29
C20015-CIR-120x120	120.00	120.00	0.63	98.77	99.00	0.52	3.27	10.49	45.44	21.55	2.08	0.47
C20015-SLT-120x240-1	240.00	120.00	0.63	223.77	99.36	0.52	1.77	5.69	45.26	11.82	2.82	0.26
C20015-SLT-120x240-2	240.00	120.00	0.63	223.77	99.36	0.52	1.77	5.69	45.26	11.65	2.82	0.26
C20015-SLT-120x360-1	360.00	120.00	0.63	347.87	99.72	0.52	0.86	2.77	45.09	7.59	4.04	0.17
C20015-SLT-120x360-2	360.00	120.00	0.63	347.87	99.72	0.52	0.86	2.77	45.09	7.62	4.04	0.17

Appendix C: Shear test results based on V_{yh} versus DSM shear curves

Designation	L_h (mm)	d_h (mm)	d_h / h	L_{h-eq} (mm)	d_{h-eq} (mm)	d_{h-eq} / h	k_v	V_{cr} (kN)	V_y (kN)	$V_{vrd,0.6}$ (kN)	V_{vrd} (kN)	V_{yh} (kN)	$V_{n,test}$ (kN)	$\lambda_v = \sqrt{V_{yh} / V_{cr}}$	$V_{n,test} / V_{yh}$
C20015-SQR-40x40	40.00	40.00	0.21	40.00	40.00	0.21	5.90	18.95	93.81	30.47		80.08	43.25	2.06	0.54
C20015-REC-40x80-1	80.00	40.00	0.21	80.00	40.00	0.21	4.85	15.58	93.81	15.24		76.78	38.05	2.22	0.50
C20015-REC-40x80-2	80.00	40.00	0.21	80.00	40.00	0.21	4.85	15.58	93.81	15.24		76.78	38.55	2.22	0.50
C20015-REC-40x120-1	120.00	40.00	0.21	120.00	40.00	0.21	4.03	12.94	93.81	10.16		75.68	34.58	2.42	0.46
C20015-REC-40x120-2	120.00	40.00	0.21	120.00	40.00	0.21	4.03	12.94	93.81	10.16		75.68	33.62	2.42	0.44
C20015-SQR-80x80	80.00	80.00	0.42	80.00	80.00	0.42	3.94	12.66	93.81	30.47		53.69	29.00	2.06	0.54
C20015-REC-80x160-1	160.00	80.00	0.42	160.00	80.00	0.42	2.61	8.37	93.81	15.24		44.05	21.41	2.29	0.49
C20015-REC-80x160-2	160.00	80.00	0.42	160.00	80.00	0.42	2.61	8.37	93.81	15.24		44.05	21.21	2.29	0.48
C20015-REC-80x240-1	240.00	80.00	0.42	240.00	80.00	0.42	1.80	5.79	93.81	10.16		40.83	16.13	2.65	0.40
C20015-REC-80x240-2	240.00	80.00	0.42	240.00	80.00	0.42	1.80	5.79	93.81	10.16		40.83	15.69	2.65	0.38
C20015-SQR-120x120	120.00	120.00	0.63	120.00	120.00	0.63	2.70	8.67	93.81		26.54	26.54	15.28	1.75	0.58
C20015-REC-120x240-1	240.00	120.00	0.63	240.00	120.00	0.63	1.51	4.85	93.81		13.27	13.27	8.76	1.65	0.66
C20015-REC-120x240-2	240.00	120.00	0.63	240.00	120.00	0.63	1.51	4.85	93.81		13.27	13.27	8.77	1.65	0.66
C20015-REC-120x360-1	360.00	120.00	0.63	360.00	120.00	0.63	0.73	2.36	93.81		8.85	8.85	6.08	1.94	0.69
C20015-REC-120x360-2	360.00	120.00	0.63	360.00	120.00	0.63	0.73	2.36	93.81		8.85	8.85	6.00	1.94	0.68
C20015-CIR-40x40	40.00	40.00	0.21	32.92	33.00	0.17	6.28	20.17	93.81	30.54		84.71	44.20	2.05	0.52
C20015-SLT-40x80-1	80.00	40.00	0.21	74.59	33.12	0.17	5.19	16.67	93.81	13.53		82.17	41.39	2.22	0.50
C20015-SLT-40x80-2	80.00	40.00	0.21	74.59	33.12	0.17	5.19	16.67	93.81	13.53		82.17	41.44	2.22	0.50
C20015-SLT-40x120-1	120.00	40.00	0.21	115.96	33.24	0.17	4.31	13.85	93.81	8.73		81.37	35.90	2.42	0.44
C20015-SLT-40x120-2	120.00	40.00	0.21	115.96	33.24	0.17	4.31	13.85	93.81	8.73		81.37	36.04	2.42	0.44
C20015-CIR-80x80	80.00	80.00	0.42	65.85	66.00	0.34	4.56	14.63	93.81	30.54		62.97	32.98	2.05	0.54
C20015-SLT-80x160-1	160.00	80.00	0.42	149.18	66.24	0.35	2.96	9.50	93.81	13.53		54.47	24.21	2.39	0.44
C20015-SLT-80x160-2	160.00	80.00	0.42	149.18	66.24	0.35	2.96	9.50	93.81	13.53		54.47	24.09	2.39	0.44
C20015-SLT-80x240-1	240.00	80.00	0.42	231.92	66.48	0.35	2.04	6.54	93.81	8.73		51.91	18.00	2.82	0.35
C20015-SLT-80x240-2	240.00	80.00	0.42	231.92	66.48	0.35	2.04	6.54	93.81	8.73		51.91	18.00	2.82	0.35
C20015-CIR-120x120	120.00	120.00	0.63	98.77	99.00	0.52	3.27	10.49	93.81	30.54		41.22	21.55	1.98	0.52
C20015-SLT-120x240-1	240.00	120.00	0.63	223.77	99.36	0.52	1.77	5.69	93.81	13.53		26.78	11.82	2.17	0.44
C20015-SLT-120x240-2	240.00	120.00	0.63	223.77	99.36	0.52	1.77	5.69	93.81	13.53		26.78	11.65	2.17	0.44
C20015-SLT-120x360-1	360.00	120.00	0.63	347.87	99.72	0.52	0.86	2.77	93.81	8.73		22.45	7.59	2.85	0.34
C20015-SLT-120x360-2	360.00	120.00	0.63	347.87	99.72	0.52	0.86	2.77	93.81	8.73		22.45	7.62	2.85	0.34

Appendix D: Shear test results based on $V_{y,proposed}$ versus DSM shear curves

Designation	L_{h-eq} (mm)	d_{h-eq} (mm)	d_{h-eq}/h	k_v	V_{cr} (kN)	V_y (kN)	m	v_i	$V_{vrd,m}$ (kN)	V_{vrd} (kN)	$V_{y,proposed}$ (kN)	$V_{n,test}$ (kN)	$\lambda_v = \sqrt{V_{y,proposed}/V_{cr}}$	$V_{n,test}/V_{y,proposed}$
C20015-SQR-40x40	40.00	40.00	0.21	5.90	18.95	93.81	0.60	1.00	30.47		80.08	43.25	2.06	0.54
C20015-REC-40x80-1	80.00	40.00	0.21	4.85	15.58	93.81	0.51	1.21	25.35		76.89	38.05	2.22	0.49
C20015-REC-40x80-2	80.00	40.00	0.21	4.85	15.58	93.81	0.51	1.21	25.35		76.89	38.55	2.22	0.50
C20015-REC-40x120-1	120.00	40.00	0.21	4.03	12.94	93.81	0.43	1.36	25.10		74.22	34.58	2.40	0.47
C20015-REC-40x120-2	120.00	40.00	0.21	4.03	12.94	93.81	0.43	1.36	25.10		74.22	33.62	2.40	0.47
C20015-SQR-80x80	80.00	80.00	0.42	3.94	12.66	93.81	0.60	1.00	30.47		53.69	29.00	2.06	0.54
C20015-REC-80x160-1	160.00	80.00	0.42	2.61	8.37	93.81	0.51	1.21	25.35		44.35	21.41	2.30	0.48
C20015-REC-80x160-2	160.00	80.00	0.42	2.61	8.37	93.81	0.51	1.21	25.35		44.35	21.21	2.30	0.48
C20015-REC-80x240-1	240.00	80.00	0.42	1.80	5.79	93.81	0.43	1.36	25.10		36.55	16.13	2.51	0.44
C20015-REC-80x240-2	240.00	80.00	0.42	1.80	5.79	93.81	0.43	1.36	25.10		36.55	15.69	2.51	0.43
C20015-SQR-120x120	120.00	120.00	0.63	2.70	8.67	93.81	0.60	1.00		26.54	26.54	15.28	1.75	0.58
C20015-REC-120x240-1	240.00	120.00	0.63	1.51	4.85	93.81	0.51	1.21		13.27	15.99	8.76	1.81	0.55
C20015-REC-120x240-2	240.00	120.00	0.63	1.51	4.85	93.81	0.51	1.21		13.27	15.99	8.77	1.81	0.55
C20015-REC-120x360-1	360.00	120.00	0.63	0.73	2.36	93.81	0.43	1.36		8.85	12.03	6.08	2.26	0.50
C20015-REC-120x360-2	360.00	120.00	0.63	0.73	2.36	93.81	0.43	1.36		8.85	12.03	6.00	2.26	0.50
C20015-CIR-40x40	32.92	33.00	0.17	6.28	20.17	93.81	0.60	1.00	30.47		84.71	44.20	2.05	0.52
C20015-SLT-40x80-1	74.59	33.12	0.17	5.19	16.67	93.81	0.48	1.25	25.12		82.03	41.39	2.22	0.50
C20015-SLT-40x80-2	74.59	33.12	0.17	5.19	16.67	93.81	0.48	1.25	25.12		82.03	41.44	2.22	0.51
C20015-SLT-40x120-1	115.96	33.24	0.17	4.31	13.85	93.81	0.40	1.42	25.17		79.67	35.90	2.40	0.45
C20015-SLT-40x120-2	115.96	33.24	0.17	4.31	13.85	93.81	0.40	1.42	25.17		79.67	36.04	2.40	0.45
C20015-CIR-80x80	65.85	66.00	0.34	4.56	14.63	93.81	0.60	1.00	30.47		62.95	32.98	2.05	0.54
C20015-SLT-80x160-1	149.18	66.24	0.35	2.96	9.50	93.81	0.48	1.25	25.12		54.00	24.21	2.38	0.45
C20015-SLT-80x160-2	149.18	66.24	0.35	2.96	9.50	93.81	0.48	1.25	25.12		54.00	24.09	2.38	0.45
C20015-SLT-80x240-1	231.92	66.48	0.35	2.04	6.54	93.81	0.40	1.42	25.17		46.20	18.00	2.66	0.40
C20015-SLT-80x240-2	231.92	66.48	0.35	2.04	6.54	93.81	0.40	1.42	25.17		46.20	18.00	2.66	0.40
C20015-CIR-120x120	98.77	99.00	0.52	3.27	10.49	93.81	0.60	1.00	30.47		41.20	21.55	1.98	0.52
C20015-SLT-120x240-1	223.77	99.36	0.52	1.77	5.69	93.81	0.48	1.25		21.08	26.32	11.82	2.15	0.45
C20015-SLT-120x240-2	223.77	99.36	0.52	1.77	5.69	93.81	0.48	1.25		21.08	26.32	11.65	2.15	0.44
C20015-SLT-120x360-1	347.87	99.72	0.52	0.86	2.77	93.81	0.40	1.42		13.47	19.10	7.59	2.63	0.44
C20015-SLT-120x360-2	347.87	99.72	0.52	0.86	2.77	93.81	0.40	1.42		13.47	19.10	7.62	2.63	0.44

Appendix E.1: Verification of $V_{y,proposed}$ with C200 channel members with various web hole sizes

Designation	L_{h-eq} (mm)	d_{h-eq} (mm)	d_{h-eq}/h	V_{cr} (kN)	V_y (kN)	m	v_i	$V_{vrd,m}$ (kN)	V_{vrd} (kN)	$V_{y,proposed}$ (kN)	V_n (kN)	$\lambda_v = \sqrt{V_{y,proposed}/V_{cr}}$	$V_n/V_{y,proposed}$
C20010-SQR-40x40	40.00	40.00	0.21	5.62	67.40	0.60	1.00	21.73		57.51	22.46	3.20	0.39
C20010-SQR-80x80	80.00	80.00	0.42	3.78	67.40	0.60	1.00	21.73		38.48	15.31	3.19	0.40
C20010-SQR-120x120	120.00	120.00	0.63	2.60	67.40	0.60	1.00		18.90	18.90	8.20	2.69	0.43
C20010-REC-40x80	80.00	40.00	0.21	4.63	67.40	0.51	1.21	18.14		55.22	20.18	3.45	0.37
C20010-REC-80x160	160.00	80.00	0.42	2.51	67.40	0.51	1.21	18.14		31.80	11.32	3.56	0.36
C20010-REC-120x240	240.00	120.00	0.63	1.45	67.40	0.51	1.21		9.45	11.39	4.93	2.81	0.43
C20010-REC-40x120	120.00	40.00	0.21	3.86	67.40	0.43	1.36	17.99		53.31	18.43	3.72	0.35
C20010-REC-80x240	240.00	80.00	0.42	1.72	67.40	0.43	1.36	17.99		26.20	8.71	3.90	0.33
C20010-REC-120x360	360.00	120.00	0.63	0.70	67.40	0.43	1.36		6.30	8.57	3.47	3.50	0.40
C20015-SQR-40x40	40.00	40.00	0.21	18.95	93.81	0.60	1.00	30.47		80.08	43.25	2.06	0.54
C20015-SQR-80x80	80.00	80.00	0.42	12.66	93.81	0.60	1.00	30.47		53.69	29.00	2.06	0.54
C20015-SQR-120x120	120.00	120.00	0.63	8.67	93.81	0.60	1.00		26.54	26.54	15.28	1.75	0.58
C20015-REC-40x80	80.00	40.00	0.21	15.58	93.81	0.51	1.21	25.35		76.89	38.30	2.22	0.50
C20015-REC-80x160	160.00	80.00	0.42	8.37	93.81	0.51	1.21	25.35		44.35	21.30	2.30	0.48
C20015-REC-120x240	240.00	120.00	0.63	4.85	93.81	0.51	1.21		13.27	15.99	8.76	1.81	0.55
C20015-REC-40x120	120.00	40.00	0.21	12.94	93.81	0.43	1.36	25.10		74.22	34.60	2.40	0.47
C20015-REC-80x240	240.00	80.00	0.42	5.79	93.81	0.43	1.36	25.10		36.55	15.85	2.51	0.43
C20015-REC-120x360	360.00	120.00	0.63	2.36	93.81	0.43	1.36		8.85	12.03	6.04	2.26	0.50
C20019-SQR-40x40	40.00	40.00	0.21	37.69	111.73	0.60	1.00	36.51		95.44	62.46	1.59	0.65
C20019-SQR-80x80	80.00	80.00	0.42	25.03	111.73	0.60	1.00	36.51		64.09	41.20	1.60	0.64
C20019-SQR-120x120	120.00	120.00	0.63	17.07	111.73	0.60	1.00		31.83	31.83	21.23	1.37	0.67
C20019-REC-40x80	80.00	40.00	0.21	30.90	111.73	0.51	1.21	30.30		91.61	54.64	1.72	0.60
C20019-REC-80x160	160.00	80.00	0.42	16.51	111.73	0.51	1.21	30.30		52.92	29.07	1.79	0.55
C20019-REC-120x240	240.00	120.00	0.63	9.63	111.73	0.51	1.21		15.92	19.18	12.11	1.41	0.63

Designation	L_{h-eq} (mm)	d_{h-eq} (mm)	d_{h-eq}/h	V_{cr} (kN)	V_y (kN)	m	v_i	$V_{vrd,m}$ (kN)	V_{vrd} (kN)	$V_{y,proposed}$ (kN)	V_n (kN)	$\lambda_v = \sqrt{V_{y,proposed}/V_{cr}}$	$V_n/V_{y,proposed}$
C20019-REC-40x120	120.00	40.00	0.21	25.58	111.73	0.43	1.36	29.96		88.43	47.32	1.86	0.54
C20019-REC-80x240	240.00	80.00	0.42	11.47	111.73	0.43	1.36	29.96		43.61	22.00	1.95	0.50
C20019-REC-120x360	360.00	120.00	0.63	4.68	111.73	0.43	1.36		10.61	14.43	8.35	1.76	0.58
C20024-SQR-40x40	40.00	40.00	0.21	75.01	128.15	0.60	1.00	42.20		109.52	89.00	1.21	0.81
C20024-SQR-80x80	80.00	80.00	0.42	49.47	128.15	0.60	1.00	42.20		73.71	58.77	1.22	0.80
C20024-SQR-120x120	120.00	120.00	0.63	33.59	128.15	0.60	1.00		36.84	36.84	29.72	1.05	0.81
C20024-REC-40x80	80.00	40.00	0.21	61.32	128.15	0.51	1.21	34.91		105.12	78.35	1.31	0.75
C20024-REC-80x160	160.00	80.00	0.42	32.53	128.15	0.51	1.21	34.91		60.84	40.81	1.37	0.67
C20024-REC-120x240	240.00	120.00	0.63	19.12	128.15	0.51	1.21		18.42	22.19	17.10	1.08	0.77
C20024-REC-40x120	120.00	40.00	0.21	50.56	128.15	0.43	1.36	34.45		101.46	67.33	1.42	0.66
C20024-REC-80x240	240.00	80.00	0.42	22.68	128.15	0.43	1.36	34.45		50.13	31.00	1.49	0.62
C20024-REC-120x360	360.00	120.00	0.63	9.30	128.15	0.43	1.36		12.28	16.70	11.49	1.34	0.69
C20010-CIR-40x40	32.92	33.00	0.17	5.95	67.40	0.60	1.00	21.73		60.84	24.17	3.20	0.40
C20010-CIR-80x80	65.85	66.00	0.34	4.37	67.40	0.60	1.00	21.73		45.15	18.10	3.21	0.40
C20010-CIR-120x120	98.77	99.00	0.52	3.09	67.40	0.60	1.00	21.73		29.47	10.89	3.09	0.37
C20010-SLT-40x80	74.59	33.12	0.17	4.93	67.40	0.48	1.25	17.99		58.92	21.72	3.46	0.37
C20010-SLT-80x160	149.18	66.24	0.35	2.81	67.40	0.48	1.25	17.99		38.75	13.34	3.71	0.34
C20010-SLT-120x240	223.77	99.36	0.52	1.71	67.40	0.48	1.25		15.08	18.83	6.73	3.32	0.34
C20010-SLT-40x120	115.96	33.24	0.17	4.08	67.40	0.40	1.42	18.07		57.24	19.49	3.75	0.34
C20010-SLT-80x240	231.92	66.48	0.35	1.93	67.40	0.40	1.42	18.07		33.17	9.99	4.15	0.30
C20010-SLT-120x360	347.87	99.72	0.52	0.85	67.40	0.40	1.42		9.64	13.66	4.28	4.02	0.31
C20015-CIR-40x40	32.92	33.00	0.17	20.17	93.81	0.60	1.00	30.47		84.71	44.19	2.05	0.52
C20015-CIR-80x80	65.85	66.00	0.34	14.63	93.81	0.60	1.00	30.47		62.95	32.98	2.05	0.54
C20015-CIR-120x120	98.77	99.00	0.52	10.49	93.81	0.60	1.00	30.47		41.20	21.55	1.98	0.52

Designation	L_{h-eq} (mm)	d_{h-eq} (mm)	d_{h-eq}/h	V_{cr} (kN)	V_y (kN)	m	v_i	$V_{vrd,m}$ (kN)	V_{vrd} (kN)	$V_{y,proposed}$ (kN)	V_n (kN)	$\lambda_v = \sqrt{V_{y,proposed}/V_{cr}}$	$V_n/V_{y,proposed}$
C20015-SLT-40x80	74.59	33.12	0.17	16.67	93.81	0.48	1.25	25.12		82.03	41.31	2.22	0.50
C20015-SLT-80x160	149.18	66.24	0.35	9.50	93.81	0.48	1.25	25.12		54.00	24.15	2.38	0.45
C20015-SLT-120x240	223.77	99.36	0.52	5.69	93.81	0.48	1.25		21.08	26.32	11.71	2.15	0.45
C20015-SLT-40x120	115.96	33.24	0.17	13.85	93.81	0.40	1.42	25.17		79.67	36.00	2.40	0.45
C20015-SLT-80x240	231.92	66.48	0.35	6.54	93.81	0.40	1.42	25.17		46.20	18.00	2.66	0.40
C20015-SLT-120x360	347.87	99.72	0.52	2.77	93.81	0.40	1.42		13.47	19.10	7.60	2.63	0.44
C20019-CIR-40x40	32.92	33.00	0.17	40.02	111.73	0.60	1.00	36.51		100.93	66.83	1.59	0.66
C20019-CIR-80x80	65.85	66.00	0.34	29.10	111.73	0.60	1.00	36.51		75.09	48.83	1.61	0.65
C20019-CIR-120x120	98.77	99.00	0.52	20.36	111.73	0.60	1.00	36.51		49.25	31.37	1.56	0.64
C20019-SLT-40x80	74.59	33.12	0.17	32.98	111.73	0.48	1.25	30.01		97.72	58.00	1.72	0.59
C20019-SLT-80x160	149.18	66.24	0.35	18.51	111.73	0.48	1.25	30.01		64.38	34.58	1.86	0.54
C20019-SLT-120x240	223.77	99.36	0.52	11.29	111.73	0.48	1.25		25.20	31.47	17.36	1.67	0.55
C20019-SLT-40x120	115.96	33.24	0.17	27.08	111.73	0.40	1.42	30.10		94.94	50.67	1.87	0.53
C20019-SLT-80x240	231.92	66.48	0.35	12.71	111.73	0.40	1.42	30.10		55.17	26.12	2.08	0.47
C20019-SLT-120x360	347.87	99.72	0.52	5.65	111.73	0.40	1.42		16.11	22.83	10.86	2.01	0.48
C20024-CIR-40x40	32.92	33.00	0.17	80.71	128.15	0.60	1.00	42.20		115.80	92.06	1.20	0.79
C20024-CIR-80x80	65.85	66.00	0.34	58.39	128.15	0.60	1.00	42.20		86.28	71.09	1.22	0.82
C20024-CIR-120x120	98.77	99.00	0.52	40.61	128.15	0.60	1.00	42.20		56.76	45.52	1.18	0.80
C20024-SLT-40x80	74.59	33.12	0.17	65.54	128.15	0.48	1.25	34.56		112.11	84.18	1.31	0.75
C20024-SLT-80x160	149.18	66.24	0.35	36.48	128.15	0.48	1.25	34.56		73.95	48.93	1.42	0.66
C20024-SLT-120x240	223.77	99.36	0.52	22.30	128.15	0.48	1.25		29.04	36.26	23.96	1.28	0.66
C20024-SLT-40x120	115.96	33.24	0.17	40.61	128.15	0.40	1.42	34.60		108.91	72.01	1.64	0.66
C20024-SLT-80x240	231.92	66.48	0.35	25.05	128.15	0.40	1.42	34.60		63.35	35.79	1.59	0.56
C20024-SLT-120x360	347.87	99.72	0.52	11.23	128.15	0.40	1.42		18.56	26.31	15.32	1.53	0.58

Appendix E.2: Verification of $V_{y,proposed}$ with C250 channel members with various web hole sizes

Designation	L_{h-eq} (mm)	d_{h-eq} (mm)	d_{h-eq}/h	V_{cr} (kN)	V_y (kN)	m	v_i	$V_{vrd,m}$ (kN)	V_{vrd} (kN)	$V_{y,proposed}$ (kN)	V_n (kN)	$\lambda_v = \sqrt{V_{y,proposed}/V_{cr}}$	$V_n/V_{y,proposed}$
C25010-SQR-40x40	40.00	40.00	0.17	4.72	85.68	0.60	1.00	23.63		77.41	22.15	4.05	0.29
C25010-SQR-80x80	80.00	80.00	0.33	3.42	85.68	0.60	1.00	23.63		56.72	17.14	4.07	0.30
C25010-SQR-120x120	120.00	120.00	0.5	2.44	85.68	0.60	1.00	23.63		36.04	11.75	3.84	0.33
C25010-SQR-150x150	150.00	150.00	0.63	1.95	85.68	0.60	1.00		20.66	20.66	7.95	3.25	0.38
C25010-REC-40x80	80.00	40.00	0.17	4.06	85.68	0.51	1.21	19.20		75.38	24.90	4.31	0.33
C25010-REC-80x160	160.00	80.00	0.33	2.41	85.68	0.51	1.21	19.20		49.64	16.36	4.54	0.33
C25010-REC-120x240	240.00	120.00	0.5	1.52	85.68	0.51	1.21	19.20		23.90	8.98	3.97	0.38
C25010-REC-150x300	300.00	150.00	0.63	1.12	85.68	0.51	1.21		10.33	12.45	5.00	3.33	0.40
C25010-REC-40x120	120.00	40.00	0.17	3.50	85.68	0.43	1.36	18.57		73.47	22.26	4.58	0.30
C25010-REC-80x240	240.00	80.00	0.33	1.80	85.68	0.43	1.36	18.57		42.96	12.79	4.89	0.30
C25010-REC-120x360	360.00	120.00	0.5	0.95	85.68	0.43	1.36	18.57		17.84	6.33	4.33	0.35
C25010-REC-150x450	450.00	150.00	0.63	0.55	85.68	0.43	1.36		6.89	9.37	3.34	4.13	0.36
C25015-SQR-40x40	40.00	40.00	0.17	15.44	117.26	0.60	1.00	32.26		105.93	48.56	2.62	0.46
C25015-SQR-80x80	80.00	80.00	0.33	11.07	117.26	0.60	1.00	32.26		77.59	36.06	2.65	0.46
C25015-SQR-120x120	120.00	120.00	0.5	7.80	117.26	0.60	1.00	32.26		49.26	24.04	2.51	0.49
C25015-SQR-150x150	150.00	150.00	0.63	6.22	117.26	0.60	1.00		28.22	28.22	15.88	2.13	0.56
C25015-REC-40x80	80.00	40.00	0.17	13.21	117.26	0.51	1.21	26.17		103.15	46.95	2.79	0.46
C25015-REC-80x160	160.00	80.00	0.33	7.70	117.26	0.51	1.21	26.17		67.87	29.01	2.97	0.43
C25015-REC-120x240	240.00	120.00	0.5	4.85	117.26	0.51	1.21	26.17		32.59	16.13	2.59	0.49
C25015-REC-150x300	300.00	150.00	0.63	3.65	117.26	0.51	1.21		14.11	17.00	9.35	2.16	0.55
C25015-REC-40x120	120.00	40.00	0.17	11.32	117.26	0.43	1.36	25.30		100.52	40.74	2.98	0.41
C25015-REC-80x240	240.00	80.00	0.33	5.72	117.26	0.43	1.36	25.30		58.68	23.31	3.20	0.40
C25015-REC-120x360	360.00	120.00	0.5	3.12	117.26	0.43	1.36	25.30		24.32	11.88	2.79	0.49
C25015-REC-150x450	450.00	150.00	0.63	1.82	117.26	0.43	1.36		9.41	12.79	6.50	2.65	0.51

Designation	L_{h-eq} (mm)	d_{h-eq} (mm)	d_{h-eq}/h	V_{cr} (kN)	V_y (kN)	m	v_i	$V_{vrd,m}$ (kN)	V_{vrd} (kN)	$V_{y,proposed}$ (kN)	V_n (kN)	$\lambda_v = \sqrt{V_{y,proposed}/V_{cr}}$	$V_n/V_{y,proposed}$
C25019-SQR-40x40	40.00	40.00	0.17	30.63	139.67	0.60	1.00	38.34		126.16	71.13	2.03	0.56
C25019-SQR-80x80	80.00	80.00	0.33	21.87	139.67	0.60	1.00	38.34		92.38	55.15	2.06	0.60
C25019-SQR-120x120	120.00	120.00	0.5	15.30	139.67	0.60	1.00	38.34		58.60	34.29	1.96	0.59
C25019-SQR-150x150	150.00	150.00	0.63	12.15	139.67	0.60	1.00		33.56	33.56	22.15	1.66	0.66
C25019-REC-40x80	80.00	40.00	0.17	26.17	139.67	0.51	1.21	31.06		122.84	64.68	2.17	0.53
C25019-REC-80x160	160.00	80.00	0.33	15.12	139.67	0.51	1.21	31.06		80.77	41.97	2.31	0.52
C25019-REC-120x240	240.00	120.00	0.5	9.48	139.67	0.51	1.21	31.06		38.69	22.25	2.02	0.57
C25019-REC-150x300	300.00	150.00	0.63	7.20	139.67	0.51	1.21		16.78	20.22	12.90	1.68	0.64
C25019-REC-40x120	120.00	40.00	0.17	22.36	139.67	0.43	1.36	30.02		119.70	60.64	2.31	0.51
C25019-REC-80x240	240.00	80.00	0.33	11.19	139.67	0.43	1.36	30.02		69.78	32.13	2.50	0.46
C25019-REC-120x360	360.00	120.00	0.5	6.20	139.67	0.43	1.36	30.02		28.87	16.17	2.16	0.56
C25019-REC-150x450	450.00	150.00	0.63	3.64	139.67	0.43	1.36		11.19	15.21	8.85	2.04	0.58
C25024-SQR-40x40	40.00	40.00	0.17	60.06	167.09	0.60	1.00	45.74		150.91	103.54	1.59	0.69
C25024-SQR-80x80	80.00	80.00	0.33	42.79	167.09	0.60	1.00	45.74		110.46	75.28	1.61	0.68
C25024-SQR-120x120	120.00	120.00	0.5	29.76	167.09	0.60	1.00	45.74		70.01	48.38	1.53	0.69
C25024-SQR-150x150	150.00	150.00	0.63	23.53	167.09	0.60	1.00		40.06	40.06	30.71	1.30	0.77
C25024-REC-40x80	80.00	40.00	0.17	51.29	167.09	0.51	1.21	37.01		146.93	93.69	1.69	0.64
C25024-REC-80x160	160.00	80.00	0.33	29.42	167.09	0.51	1.21	37.01		96.52	56.66	1.81	0.59
C25024-REC-120x240	240.00	120.00	0.5	18.34	167.09	0.51	1.21	37.01		46.11	30.77	1.59	0.67
C25024-REC-150x300	300.00	150.00	0.63	13.98	167.09	0.51	1.21		20.03	24.14	17.65	1.31	0.73
C25024-REC-40x120	120.00	40.00	0.17	43.72	167.09	0.43	1.36	35.74		143.16	82.36	1.81	0.58
C25024-REC-80x240	240.00	80.00	0.33	21.66	167.09	0.43	1.36	35.74		83.32	44.45	1.96	0.53
C25024-REC-120x360	360.00	120.00	0.5	12.11	167.09	0.43	1.36	35.74		34.39	21.94	1.69	0.64
C25024-REC-150x450	450.00	150.00	0.63	7.20	167.09	0.43	1.36		13.35	18.16	11.87	1.59	0.65

Designation	L_{h-eq} (mm)	d_{h-eq} (mm)	d_{h-eq}/h	V_{cr} (kN)	V_y (kN)	m	v_i	$V_{vrd,m}$ (kN)	V_{vrd} (kN)	$V_{y,proposed}$ (kN)	V_n (kN)	$\lambda_v = \sqrt{V_{y,proposed}/V_{cr}}$	$V_n/V_{y,proposed}$
C25010-CIR-40x40	32.92	33.00	0.14	4.93	85.68	0.60	1.00	23.63		81.03	26.92	4.06	0.33
C25010-CIR-80x80	65.85	66.00	0.28	3.87	85.68	0.60	1.00	23.63		63.98	19.61	4.07	0.31
C25010-CIR-120x120	98.77	99.00	0.42	2.90	85.68	0.60	1.00	23.63		46.92	14.23	4.02	0.30
C25010-CIR-150x150	123.46	123.75	0.52	2.34	85.68	0.60	1.00	23.63		34.13	10.56	3.82	0.31
C25010-SLT-40x80	74.59	33.12	0.14	4.26	85.68	0.48	1.25	18.90		79.54	23.62	4.32	0.30
C25010-SLT-80x160	149.18	66.24	0.28	2.67	85.68	0.48	1.25	18.90		57.25	15.63	4.63	0.27
C25010-SLT-120x240	223.77	99.36	0.42	1.72	85.68	0.48	1.25	18.90		34.95	9.85	4.51	0.28
C25010-SLT-150x300	279.72	124.20	0.52	1.31	85.68	0.48	1.25		16.02	20.00	6.34	3.91	0.32
C25010-SLT-40x120	115.96	33.24	0.14	3.67	85.68	0.40	1.42	18.50		78.07	20.99	4.61	0.27
C25010-SLT-80x240	231.92	66.48	0.28	1.93	85.68	0.40	1.42	18.50		50.68	12.74	5.12	0.25
C25010-SLT-120x360	347.87	99.72	0.42	1.11	85.68	0.40	1.42		17.17	24.34	7.22	4.69	0.30
C25010-SLT-150x450	434.84	124.65	0.52	0.66	85.68	0.40	1.42		10.24	14.52	4.31	4.68	0.30
C25015-CIR-40x40	32.92	33.00	0.14	16.14	117.26	0.60	1.00	32.26		110.89	50.12	2.62	0.45
C25015-CIR-80x80	65.85	66.00	0.28	12.59	117.26	0.60	1.00	32.26		87.53	40.14	2.64	0.46
C25015-CIR-120x120	98.77	99.00	0.42	9.35	117.26	0.60	1.00	32.26		64.17	29.38	2.62	0.46
C25015-CIR-150x150	123.46	123.75	0.52	7.47	117.26	0.60	1.00	32.26		46.65	21.79	2.50	0.47
C25015-SLT-40x80	74.59	33.12	0.14	13.95	117.26	0.48	1.25	25.76		108.84	47.47	2.79	0.44
C25015-SLT-80x160	149.18	66.24	0.28	8.65	117.26	0.48	1.25	25.76		78.28	32.50	3.01	0.42
C25015-SLT-120x240	223.77	99.36	0.42	5.54	117.26	0.48	1.25	25.76		47.72	19.75	2.93	0.41
C25015-SLT-150x300	279.72	124.20	0.52	4.19	117.26	0.48	1.25		21.83	27.27	12.38	2.55	0.45
C25015-SLT-40x120	115.96	33.24	0.14	11.98	117.26	0.40	1.42	25.20		106.82	42.43	2.99	0.40
C25015-SLT-80x240	231.92	66.48	0.28	6.32	117.26	0.40	1.42	25.20		69.25	26.15	3.31	0.38
C25015-SLT-120x360	347.87	99.72	0.42	3.56	117.26	0.40	1.42		23.39	33.15	14.00	3.05	0.42
C25015-SLT-150x450	434.84	124.65	0.52	2.13	117.26	0.40	1.42		13.96	19.79	8.09	3.05	0.41

Designation	L_{h-eq} (mm)	d_{h-eq} (mm)	d_{h-eq}/h	V_{cr} (kN)	V_y (kN)	m	v_i	$V_{vrd,m}$ (kN)	V_{vrd} (kN)	$V_{y,proposed}$ (kN)	V_n (kN)	$\lambda_v = \sqrt{V_{y,proposed}/V_{cr}}$	$V_n/V_{y,proposed}$
C25019-CIR-40x40	32.92	33.00	0.14	32.04	139.67	0.60	1.00	38.34		132.07	73.14	2.03	0.55
C25019-CIR-80x80	65.85	66.00	0.28	29.94	139.67	0.60	1.00	38.34		104.23	61.46	1.87	0.59
C25019-CIR-120x120	98.77	99.00	0.42	18.41	139.67	0.60	1.00	38.34		76.38	42.75	2.04	0.56
C25019-CIR-150x150	123.46	123.75	0.52	14.66	139.67	0.60	1.00	38.34		55.50	31.91	1.95	0.57
C25019-SLT-40x80	74.59	33.12	0.14	27.58	139.67	0.48	1.25	30.58		129.63	67.37	2.17	0.52
C25019-SLT-80x160	149.18	66.24	0.28	16.89	139.67	0.48	1.25	30.58		93.18	46.02	2.35	0.49
C25019-SLT-120x240	223.77	99.36	0.42	10.68	139.67	0.48	1.25	30.58		56.73	27.67	2.30	0.49
C25019-SLT-150x300	279.72	124.20	0.52	8.18	139.67	0.48	1.25		25.92	32.37	17.28	1.99	0.53
C25019-SLT-40x120	115.96	33.24	0.14	23.54	139.67	0.40	1.42	29.90		127.21	62.12	2.32	0.49
C25019-SLT-80x240	231.92	66.48	0.28	12.06	139.67	0.40	1.42	29.90		82.39	36.24	2.61	0.44
C25019-SLT-120x360	347.87	99.72	0.42	7.04	139.67	0.40	1.42		27.75	39.34	19.19	2.36	0.49
C25019-SLT-150x450	434.84	124.65	0.52	4.36	139.67	0.40	1.42		16.58	23.50	11.14	2.32	0.47
C25024-CIR-40x40	32.92	33.00	0.14	62.81	167.09	0.60	1.00	45.74		158.00	105.83	1.59	0.67
C25024-CIR-80x80	65.85	66.00	0.28	48.89	167.09	0.60	1.00	45.74		124.65	86.98	1.60	0.70
C25024-CIR-120x120	98.77	99.00	0.42	35.95	167.09	0.60	1.00	45.74		91.30	65.50	1.59	0.72
C25024-CIR-150x150	123.46	123.75	0.52	28.51	167.09	0.60	1.00	45.74		66.29	46.43	1.52	0.70
C25024-SLT-40x80	74.59	33.12	0.14	54.08	167.09	0.48	1.25	36.42		155.07	97.78	1.69	0.63
C25024-SLT-80x160	149.18	66.24	0.28	32.94	167.09	0.48	1.25	36.42		111.39	67.70	1.84	0.61
C25024-SLT-120x240	223.77	99.36	0.42	20.68	167.09	0.48	1.25	36.42		67.71	38.89	1.81	0.57
C25024-SLT-150x300	279.72	124.20	0.52	15.78	167.09	0.48	1.25		30.89	38.57	23.97	1.56	0.62
C25024-SLT-40x120	115.96	33.24	0.14	46.07	167.09	0.40	1.42	35.59		152.16	88.76	1.82	0.58
C25024-SLT-80x240	231.92	66.48	0.28	23.39	167.09	0.40	1.42	35.59		98.42	50.38	2.05	0.51
C25024-SLT-120x360	347.87	99.72	0.42	13.64	167.09	0.40	1.42		33.04	46.83	26.21	1.85	0.56
C25024-SLT-150x450	434.84	124.65	0.52	8.57	167.09	0.40	1.42		19.76	28.00	15.13	1.81	0.54

Appendix F: Verification of $V_{y,proposed}$ with critical opening sizes on channels C200 and C250

Designation	L_h (mm)	d_h (mm)	d_h / h	V_{cr} (kN)	V_y (kN)	m	v_i	$V_{vrd,m}$ (kN)	V_{vrd} (kN)	$V_{y,proposed}$ (kN)	V_n (kN)	$\lambda_v = \sqrt{V_{y,proposed} / V_{cr}}$	$V_n / V_{y,proposed}$
C20010-REC-40x360	360	40	0.21	1.10	67.40	0.40	1.24	7.03	21.29	46.21	10.30	6.49	0.22
C20010-REC-160x360	360	160	0.83	0.65	67.40	0.48	1.25	17.99	2.31	2.88	1.47	2.11	0.51
C20010-REC-160x40	40	160	0.83	3.23	67.40	0.68	0.81	53.70	20.78	16.91	7.56	2.29	0.45
C20015-REC-40x360	360	40	0.21	3.68	93.81	0.40	1.24	9.79	29.58	64.32	17.95	4.18	0.28
C20015-REC-160x360	360	160	0.83	2.17	93.81	0.48	1.25	25.13	3.32	4.14	2.70	1.38	0.65
C20015-REC-160x40	40	160	0.83	12.50	93.81	0.68	0.81	75.67	29.85	24.28	15.12	1.39	0.62
C20019-REC-40x360	360	40	0.21	7.27	111.73	0.40	1.24	11.71	35.19	76.63	25.78	3.25	0.34
C20019-REC-160x360	360	160	0.83	4.29	111.73	0.48	1.25	30.02	4.05	5.06	3.87	1.09	0.77
C20019-REC-160x40	40	160	0.83	23.15	111.73	0.68	0.81	91.04	36.44	29.64	20.70	1.13	0.70
C20024-REC-40x360	360	40	0.21	14.37	128.15	0.40	1.24	13.46	40.30	87.90	35.12	2.47	0.40
C20024-REC-160x360	360	160	0.83	8.47	128.15	0.48	1.25	34.56	4.79	5.98	5.20	0.84	0.87
C20024-REC-160x40	40	160	0.83	48.34	128.15	0.68	0.81	105.73	43.09	35.05	26.68	0.85	0.82
C25010-REC-50x450	450	50	0.21	0.85	85.68	0.40	1.24	7.19	22.57	57.96	11.10	8.27	0.19
C25010-REC-200x450	450	200	0.83	0.51	85.68	0.48	1.25	18.91	2.31	2.89	1.47	2.39	0.51
C25010-REC-200x50	50	200	0.83	2.83	85.68	0.68	0.81	58.96	20.82	16.94	7.91	2.44	0.47
C25015-REC-50x450	450	50	0.21	2.76	117.26	0.40	1.24	9.80	30.86	79.30	19.05	5.36	0.24
C25015-REC-200x450	450	200	0.83	1.67	117.26	0.48	1.25	25.77	3.21	4.01	2.57	1.55	0.64
C25015-REC-200x50	50	200	0.83	9.05	117.26	0.68	0.81	80.71	28.93	23.53	14.36	1.61	0.61
C25019-REC-50x450	450	50	0.21	5.44	139.67	0.40	1.24	11.62	36.73	94.44	25.13	4.17	0.27
C25019-REC-200x450	450	200	0.83	3.35	139.67	0.48	1.25	30.58	3.88	4.84	3.53	1.20	0.73
C25019-REC-200x50	50	200	0.83	17.75	139.67	0.68	0.81	96.14	34.88	28.37	20.69	1.26	0.73
C25024-REC-50x450	450	50	0.21	10.59	167.09	0.40	1.24	13.84	43.91	112.95	36.03	3.27	0.32
C25024-REC-200x450	450	200	0.83	6.63	167.09	0.48	1.25	36.43	4.71	5.88	4.90	0.94	0.83
C25024-REC-200x50	50	200	0.83	34.49	167.09	0.68	0.81	115.01	42.38	34.47	29.46	1.00	0.85

Appendix G: Python code for ABAQUS modelling and buckling analyses

It is noted that the blanks '...' in the script are for the values of variables (i.e. the dimensions of channel sections and material properties)

```
#INPUT VARIABLES
#===============
#DIMENSIONS Of COLD-FORMED CHANNEL SECTION
#-----------------------------------------
#Aspect ratio of shear span
AR = ...
#Overall depth of channel
H = ...
#Length of flange
B = ...
#Length of lip
l = ...
#Radius of rounded corner
r = ...
# Thickness of channel
t = ...
#Length of channel
Length = H * AR
#Hole depth
h = ...
#Hole length
L = ...
#Location of hole along the member length
m = Length/2

#MATERIAL PROPERTIES
#-------------------
#Young modulus
E = ...
#Poison ratio
v = ...

#COORDINATES Of CROSS-SECTIONAL POINTS
#-------------------------------------
#**********************************WEB
X1_Web = 0.0
Y1_Web = H/2
X2_Web = 0.0
Y2_Web = -H/2
#*****************************FLANGE
X1_Flange_Up = 0.0
```

```
Y1_Flange_Up = H/2
X2_Flange_Up = B
Y2_Flange_Up = H/2
X1_Flange_Down = 0.0
Y1_Flange_Down = -H/2
X2_Flange_Down = B
Y2_Flange_Down = -H/2
#*********************************LIP
X1_Lip_Up = B
Y1_Lip_Up = H/2
X2_Lip_Up = B
Y2_Lip_Up = H/2 - l
X1_Lip_Down = B
Y1_Lip_Down = -H/2
X2_Lip_Down = B
Y2_Lip_Down = -H/2 + l
#************************FILLET CONNER
X1_Conner_1 = 0.0
Y1_Conner_1 = H/2 - r
X2_Conner_1 = r
Y2_Conner_1 = H/2
X1_Conner_2 = 0.0
Y1_Conner_2 = -H/2 + r
X2_Conner_2 = r
Y2_Conner_2 = -H/2
X1_Conner_3 = B - r
Y1_Conner_3 = H/2
X2_Conner_3 = B
Y2_Conner_3 = H/2 - r
X1 Conner 4 = B - r
Y1_Conner_4 = -H/2
X2_Conner_4 = B
Y2_Conner_4 = -H/2 + r
#***************************WEB OPENING
X1_Hole = -L/2
Y1_Hole = h/2
X2_Hole = L/2
Y2_Hole = -h/2
X3_Hole = L/2
Y3_Hole = h/2
X4 Hole = -L/2
Y4_Hole = -h/2

#MODELLING
#=========
from part import *
from material import *
from section import *
from assembly import *
```

```
from step import *
from interaction import *
from load import *
from mesh import *
from optimization import *
from job import *
from sketch import *
from visualization import *
from connectorBehavior import *

#CREATING CHANNEL SECTION
#------------------------
mdb.models['Model-1'].ConstrainedSketch(name='__profile__', sheetSize=300.0)
mdb.models['Model-1'].sketches['__profile__'].Line(point1=(X1_Web, Y1_Web), point2=(X2_Web, Y2_Web))
mdb.models['Model-1'].sketches['__profile__'].VerticalConstraint(addUndoState=False, entity=mdb.models['Model-1'].sketches['__profile__'].geometry[2])
mdb.models['Model-1'].sketches['__profile__'].Line(point1=(X1_Flange_Up, Y1_Flange_Up), point2=(X2_Flange_Up, Y2_Flange_Up))
mdb.models['Model-1'].sketches['__profile__'].HorizontalConstraint(addUndoState=False, entity=mdb.models['Model-1'].sketches['__profile__'].geometry[3])
mdb.models['Model-1'].sketches['__profile__'].Line(point1=(X1_Flange_Down, Y1_Flange_Down), point2=(X2_Flange_Down, Y2_Flange_Down))
mdb.models['Model-1'].sketches['__profile__'].HorizontalConstraint(addUndoState=False, entity=mdb.models['Model-1'].sketches['__profile__'].geometry[4])
mdb.models['Model-1'].sketches['__profile__'].Line(point1=(X1_Lip_Up, Y1_Lip_Up), point2=(X2_Lip_Up, Y2_Lip_Up))
mdb.models['Model-1'].sketches['__profile__'].VerticalConstraint(addUndoState=False, entity=mdb.models['Model-1'].sketches['__profile__'].geometry[5])
mdb.models['Model-1'].sketches['__profile__'].Line(point1=(X1_Lip_Down, Y1_Lip_Down), point2=(X2_Lip_Down, Y2_Lip_Down))
mdb.models['Model-1'].sketches['__profile__'].VerticalConstraint(addUndoState=False, entity=mdb.models['Model-1'].sketches['__profile__'].geometry[6])
mdb.models['Model-1'].Part(dimensionality=THREE_D, name='Part-1', type=DEFORMABLE_BODY)
mdb.models['Model-1'].parts['Part-1'].BaseShellExtrude(depth=Length, sketch=mdb.models['Model-1'].sketches['__profile__'])
del mdb.models['Model-1'].sketches['__profile__']

mdb.models['Model-1'].ConstrainedSketch(name='__edit__', objectToCopy=mdb.models['Model-1'].parts['Part-1'].features['Shell extrude-1'].sketch)
mdb.models['Model-1'].parts['Part-1'].projectReferencesOntoSketch(
        filter=COPLANAR EDGES,
        sketch=mdb.models['Model-1'].sketches['__edit__'],
        upToFeature=mdb.models['Model-1'].parts['Part-1'].features['Shell extrude-1'])
mdb.models['Model-1'].sketches['__edit__'].FilletByRadius(
        curve1=mdb.models['Model-1'].sketches['__edit__'].geometry[2],
        curve2=mdb.models['Model-1'].sketches['__edit__'].geometry[3],
        nearPoint1=(X1_Conner_1, Y1_Conner_1),
        nearPoint2=(X2_Conner_1, Y2_Conner_1),
        radius=r)
mdb.models['Model-1'].sketches['__edit__'].FilletByRadius(
        curve1=mdb.models['Model-1'].sketches['__edit__'].geometry[2],
        curve2=mdb.models['Model-1'].sketches['__edit__'].geometry[4],
        nearPoint1=(X1_Conner_2, Y1_Conner_2),
        nearPoint2=(X2_Conner_2, Y2_Conner_2),
        radius=r)
mdb.models['Model-1'].sketches['__edit__'].FilletByRadius(
        curve1=mdb.models['Model-1'].sketches['__edit__'].geometry[3],
        curve2=mdb.models['Model-1'].sketches['__edit__'].geometry[5],
        nearPoint1=(X1_Conner_3, Y1_Conner_3),
        nearPoint2=(X2_Conner_3, Y2_Conner_3),
```

```
        radius=r)
mdb.models['Model-1'].sketches['__edit__'].FilletByRadius(
        curve1=mdb.models['Model-1'].sketches['__edit__'].geometry[4],
        curve2=mdb.models['Model-1'].sketches['__edit__'].geometry[6],
        nearPoint1=(X1_Conner_4, Y1_Conner_4),
        nearPoint2=(X2_Conner_4, Y2_Conner_4),
        radius=r)
mdb.models['Model-1'].parts['Part-1'].features['Shell extrude-1'].setValues(sketch=mdb.models['Model-1'].sketches['__edit__'])
del mdb.models['Model-1'].sketches['__edit__']
mdb.models['Model-1'].parts['Part-1'].regenerate()

#CREATING WEB OPENING
#--------------------
mdb.models['Model-1'].ConstrainedSketch(gridSpacing=22.14, name='__profile__',
        sheetSize=885.66, transform=
        mdb.models['Model-1'].parts['Part-1'].MakeSketchTransform(
        sketchPlane=mdb.models['Model-1'].parts['Part-1'].faces[4],
        sketchPlaneSide=SIDE1,
        sketchUpEdge=mdb.models['Model-1'].parts['Part-1'].edges[15],
        sketchOrientation=RIGHT, origin=(0.0, 0.0 , m)))
mdb.models['Model-1'].parts['Part-1'].projectReferencesOntoSketch(filter=COPLANAR_EDGES, sketch=mdb.models['Model-1'].sketches['__profile__'])
mdb.models['Model-1'].sketches['__profile__'].rectangle(point1=(X1_Hole, Y1_Hole), point2=(X2_Hole, Y2_Hole))
mdb.models['Model-1'].parts['Part-1'].CutExtrude(flipExtrudeDirection=OFF,
        sketch=mdb.models['Model-1'].sketches['__profile__'],
        sketchOrientation=RIGHT,
        sketchPlane=mdb.models['Model-1'].parts['Part-1'].faces[4],
        sketchPlaneSide=SIDE1, sketchUpEdge=mdb.models['Model-1'].parts['Part-1'].edges[15])
del mdb.models['Model-1'].sketches['__profile__']

#CREATING MATERIALS
#------------------
mdb.models['Model-1'].Material(name='HSS')
mdb.models['Model-1'].materials['HSS'].Elastic(table=((E, v), ))

#SECTIONS ASSIGNMENT
#-------------------
mdb.models['Model-1'].HomogeneousShellSection(idealization=NO_IDEALIZATION,
        integrationRule=SIMPSON, material='HSS', name='Section-1', numIntPts=5,
        poissonDefinition=DEFAULT, preIntegrate=OFF, temperature=GRADIENT,
        thickness= t, thicknessField='', thicknessModulus=None, thicknessType=
        UNIFORM, useDensity=OFF)
mdb.models['Model-1'].parts['Part-1'].SectionAssignment(offset=0.0,
        offsetField='', offsetType=MIDDLE_SURFACE, region=Region(
        faces=mdb.models['Model-1'].parts['Part-1'].faces.getSequenceFromMask(
        mask=('[#1ff ]', ), )), sectionName='Section-1', thicknessAssignment=
        FROM_SECTION)

#CREATING ASSEMBLY
#-----------------
```

```
mdb.models['Model-1'].rootAssembly.DatumCsysByDefault(CARTESIAN)
mdb.models['Model-1'].rootAssembly.Instance(dependent=OFF, name='Part-1-1',
        part=mdb.models['Model-1'].parts['Part-1'])

#CREATING STEPS
#--------------
mdb.models['Model-1'].BuckleStep(maxIterations=300, name='Step-1', numEigen=2, previous='Initial', vectors=4)

#CREATING PARTITIONS
#-------------------
mdb.models['Model-1'].rootAssembly.PartitionEdgeByPoint(edge=
        mdb.models['Model-1'].rootAssembly.instances['Part-1-1'].edges[17], point=
        mdb.models['Model-1'].rootAssembly.instances['Part-1-1'].InterestingPoint(
        mdb.models['Model-1'].rootAssembly.instances['Part-1-1'].edges[17],
        MIDDLE))
mdb.models['Model-1'].rootAssembly.PartitionEdgeByPoint(edge=
        mdb.models['Model-1'].rootAssembly.instances['Part-1-1'].edges[20], point=
        mdb.models['Model-1'].rootAssembly.instances['Part-1-1'].InterestingPoint(
        mdb.models['Model-1'].rootAssembly.instances['Part-1-1'].edges[20],
        MIDDLE))
mdb.models['Model-1'].ConstrainedSketch(gridSpacing=22.14, name='__profile__',
        sheetSize=885.66, transform=
        mdb.models['Model-1'].rootAssembly.MakeSketchTransform(
        sketchPlane=mdb.models['Model-1'].rootAssembly.instances['Part-1-1'].faces[4],
        sketchPlaneSide=SIDE1,
        sketchUpEdge=mdb.models['Model-1'].rootAssembly.instances['Part-1-1'].edges[15],
        sketchOrientation=RIGHT, origin=(0.0, 0.0 , m)))
mdb.models['Model-1'].rootAssembly.projectReferencesOntoSketch(filter=
        COPLANAR_EDGES, sketch=mdb.models['Model-1'].sketches['__profile__'])
mdb.models['Model-1'].sketches['  profile  '].Line(point1=(X3 Hole, Y3_Hole), point2=(200.0, Y3_Hole))
mdb.models['Model-1'].sketches['__profile__'].HorizontalConstraint(
        addUndoState=False, entity=
        mdb.models['Model-1'].sketches['__profile__'].geometry[14])
mdb.models['Model-1'].sketches['__profile__'].ParallelConstraint(addUndoState=
        False, entity1=mdb.models['Model-1'].sketches['__profile__'].geometry[4],
        entity2=mdb.models['Model-1'].sketches['__profile__'].geometry[14])
mdb.models['Model-1'].sketches['__profile__'].CoincidentConstraint(
        addUndoState=False, entity1=
        mdb.models['Model-1'].sketches['__profile__'].vertices[10], entity2=
        mdb.models['Model-1'].sketches['__profile__'].geometry[11])
mdb.models['Model-1'].sketches['  profile  '].Line(point1=(X2 Hole, Y2_Hole), point2=(200.0, Y2_Hole))
mdb.models['Model-1'].sketches['__profile__'].HorizontalConstraint(
        addUndoState=False, entity=
        mdb.models['Model-1'].sketches['__profile__'].geometry[15])
mdb.models['Model-1'].sketches['__profile__'].PerpendicularConstraint(
        addUndoState=False, entity1=
        mdb.models['Model-1'].sketches['  profile  '].geometry[5], entity2=
        mdb.models['Model-1'].sketches['__profile__'].geometry[15])
mdb.models['Model-1'].sketches['__profile__'].CoincidentConstraint(
```

```
        addUndoState=False, entity1=
        mdb.models['Model-1'].sketches['__profile__'].vertices[11], entity2=
        mdb.models['Model-1'].sketches['__profile__'].geometry[10])
mdb.models['Model-1'].sketches['__profile__'].Line(point1=(X1_Hole, Y1_Hole), point2=(-200.0, Y1_Hole))
mdb.models['Model-1'].sketches['__profile__'].HorizontalConstraint(
        addUndoState=False, entity=
        mdb.models['Model-1'].sketches['__profile__'].geometry[16])
mdb.models['Model-1'].sketches['__profile__'].PerpendicularConstraint(
        addUndoState=False, entity1=
        mdb.models['Model-1'].sketches['__profile__'].geometry[3], entity2=
        mdb.models['Model-1'].sketches['__profile__'].geometry[16])
mdb.models['Model-1'].sketches['__profile__'].CoincidentConstraint(
        addUndoState=False, entity1=
        mdb.models['Model-1'].sketches['__profile__'].vertices[12], entity2=
        mdb.models['Model-1'].sketches['__profile__'].geometry[7])
mdb.models['Model-1'].sketches['__profile__'].Line(point1=(X4_Hole, Y4_Hole), point2=(-200.0, Y4_Hole))
mdb.models['Model-1'].sketches['__profile__'].HorizontalConstraint(
        addUndoState=False, entity=
        mdb.models['Model-1'].sketches['__profile__'].geometry[17])
mdb.models['Model-1'].sketches['__profile__'].PerpendicularConstraint(
        addUndoState=False, entity1=
        mdb.models['Model-1'].sketches['__profile__'].geometry[3], entity2=
        mdb.models['Model-1'].sketches['__profile__'].geometry[17])
mdb.models['Model-1'].sketches['__profile__'].CoincidentConstraint(
        addUndoState=False, entity1=
        mdb.models['Model-1'].sketches['__profile__'].vertices[13], entity2=
        mdb.models['Model-1'].sketches['__profile__'].geometry[8])
mdb.models['Model-1'].rootAssembly.PartitionFaceBySketch(faces=
        mdb.models['Model-1'].rootAssembly.instances['Part-1-1'].faces.getSequenceFromMask(
        ('[#10 ]', ), ), sketch=mdb.models['Model-1'].sketches['__profile__'],
        sketchUpEdge=
        mdb.models['Model-1'].rootAssembly.instances['Part-1-1'].edges[15])
del mdb.models['Model-1'].sketches['__profile__']

#CREATING BOUNDARY CONDITIONS
#----------------------------
mdb.models['Model-1'].DisplacementBC(amplitude=UNSET, createStepName='Initial',
        distributionType=UNIFORM, fieldName='', localCsys=None, name='Fix-Z',
        region=Region(
        vertices=mdb.models['Model-1'].rootAssembly.instances['Part-1-1'].vertices.getSequenceFromMask(
        mask=('[#200010 ]', ), )), u1=UNSET, u2=UNSET, u3=SET, ur1=UNSET, ur2=UNSET
        , ur3=UNSET)
mdb.models['Model-1'].DisplacementBC(amplitude=UNSET, createStepName='Initial',
        distributionType=UNIFORM, fieldName='', localCsys=None, name='Fix-X,Y',
        region=Region(
        edges=mdb.models['Model-1'].rootAssembly.instances['Part-1-1'].edges.getSequenceFromMask(
        mask=('[#5f6ad298 #2db ]', ), )), u1=SET, u2=SET, u3=UNSET, ur1=UNSET, ur2=
        UNSET, ur3=UNSET)
```

```
#CREATING LOADINGS
#------------------
mdb.models['Model-1'].ExpressionField(description='', expression=
        '0.0000842933*Y', localCsys=None, name='Normal-Distribution')
mdb.models['Model-1'].ShellEdgeLoad(createStepName='Step-1', distributionType=
        FIELD, field='Normal-Distribution', localCsys=None, magnitude=-1.0, name=
        'Moment-Left', region=Region(
        side1Edges=mdb.models['Model-1'].rootAssembly.instances['Part-1-1'].edges.getSequenceFromMask(
        mask=('[#5a48c080 #92 ]', ), )))
mdb.models['Model-1'].ShellEdgeLoad(createStepName='Step-1', distributionType=
        FIELD, field='Normal-Distribution', localCsys=None, magnitude=1.0, name=
        'Moment-Right', region=Region(
        side1Edges=mdb.models['Model-1'].rootAssembly.instances['Part-1-1'].edges.getSequenceFromMask(
        mask=('[#5221218 #249 ]', ), )))

#SEEDING And MESHING
#--------------------
mdb.models['Model-1'].rootAssembly.seedPartInstance(deviationFactor=0.1,
        minSizeFactor=0.1, regions=(
        mdb.models['Model-1'].rootAssembly.instances['Part-1-1'], ), size=5.0)
mdb.models['Model-1'].rootAssembly.generateMesh(regions=(
        mdb.models['Model-1'].rootAssembly.instances['Part-1-1'], ))

#CREATING JOBS
#-------------
mdb.Job(atTime=None, contactPrint=OFF, description='', echoPrint=OFF,
        explicitPrecision=SINGLE, getMemoryFromAnalysis=True, historyPrint=OFF,
        memory=90, memoryUnits=PERCENTAGE, model='Model-1', modelPrint=OFF,
        multiprocessingMode=DEFAULT, name='Buckle-Analysis-CASE-C', nodalOutputPrecision=
        SINGLE, numCpus=1, numGPUs=0, queue=None, resultsFormat=ODB, scratch='',
        type=ANALYSIS, userSubroutine='', waitHours=0, waitMinutes=0)

#SUBMITTING JOBS
#---------------
mdb.jobs['Buckle-Analysis-CASE-C'].submit(consistencyChecking=OFF)
mdb.jobs['Buckle-Analysis-CASE-C'].waitForCompletion()

#EXTRACTING RESULTS
#==================
import odbAccess
odb = openOdb(path = 'Buckle-Analysis-CASE-C.odb')
STEP = odb.steps.values()[0]
for i_frame in STEP.frames:
        eigenvalue = str(i_frame.description[29:37])
        print (eigenvalue)
```